NAVAL POSTGRADUATE SCHOOL
MONTEREY, CALIFORNIA

DISSERTATION

MAXIMUM-LIKELIHOOD ESTIMATORS FOR THE
TIME AND FREQUENCY DIFFERENCES OF
ARRIVAL OF CYCLOSTATIONARY DIGITAL
COMMUNICATIONS SIGNALS

by

David A. Streight

June 1999

Dissertation Supervisor: Herschel H. Loomis, Jr.

Approved for public release; distribution is unlimited.

19991227 030

REPORT DOCUMENTATION PAGE			Form Approved OMB No. 0704-0188

1. AGENCY USE ONLY *(Leave blank)*	2. REPORT DATE June 1999	3. REPORT TYPE AND DATES COVERED Doctoral Dissertation

4. TITLE AND SUBTITLE : Maximum-Likelihood Estimators For The Time And Frequency Differences Of Arrival Of Cyclostationary Digital Communications Signals	5. FUNDING NUMBERS
6. AUTHOR(S) David A. Streight	

7. PERFORMING ORGANIZATION NAME(S) AND ADDRESS(ES) Naval Postgraduate School Monterey CA 93943-5000	8. PERFORMING ORGANIZATION REPORT NUMBER

9. SPONSORING/MONITORING AGENCY NAME(S) AND ADDRESS(ES)	10. SPONSORING/MONITORING AGENCY REPORT NUMBER

11. SUPPLEMENTARY NOTES The views expressed in this thesis are those of the author and do not reflect the official policy or position of the Department of Defense or the U.S. Government.

12a. DISTRIBUTION/AVAILABILITY STATEMENT Approved for public release; distribution is unlimited.	12b. DISTRIBUTION CODE

13. ABSTRACT *(maximum 200 words)*

Advanced techniques have been employed for decades in the location of emitted communications signals. The use of cyclostationary maximum-likelihood estimators (MLE) applied to time difference of arrival (TDOA) and frequency difference of arrival (FDOA) techniques for target emitter location is a newly developed approach. This dissertation provides an introduction to traditional TDOA and FDOA methods and the underlying cyclostationary theory of pseudo-random signals. A survey of current cyclostationary TDOA and FDOA methods, the description of new maximum likelihood estimators (MLEs) and descriptions of Monte Carlo simulations follow this.

By comparing performance results to those of the Complex Ambiguity Function (CAF), it is shown that the new MLE(s) outperform the CAF in nearly all cases. Also, by comparison to the Cramer-Rao lower bound, the new MLE(s) provide a hint of the ultimate power of cyclostationary techniques over stationary techniques, exceeding this stationary theoretical lower bound on performance in many cases. Finally, the new MLE(s) perform comparably in the measurement of TDOA to those cyclostationary algorithms previously derived, when adjustments are made for the different signal environments used in the heritage work.

14. SUBJECT TERMS cyclostationary; time difference of arrival; TDOA; frequency difference of arrival; FDOA, maximum likelihood estimation .	15. NUMBER OF PAGES 162
	16. PRICE CODE

17. SECURITY CLASSIFICATION OF REPORT Unclassified	18. SECURITY CLASSIFICATION OF THIS PAGE Unclassified	19. SECURITY CLASSIFICATION OF ABSTRACT Unclassified	20. LIMITATION OF ABSTRACT UL

MAXIMUM-LIKELIHOOD ESTIMATORS FOR THE TIME AND FREQUENCY DIFFERENCES OF ARRIVAL OF CYCLOSTATIONARY DIGITAL COMMUNICATIONS SIGNALS

David A. Streight
Lieutenant, United States Navy
B.S., United States Naval Academy, 1990
M.B.A., National University, 1994
M.S.E.E., Naval Postgraduate School, 1997
E.E., Naval Postgraduate School, 1997

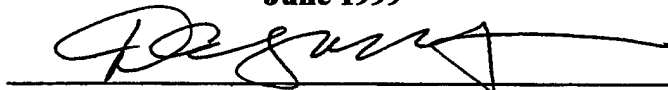Submitted in partial fulfillment of the requirements for the degree of

DOCTOR OF PHILOSOPHY IN ELECTRICAL ENGINEERING

from the

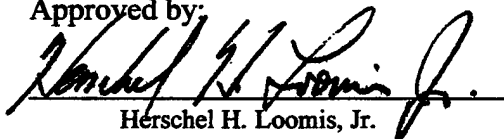## NAVAL POSTGRADUATE SCHOOL
June 1999

Author: _____

David A. Streight
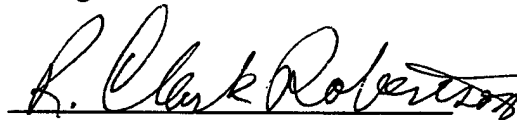
Approved by:

Herschel H. Loomis, Jr.
Professor of
Electrical and Computer Engineering
Dissertation Supervisor
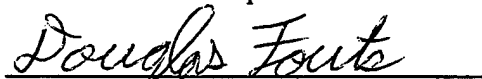
R. Clark Robertson
Professor of
Electrical and Computer Engineering

Douglas Fouts
Associate Professor of
Electrical and Computer Engineering

Gus K. Lott, Jr.
YarCom, Incorporated

William A. Brown, III
Mission Research Corporation

Approved by: _____

Jeffery B. Knorr, Chairman, Department of Electrical and Computer Engineering

Approved by: _____

Anthony P. Ciavarelli, Associate Provost for Instruction

iii

ABSTRACT

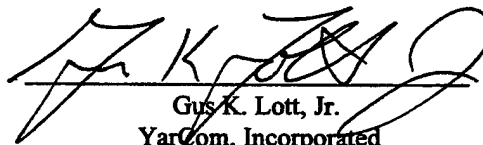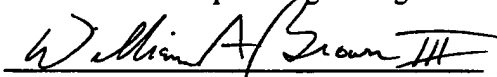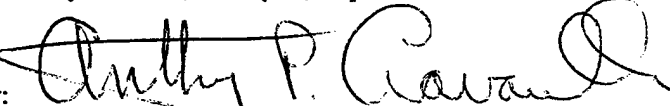Advanced techniques have been employed for decades in the location of emitted communications signals. The use of cyclostationary maximum-likelihood estimators (MLE) applied to time difference of arrival (TDOA) and frequency difference of arrival (FDOA) techniques for target emitter location is a newly developed approach. This dissertation provides an introduction to traditional TDOA and FDOA methods and the underlying cyclostationary theory of pseudo-random signals. A survey of current cyclostationary TDOA and FDOA methods, the description of new maximum likelihood estimators (MLEs) and descriptions of Monte Carlo simulations follow this.

By comparing performance results to those of the Complex Ambiguity Function (CAF), it is shown that the new MLE(s) outperform the CAF in nearly all cases. Also, by comparison to the Cramer-Rao lower bound, the new MLE(s) provide a hint of the ultimate power of cyclostationary techniques over stationary techniques, exceeding this stationary theoretical lower bound on performance in many cases. Finally, the new MLE(s) perform comparably in the measurement of TDOA to those cyclostationary algorithms previously derived, when adjustments are made for the different signal environments used in the heritage work.

TABLE OF CONTENTS

ACKNOWLEDGEMENTS

This journey started for me in 1994 when I took my first digital logic course and was hooked on electrical engineering. Now several years, one dog, one son, two houses, two jobs and a quarter-of-a-million airline miles later, there are a great many people without whom this would not have been possible. Hopefully I have managed to include them all here.

First to my committee I send a heartfelt thanks. Having a nagging, email-sending, phone message-leaving Ph.D candidate that is 3000 miles away (makes strangulation difficult) who tries to demand very fast responses and tough scheduling, could not have been easy. I thank you all in general for your tolerance of this unique and certainly at times, frustrating endeavor.

More specifically, to Dr. Robertson, thanks for your easy Texas manners and your amazing ability to *really teach* the complicated mathematics that makes up modern digital communications processes. I actually chose communications as my major area because of what I learned from you in all those classes and well-spent hours in the lab.

To Dr. Fouts- thanks for your help during my Written Screening Preparation as well as your calm and logical examination of me during both my Oral Screening Exam and Oral Qualifiers. I never ceased to learn a new point of view when preparing for an exam, reviewing problems or answering your examination questions. In addition, thanks for always working Space Systems Engineering into what we were doing – the minor area should never be forgotten and you were sure that it was not.

My gratitude extends to Dr. Brown for giving more of his time and attention than he probably thought would be needed when he agreed to do this. With you, I was able to learn not to fear working from first principles – a lesson I will always remember. Without you, never would I have been able to wade through the reams of previously derived cyclostationary algorithms that were the basis for this work.

I am indebted to Dr. Lott for the many hours of general counseling and the seemingly endless answers he had to the equally endless list of questions I had for him. I found that it is important to have one person on your committee that you can always call

(at any hour) and ask any question no matter how trivial or stupid it may seem – you were he. It is rare indeed when a student gets the opportunity to interact with, on a regular basis, someone who has seemingly done everything there is to do in electrical engineering. I know of no other person that has accomplished so much at such a young age and still has the time to be such a great mentor. I hope to continue to learn from your wealth of experience for many years.

Finally, I am truly grateful to Dr. Loomis. For over five years you have expertly guided me through a maze of academic achievements – all of which I never dreamed I'd see. Phenomenally, we have managed to squeeze out three graduate degrees in that time – all because you always knew exactly what to do, where I should go and who I needed to see. You always gave me an incredible amount of latitude – certainly enough rope with which to hang myself if I so chose. However, you never let me quite drop and I learned an enormous amount about how to think, how to work and how to keep all the balls in the air at the same time. Thank you sir, for all those years and all that time. I look forward to working with you in the years to come.

Now to the many people that also played important roles I'd also like to express my gratitude. Thanks to Dr. Charles Therrien for his assistance with discrete jointly-Gaussian pdfs and for always having time for me to ask questions of a true giant in the field of signal processing and random processes; to Cal Larvick for his help on the commercial uses of this research area and for reading the early, extremely rough draft of this dissertation and providing very thorough comments; to my friends Val Johnson and Mitch Darling (for some major CMA) and the men and women of ACG who encouraged me throughout; to the GeoLITE program office for epitomizing the notion that it's what you do with it once you have it that counts in the end and specifically to my boss, Randi Moore for her constant support of this work.

Finally, there have been several other people without whom my academic career would have ended in December 1996 with my departure from NPS. First, Linda Whitaker, my first post-graduate-school boss, has since taught me everything I know about acquisition, perseverance through her personal example, some humility along the way and the absolute importance of taking care of your people. At times she played mother, boss and sister but always friend. Without her unquestioning support, constant

encouragement and the unprecedented time she gave me, this work would never have been completed. Thank you Linda – we will surely work together again someday.

To my great friend Gus Lott and his wonderful wife Mary - you are two tremendous human beings that I have cherished since the day we met. You have helped me in many ways well beyond careers and the pursuit of graduate degrees. Gus, you got me started, kept me going and never gave up on me. You taught me and continue to teach me something new about life every time I talk to you. After all, you are the first guy I found as weird as I am when it comes to learning things simply from reading books! Your influence extends far beyond circuits and antennas – you have truly helped shape my career and helped me to realize what I want to be when I grow up someday. At times I still wonder if your steadfast support of me in those early years wasn't to you own detriment. In the end though, I guess you could say we are both better off anyway... Mary, you certainly didn't need (and are not nearly old enough) to have a 30 year-old kid - but you adopted one anyway. Thanks for playing Mom and for being the beautiful, caring friend that you are. Your zest for life and your constant positive outlook on everything is infectious. Thank you both for the great years past and the many better ones to come.

Next, to the best friend I've had for 26 of my 30 years, what can I say? There isn't anything we've done within our memories that the other wasn't around for. This time around I have to thank you for reminding me that the good life is often more about red felt pool tables and muddy mountain bikes than it is about algorithms and derivations. You are and will always be my alter ego – remember, we still share this brain, of that I am certain...thanks Rick.

Lastly, I would be truly lost without my amazing family. I am indebted to my brother Christopher and my soon-to-be sister-in-law, Tina for all the help they've given me. From your tireless nephew entertainment to taking care of the house and all its animal inhabitants while we've been gone, you've been a great help. I hope to repay you someday for all the time you've given.

To my wonderful mother-in-law, Carolyn, I cannot possibly thank you for all you've given me. The personal example you set in support of education every day and the endless list of things you've done for us, especially while I've been in school, are

xiii

staggering. Thank you for your unconditional support, your prayers and most especially, your daughter. I was truly blessed the day I met Shannon because I was able to gain not only a wife but also another Mom in the process.

Mom and Dad - you have always, since I can remember, stressed the importance of education, of applying oneself to the fullest and of pursuing dreams. Dad - you taught me how to print zeros and sevens correctly, the futility of intelligence without skilled written and oral expression and that learning is always superior to mere grades. Mom – you never let science and engineering completely consume me with trips to see Carol Channing as Dolly and James Earl Jones as Othello, plane tickets to England and trips to the Folger. You both made many sacrifices when I was younger to send me to the right schools, to support me in the pool and to keep me out of trouble. You drove back and forth to Annapolis more times than you care to help me survive at USNA. You have bought me books (one by Dr. Seuss in particular made quite a difference), paid for tuition, dog and cat watched and babysat. Perhaps most nobly, you have suffered through my endless descriptions of how the research is going, what's left and what doesn't work. I cannot think of two people who could have gotten me here better than you did. I only hope that I can be half the parent for Reilly that you have been for me. Thank you for everything.

Finally, I have been blessed with a remarkable son, Reilly and an extraordinary wife, Shannon. To my best buddy, you probably won't remember much of this, but let it be known that you possess, at the ripe old age of three, a depth of understanding, reasoning and maturity that astounds me every day. You have always understood when Dad had work to do and always tried to find any way to help. Though I tried to limit the impact on your life, you certainly did not get all of Dad, all of the time, but that never seemed to bother you. Couldn't have done without you, this is as much yours as mine - thanks for helping out my friend.

My dearest - though I certainly have given you enough reasons to do so, you have never doubted my ability for a second. Even in my darkest moments you've always managed to drag me up, dust me off and shove me back out into the game. You have tolerated my inexplicable obsession with this insane exercise (and many others along the way, as well as the ones currently in the works) with the grace and poise of a queen. You

are my one true thing, with all that I know that means to you. I love you very much –
only 72 or so to go. TTDT!!

I. INTRODUCTION

A. MOTIVATIONS FOR EMITTER LOCATION

1. Civil and Military Application

Emitter location enjoys extensive civil and military use as it contributes to a broad range of services. It finds use in law enforcement during the tracking and recovery of stolen vehicles. It is vital to search and rescue operations – seeking anything from ships adrift to downed aircraft and lost hikers. In navigation emitter location uses range from the multitude of Global Positioning System (GPS) based applications to the LORAN, OMEGA and TRANSIT systems that proceeded it. Finally, it has found extensive employment in the enforcement of communications regulations against unlicensed transmissions and intentional or unintentional interference of legitimate communications resources recently.

By far the most well known civil application is GPS. GPS receivers use the difference in arrival times (or time difference of arrival – TDOA) between the signals, ideally from four or more GPS satellites, to determine the user's position on the earth in all three dimensions to within 100 m routinely.

In military use, emitter location supports the three prongs of Information Operations: protect, exploit and attack. All rely upon the knowledge of the enemy's location. Protection of friendly communications requires the elimination of enemy jamming and interference equipment. Locating such equipment is the vital first step in that process. Exploiting enemy systems too requires knowledge of their locations. Finally, in order to attack enemy information systems, location data must be available.

2. The Changing Signal Environment

Obviously the field of emitter location has a multitude of applications and draws its motivation from both civil and military uses. It has for many years been the subject of

1

intensive study, providing a profusion of information on any of the common techniques and their subsets of hybrids and derivatives. The various algorithms and implementations have been developed, optimized and tested thoroughly, producing volumes of significant work in these traditional areas. However, given the increasingly dense radio frequency (RF) environments throughout the world, interference tolerant methods are becoming more sought after. As the RF environmental density increases, the methods must improve to still meet the accuracies demanded of users.

Fortunately, a recent development in signal processing offers the possibility of counteracting some of the deleterious effects of these increasingly populated RF environments. By modeling signals as cyclostationary and taking advantage of the unique features that these models unmask, newly developed signal processing algorithms are able to be highly signal selective even in the presence of noise and interference normally debilitating to traditional techniques. Emitter location methods benefit substantially from the application of cyclostationarity, particularly in the dense signal environments where the signal of interest (SOI) shares its channel with many spectrally, spatially and temporally overlapping signals not of interest (SNOI).

Traditional methods of parameter estimation for emitter location perform well in fairly benign signal environments. That is, with a SOI with a significant positive signal to noise ratio (SNR), in the absence of jammers and other SNOI(s) in the frequency band around the SOI, the traditional estimators of angle-of-arrival (AOA), frequency-difference-of-arrival (FDOA) and time-difference-of-arrival (TDOA) are superb. However, in a peacetime EM spectrum increasingly packed with signals, and a battlespace spectrum potentially flooded with SNOI(s), hostile jamming and weak SOI(s), these methods suffer from severely decreased signal to noise and interference ratio (SNIR) as well as little signal selectivity capability.

Clearly for the future, the move is to ever higher portions of the frequency spectrum, heavy frequency reuse, interference problems currently within the existing spectrum and the periodic reallocation of frequencies from one sector to another (e.g. military/ government to civil/commercial and vise-versa). All of these frequency allocations are worked within the bounds of the Federal Communications Commission

(FCC) for U.S. domestic matters and via the National Telecommunications and Information Administration to United Nations sanctioned bodies for international issues, the International Telecommunications Union. Additionally, the Worldwide Administrative Radio Committee (WARC) meets in Geneva, Switzerland every two years to debate the regional and global application of all portions of the RF spectrum. It is at these sessions that many of the key decisions concerning the use of the ever-smaller available portions of the RF spectrum are made.

Additionally, because the demand has far outpaced the allocations in many venues (U.S., Europe and Japan), commercial wireless communications vendors have moved to advanced techniques for interference mitigation. Taking advantage of both hardwired digital signal processing techniques and advanced software, they struggle to produce handsets, base stations and systems capable of meeting demand and maintaining quality of service.

Further, by U.S. and international regulation, an increasing awareness of the benefits of mandatory emergency-distress-calling emitter location has placed new burdens of implementation on the service providers. In this case, if a cellular telephone caller in the United States makes a 9-1-1 call in an emergency, the service provider within a very short time, is asked to provide location information to emergency service crews to find this distressed caller. Similar mandates are being imposed on international cellular (e.g. Global Service Mobile (GSM), IS95 (CDMA standard), etc.) and also on satellite mobile handsets (e.g. Iridium, Globalstar etc.)[2] [3]. The techniques implied in this dissertation may have utility to commercial wireless providers in implementing local, regional, or global positioning schemes within their systems.

Finally, other possible civil, commercial and military applications for these techniques include: (1) Cellular/Personal Communications System (PCS) interference mitigation rejection -- caller and tower location information can be used to control smart (dynamic) antennas on both the tower and the mobile subscriber to block out interfering signal sources, enabling greater geo-frequency reuse. (2) Transportation Management Applications -- some systems such as Omnitracs by Qualcomm have already implemented within which mobile units report out their location to a mother node by query to GPS

3

receivers. If the implied techniques here were implemented, perhaps the GPS component would not be required and the communication system itself could determine relative location of the mobile units, eliminating the need for anything but a radio on the mobile units and smart software in the base nodes. (3) Within the U.S. Department of Defense, Blue (friendly) force location services could be managed using automated emitter location techniques. (4) Finally, improved tracking of attached, small beacons on the animals under intensive study could support the tracking of migratory animals such as whales, birds and polar bears. This is done today, in a crude sense, using the U.S. and French Argos satellite but perhaps could be more easily implemented using simple satellite communications devices and service from two or more satellites[1].

B. TECHNICAL PROBLEM DESCRIPTION

1. Problem of Interest

The simplified technical problem addressed by this research is that of estimating TDOA and FDOA for SOIs in a co-channel interference (CCI) environment for the purpose of emitter location. The relative difference between correlated signal components both in the time domain as well as the frequency domain at two or more spatially-separated sensors makes possible the determination of the direction-of-arrival (DOA) of the signal. Those sensors may be located on the same platform or disparate platforms. Sensors on the same platform tend to employ phase-difference techniques to calculate the angle of arrival of the SOI – a technique related to the DOA solution from above. Nonetheless, with multiple DOA(s) from any method, it is then possible to determine the location of the emitter.

The challenge in this signal in interference environment and the focus of this research lies in correctly selecting the SOI among many SNOI and in correctly determining the TDOA and FDOA of the SOI, in collection environments where negative SNIR is common. Traditional methods are susceptible to spatial, spectral and temporal

overlap rendering the task of geolocating a weak emitter among many strong emitters difficult and at times imprecise. Thus, a method that is both highly signal-selective and operates with high fidelity in poor SINR scenarios is required.

The estimators derived herein gain their heritage from a revolutionary approach begun by Dr. William A. Gardner and his colleagues (see reference list and bibliography further reading). They exploit a statistical property in the man-made signals known as cyclostationarity. This cyclostationarity is conspicuous in both the time domain and the frequency domain manifesting itself as periodic components in the mean and autocorrelation function (as well as higher order moments) in the time domain, as well as power spectral density function (again as well as higher order moments) in the frequency-domain. Often the cyclostationary statistical characteristics of each signal in a bandwidth are unique, providing an identifying signature that enables outstanding signal-selectivity. In addition, the cyclostationary characteristics used for such a high degree of signal selectivity lend themselves to extracting very low SNIR signals from a highly corrupt environment. To that end, cyclostationary signal processing techniques have been developed for numerous purposes including weak-signal detection, signal separation in co-channel interference, array processing, spatial and temporal filtering, modulation classification and of course TDOA and FDOA estimation.

2. Signal Models

This effort revolves around a series of increasingly realistic and complicated signal models for the location of an EM emitter through passive means based upon measurement of both the TDOA and FDOA of the SOI. In Spooner and Gardner [4], the signal models begin with a simple two receiver, single SOI in Gaussian noise model. This model represents the simplified situation that exists when the SOI, radiating from a source remote to both receivers, impinges upon two spatially separated receivers with no relative motion in the system. In addition, the SOI is received in the presence of Gaussian noise only. The observables for this model, denoted Model A, are

5

$$x(t) = s(t) + n_x(t) \tag{1-1}$$

$$y(t) = s(t-D) + n_y(t) \tag{1-2}$$

Note that $s(t)$ represents the single SOI and $n_x(t)$ and $n_y(t)$ are zero-mean Gaussian noise terms. The parameter of interest in this model is D the TDOA. While this model includes some of the most important aspects of the situation and has been used extensively to simplify the mathematics of past work in TDOA, it makes some critical simplifying assumptions that reduce its applicability to real-world situations.

First, Model A makes no allowance for amplitude and phase mismatch at the receivers. Complete coherence between receiver platforms, a situation not always encountered, is presupposed without regard to the possible degradation in performance the mismatch can have on TDOA and FDOA estimation. Second, this model allows for no relative motion in the collection space, discounting or assuming a lack of consequential Doppler at each receiver. Should there be relative motion in the collection space, the frequency-shifted versions of the SOI likely will not correlate with any significance using traditional correlation based methods (depending primarily on the SOI characteristics and the induced Doppler). Thus, while this omission is perfectly reasonable in known static situations, it fails to generalize the model for the collection space to include a broader range of possible scenarios. Thirdly, the assumption of a single SOI alone in Gaussian noise is only applicable in a limited number of situations. Either indeed one signal is detectable amidst Gaussian noise (highly unlikely other than in the laboratory) or the SOI has such high SNR that it can safely be considered dominant enough in the environment to validate the assumption.

Finally, in most previous work (see [5], [6] and [7] for instance), the noise terms are assumed independent, identically distributed, Gaussian distributions and uncorrelated with the SOI as well. While simplifying the mathematics tremendously, this assumption can lead to unaccountable errors in the final analysis of the performance of TDOA and FDOA estimators. This unaccountable error is the result of contributions to the error budget made by the cross-terms in the covariance matrix that are directly attributable to

6

the correlation among the three variables. Indeed, there exists many situations where the interdependence of the SOI and noise terms at each receiver cause them to be correlated but to such a miniscule degree that the assumption remains essentially valid. However, depending on the relative distances of the emitter and receivers, the atmospheric conditions, frequency of transmission, instrumentation and innumerable other factors, the SOI and associated noise terms at each receiver are correlated to a significant degree (despite the normalcy of the noise probability density), thus requiring special consideration and invalidating this assumption. These four shortcomings will be addressed by four additional signal models, each increasingly complicated but more realistic than the last. They will be designated Models B, C, D and E and referred to throughout this work.

The four additional signal models for the TDOA and FDOA emitter location problem described above begin with a model to accomodate the amplitude and phase mismatch found between receivers. Denoted Model B, its observables

$$x(t) = s(t) + n_x(t) \tag{1-3}$$

$$y(t) = A_r s(t - \mathrm{D}) + n_y(t) \tag{1-4}$$

include the complex constant A_r which represents the relative amplitude and phase mismatch between receivers. Of course, this mismatch could be represented by a general complex exponential, $Ae^{j\phi}$, but for the sake of simplicity in notation, the complex constant serves the same purpose in a more fundamental fashion.

Unfortunately, while dealing well with the receiver mismatch, Model B does not address the issues of Doppler, multiple interfering signals or correlated SOI and noise. In order to introduce Doppler to the collection space, Model C must be used. While maintaining the TDOA, amplitude and phase term and Gaussian noise terms, it includes a Doppler shift for the second receiver relative to the first (an FDOA). The observables for Model C are

7

$$x(t) = s(t) + n_x(t) \qquad (1\text{-}5)$$

$$y(t) = A_r s(t - D)e^{j2\pi f_d t} + n_y(t) \qquad (1\text{-}6)$$

where the addition of f_d represents the FDOA in the SOI.

The fourth model takes into account signals in the collection space that are not the SOI but yet appear at both receivers. These dual-receiver SNOI can severely interfere with both TDOA and FDOA estimation (see next Chapter) and are commonly encountered in the signal environments of today. Because they appear at both receivers, they contribute unwanted correlations between the data sets of the receivers, corrupting the measurement of TDOA and FDOA for the SOI. The observables for this model, Model D, become very complicated and nearly intractable for theoretical work. Nonetheless, it is important to realize them. They are

$$x(t) = s(t) + \sum_{i=1}^{I} s_i(t) + n_x(t) \qquad (1\text{-}7)$$

$$y(t) = A_r s(t - D)e^{j2\pi f_d t} + \sum_{i=1}^{I} A_i s_i(t - D_i)e^{j2\pi f_{d_i} t} + n_y(t) \qquad (1\text{-}8)$$

where the summation represents an unknown number of SNOI, I, each with their own TDOA, D_i and FDOA, f_{d_i}.

One final signal model improves upon the realism of Model D one step further. This model, Model E, accounts for SNOI in the collection-space that appear at one but not the other receiver. In fact, many collection space situations can exist where the contributions from these signals to the analysis domains results in additional error in the estimation of the parameters of the SOI, further complicating the analysis. Model E can be represented as

8

$$x(t) = s(t) + \sum_{i=1}^{I} s_i(t) + \sum_{k=1}^{K} s_k(t) + n_x(t) \qquad (1\text{-}9)$$

$$y(t) = A_r s(t-D)e^{j2\pi f_d t} + \sum_{i=1}^{I} A_i s_i(t-D_i)e^{j2\pi f_{d_i} t} + \sum_{l=1}^{L} A_l s_l(t) + n_y(t) \quad (1\text{-}10)$$

where the addition of an unknown number, K and L, of single-receiver SNOI, $s_k(t)$ and $s_l(t)$, are added to the received signals $x(t)$ and $y(t)$ respectively. In addition, note that while the single-receiver SNOI have neither a TDOA nor an FDOA.

In the research presented here, all five models will be used either as illustrations in the presentation of underlying theory, in the derivation of new TDOA and FDOA estimators, in the extension of lower bounds or in the description of the collection space used to test the new algorithms and lower bound extensions. While Models B and C are used extensively in the theoretical work contained herein, Models D and E more adequately represent the signal environment of real-world situations. Thus, they are used as guidelines in the synthesis of test signals and to represent real-world data. Awareness of the differences in the signal models allows for intelligent, qualitative comments to be made regarding the effects of using estimators derived for use in a collection environment characterized by Model C but used in an environment characterized by Models D or E for instance. While not quantitative, the conclusions are valuable and may lead to further work that will aid in optimizing algorithms for use in environments like those represented by Model E.

C. OBJECTIVES OF THE RESEARCH

1. Maximum-Likelihood Cyclostationary TDOA and FDOA Algorithms

The primary objective presented here is the development of two new cyclostationary TDOA and FDOA estimator through the maximization of a likelihood function. Through a new derivation with a unique signal model and the multitude of options that are available with the selection of valid mathematical substitutions, one ideal and two approximated maximum-likelihood estimators have emerged.

2. Lower Bound Selection and Computation

A secondary objective involves the survey, selection and possible modification of an appropriate theoretical lower bound (LB) on the estimates for TDOA and FDOA obtained from cyclostationary estimators. Ideally, following a complete survey and evaluation of related LBs from past work in emitter location, the application of an appropriate LB is possible. Such a LB must be fully congruent with the assumptions and basic theory of the cyclostationary signal models and must be easily calculable.

Unfortunately, no such LB exists currently despite of the recent work by Schell on the extension of Whittle's Theorem to the cyclostationary case [8]. Thus, while no modifications to existing LBs are presented here, a comparison to the stationary Cramer-Rao bound (CRB) developed for both TDOA in [5] and [6] and joint TDOA-FDOA in [7], serves to satisfy this secondary objective.

3. Monte Carlo Testing and Comparison

The tertiary objective involves the thorough simulation of the estimators' performance in the presence of various challenges to traditional estimators. Using a Monte Carlo method, designed both for ease of comparison to previous algorithm testing and for the assessment of specific signal-selectivity properties, the performance of the new

ML algorithms is compared to both the calculated theoretical LB and the performance of previously derived estimators. Performance conclusions with respect to several key real-world parameters are strongly supported by this testing and are commented upon in the final section.

D.   TECHNICAL APPROACH

1.   Fraction-of-Time Probability Approach

The theoretical basis for the models used in the estimation of the parameters of TDOA and FDOA is pivotal to the development of the ML estimators. Central to that theory are the two different schools of thought related to the estimation of parameters such as TDOA and FDOA from finite time-series, the traditional stochastic approach and the fraction-of-time (FOT) probability approach.

The traditional stochastic process approach can be traced through many years of use in statistical problems, particularly statistical signal processing. This tradition makes it a popular and comfortable choice for the theoretical underpinnings of the estimation of parameters process. However, it suffers in practical application to actual finite time-series signal data and from abstractions like the expectation operator that are counter-intuitive.

On the other hand, the FOT probability approach defined by Gardner in [9] and refined by Brown in [10] lends itself well to both the analytical and empirical analysis of man-made signals represented by finite time-series. The FOT probability theory overcomes many of the shortcomings of the stochastic approach and avoids the troublesome abstractions in the process. For these reasons and more (see Chapter III), the FOT theory serves as the theoretical basis for the development of both ML estimators in this work.

2. Algorithm Development

In previous work dating to 1992, Gardner and his associates have explored the benefits of cyclostationary techniques in the estimation of TDOA and to a lesser extent, FDOA in corrupt signal environments. In [4], Spooner and Gardner began the development and evaluation of an ML estimator for TDOA based upon a signal model that included a weak cyclostationary signal in white Gaussian noise with arbitrary receiver gain and phase mismatch. In the work presented here, an ML approach is again pursued but with a more complicated and realistic signal model, a greatly differing mathematical model and several differing assumptions guiding the derivation. From that approach emerges an ideal algorithm optimized for both TDOA and FDOA estimation.

In addition, two additional algorithms are developed based upon the investigation of the individual terms of the ideal ML algorithm. Making simple but effective substitutions yields the first approximation. Eliminating some weak terms to improve computation speed produces the second approximation and aids in an initial evaluation as to the feasibility of simplifying the algorithm further to benefit implementation with little effect on performance. Details of the algorithms' development appear in Chapter V.

E. DISSERTATION ORGANIZATION

1. Part I: Underlying Theories

In order to appreciate better, the advantages that cyclostationary theory has to offer the emitter location problem, traditional TDOA and FDOA methods and their applications are briefly addressed in Chapter II with an emphasis on their breakdown in highly corrupt environments using a Binary Phase Shift Keying (BPSK) signal in various environments as a recurring example. Chapter III traces the development of cyclostationary theory from the traditional auto and cross-correlation functions and the power spectral density function to the cyclic auto and cross-correlation functions and the

spectral correlation density function. This chapter serves as an extensive introduction to the signal-selective capabilities of cyclostationary processing techniques and provides an excellent transition to cyclostationary emitter location techniques. Chapter IV introduces the abbreviated derivation and discussion of some current cyclostationary TDOA techniques.

2.   Part II: Development of New Algorithms

Chapter V offers the derivation of one ideal and two approximated cyclostationary joint TDOA/FDOA algorithms. Each is derived in exhaustive detail to permit close examination of the models used, assumptions made and substitutions used.

3.   Part III: Monte Carlo Testing and Conclusions

Chapter VI tests the algorithms' performance with simulated data in a Monte Carlo fashion, reporting the results in terms of the Root Mean Square Error of the TDOA and FDOA estimates for a variety of signal environments. In Chapter VII, by comparing the results to those obtained for the traditional Cross Ambiguity Function and those predicted by the stationary CRB, the performance of the new estimators relative to that of traditional techniques is presented. Finally, a comparison to results from the testing of previously derived cyclostationary estimators precedes conclusions and suggestions for further research.

II. TRADITIONAL TDOA AND FDOA METHODS

A. TRADITIONAL GENERALIZED SIGNAL MODEL

1. Model B Revisited

For the development of the two traditional methods of TDOA determination, assume a stationary signal from a remote emitter impinges upon two spatially separated antenna elements. This situation may be represented by signal Model B and is repeated here for consistency as

$$x(t) = s(t) + n_x(t) \tag{2-1}$$

$$y(t) = A_r s(t - D) + n_y(t) \tag{2-2}$$

Recall $n_x(t)$ and $n_y(t)$ are assumed to contain only AWGN with no strong SNOI(s) in the frequency band of interest for the SOI, $s(t)$; A_r is the relative magnitude and phase mismatch between the receivers; D is the TDOA of the SOI.

It follows that the auto-correlation and cross-correlation functions are given by

$$R_x(\tau) = R_s(\tau) + R_{n_x}(\tau) \tag{2-3}$$

$$R_y(\tau) = |A_r|^2 R_s(\tau) + R_{n_y}(\tau) \tag{2-4}$$

$$R_{yx}(\tau) = A_r \cdot R_s(\tau - D) + R_{n_x n_y}(\tau) \tag{2-5}$$

and the respective spectral density functions are

15

$$S_x(f) = S_s(f) + S_{n_x}(f) \qquad\qquad\text{(2-6)}$$

$$S_y(f) = |A_r|^2 S_s(f) + S_{n_y}(f) \qquad\qquad\text{(2-7)}$$

$$S_{yx}(f) = A_r \cdot S_s(f) \cdot e^{-j2\pi fD} + S_{n_x n_y}(f) \qquad\qquad\text{(2-8)}$$

These relationships contain the parameter of interest, specifically, D, the TDOA.
The next two sections illustrate two traditional methods used to extract D from these
equations. The first, the Generalized Cross Correlation (GCC) function, can be used in
the absence of relative motion between the two receivers and the emitter. The second, the
Complex Ambiguity Function (CAF), can be used to estimate FDOA and TDOA
simultaneously as is necessary when relative motion between the receivers and emitter
exists causing the use of Model C to accommodate the Doppler.

2.   Comments on Simplifying Assumptions

As alluded to in Chapter I, of key importance to the development illustrated here is
the statistical independence of $s(t)$, $n_x(t)$ and $n_y(t)$ and the absence of in-band interference.
While it may be argued that the signals as well as noise measured at the two receivers can
be correlated to some extent, that scenario greatly complicates this case and is beyond the
scope of this discussion. The derivations that follow are drawn from [5], [6], which treat
the GCC more specifically and [7] and [11] which address the CAF more so than the
GCC. All assume the three components to be uncorrelated. For an initial treatment of
correlated noise samples at the two receivers which produce non-zero off-diagonal terms
in the covariance matrix of the TDOA estimate, see [12].

B. GENERALIZED CROSS-CORRELATION FUNCTION

1. Derivation

Applying (2-5) in the absence of SNOI in the SOI band of interest and assuming statistically independent $s(t)$, $n_x(t)$ and $n_y(t)$ yields

$$R_{yx}(\tau) = A_r \cdot R_s(\tau - D) + R_{n_x n_y}(\tau) \tag{2-9}$$

This function will peak at $\tau = D$, the TDOA between receivers 1 and 2. Because $n_x(t)$ and $n_y(t)$ contain merely AWGN, their cross-correlation term in (2-9) above reduces the SNR of the measurement but does not add interference in the form of SNOI(s). Further analysis using (2-6) – (2-8) in a similar manner reveals

$$S_x(f) = S_s(f) + S_{n_x}(f) \tag{2-10}$$

$$S_y(f) = |A_r|^2 S_s(f) + S_{n_y}(f) \tag{2-11}$$

$$S_{yx}(f) = A_r \cdot S_s(f) \cdot e^{-j2\pi f D} + S_{n_x n_y}(f) \tag{2-12}$$

To extract D from (2-12), first note

$$S_s(f) = \begin{cases} > 0 & f_0 - \dfrac{B}{2} \leq f \leq f_0 + \dfrac{B}{2} \\ = 0 & \textit{otherwise} \end{cases} \tag{2-13}$$

which assumes the SOI effectively occupies a finite bandwidth B around the carrier or intermediate frequency f_0. If sufficiently high SNR is assumed, the noise terms in (2-10) –

(2-12) may be disregarded. Thus, the ratio of the spectra using (2-10) with (2-13) becomes,

$$\frac{S_{yx}(f)}{S_x(f)} = A_r \cdot e^{-j2\pi fD}, \quad f_o - \frac{B}{2} \le f \le f_o + \frac{B}{2} \tag{2-14}$$

and taking the inverse Fourier transform of this ratio gives

$$h_o(\tau) = \int_{f_o-B/2}^{f_o+B/2} \frac{S_{yx}(f)}{S_x(f)} e^{+j2\pi ft} df$$

$$= \frac{A \sin[\pi B(\tau - D)]}{\pi(\tau - D)/2} \cos[2\pi f_o(\tau - D)] \tag{2-15}$$

which peaks at $\tau = D$. The noise terms in (2-14) are dropped in (2-15) because they are identically zero due to the statistical independence of the signals and the noise assumed in this model. Equation (2-15) in turn may be rewritten as

$$h_0'(\tau) = \int_{f_o-B/2}^{f_o+B/2} W(f) S_{yx}(f) e^{+j2\pi ft} df \tag{2-16}$$

The weighting function, $W(f)$, is defined in this instance as $1/S_x(f)$ in (2-16) which is the best choice given no a priori information about the SOI [5]. In addition, it distinguishes this case as the generalized cross correlation method. Assigning a weighting function, $W(f) = 1$ reduces the TDOA determination to a simple cross-correlation as in (2-5). Given prior knowledge of the noise and interference characteristics it is possible to make other choices for $W(f)$ including the Roth impulse, SCOT and PHAT among many others which are designed to reduce specific noise and interference problems [5]. A more comprehensive list of weighting functions and associated uses appears in Table 2-1.

18

It is clear that, in the absence of significant noise, co-channel interference and relative motion between receivers and emitter, finding the peak in the GCC produces the desired estimate of the TDOA of a signal from the ratio of the estimates of the power spectral density function of the signal at one receiver and the cross power spectral density function of the two received signals. Figure 2-1 below illustrates the generalized cross correlation.

PROCESSOR NAME	WEIGHTING FUNCTIONS	DESIGN GOAL
Cross Correlation	1	None
Roth Impulse Response	$\dfrac{1}{S_{xx}(f)}$	Suppress noise in receiver #1 for the frequency region surrounding the SOI
SCOT	$\dfrac{1}{\sqrt{S_{xx}(f)S_{yy}(f)}}$	Suppress noise in both receivers for the frequency region surrounding the SOI
PHAT	$\dfrac{1}{\left|S_{xy}(f)\right|}$	Developed purely as an ad hoc technique
Eckart	$\dfrac{S_{ss}(f)}{\left[S_{n_x n_x}(f)S_{n_y n_y}(f\right.}$	Maximizes the difference in the mean correlator output for a signal present versus just noise present (deflection)

Table 2-1 – Candidate weighting functions, from [5]

19
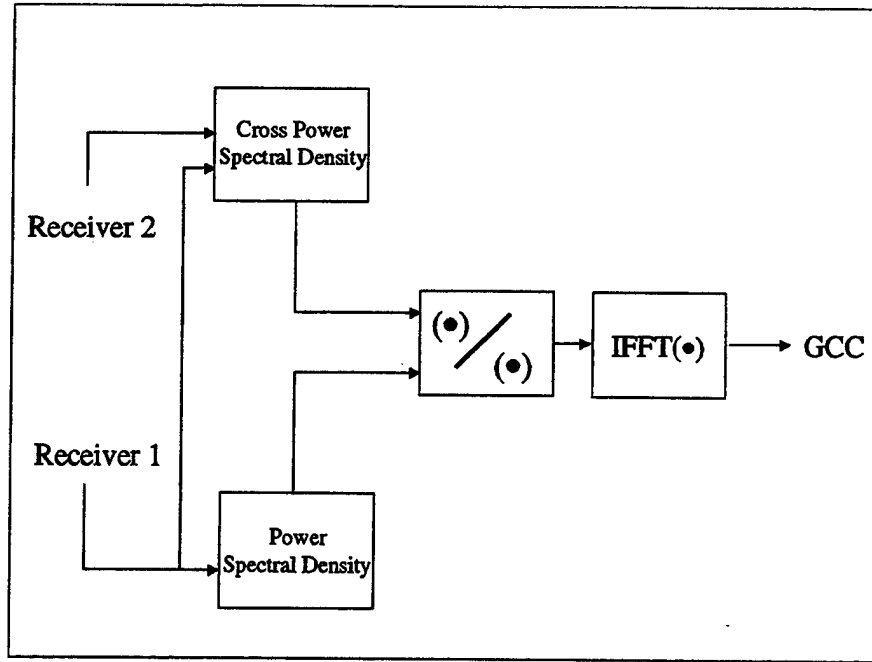
Figure 2-1 - GCC block diagram

2. Estimation Variance

Beginning in [5], Knapp and Carter developed an expression for the variance of the TDOA estimate resulting from the GCC. In [6], Azaria and Hertz refined the expression relating the variance of the estimate to the integration time, signal bandwidth and equivalent SNR at each receiver. Given those inputs,

$$E(\hat{D}-D)^2 = \frac{3}{4\pi^2} \frac{1}{T} \frac{1}{B_s^3} \frac{1}{\gamma} \tag{2-17}$$

where $\hat{D}$ is the TDOA estimate; D is the actual TDOA; T represents the integration time; B_s the signal and noise bandwidths; $\frac{1}{\gamma}$ is defined as the equivalent SNR as follows

$$\frac{1}{\gamma} = \frac{1}{2}\left[\frac{1}{\gamma_1} + \frac{1}{\gamma_2} + \frac{1}{\gamma_1\gamma_2}\right] \qquad (2\text{-}18)$$

3.   Binary Phase Shift Keying Example

To best illustrate the performance of the GCC in both benign and corrupt environments, assume a single SOI in AWGN as represented by signal Model B. A BPSK signal with the characteristics listed in the Appendix serves as the SOI. The TDOA of this signal is clearly 50 samples as the plot of the output of the GCC function for this case (GCC-1) illustrates in Figure 2-2.
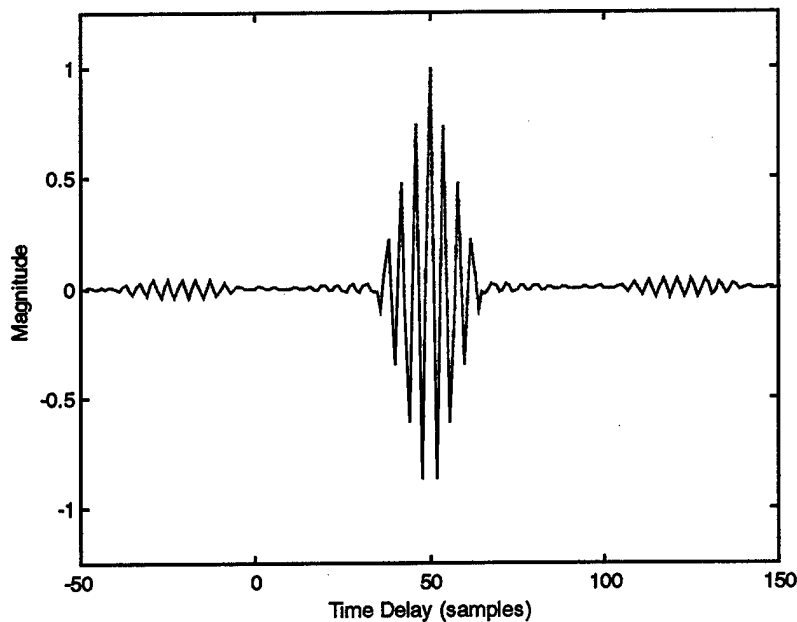

Figure 2-2 – Plot of GCC output, high SNR (GCC-1)

For comparison, change the SNR of the BPSK signal to –10 dB. The output of the GCC for this case (GCC-2) appears in Figure 2-3. Note that in the presence of severe AWGN, the GCC begins to produce errors in the estimate of the TDOA.

Thirdly, the BPSK signal is restored to its original SNR but now has an FDOA of 20 kHz introduced to the SOI, measured at the two receivers as in Model C. Figure 2-4 illustrates the results produced by the GCC in this situation (GCC-3). The shifting of the frequency components of the SOI was enough to produce errors in the estimation.
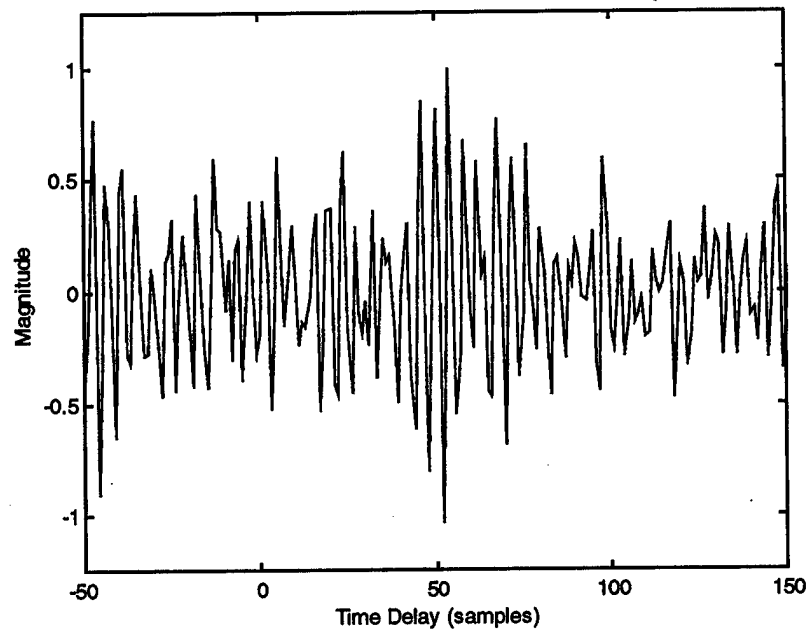
Figure 2-3 – Plot of GCC output, SNR = -10 (GCC-2)

As a fourth illustration, the environment of GCC-2, low SNR and GCC-3, Doppler, are combined and the results displayed in Figure 2-5 (GCC-4). Note the combination of poor SNR and Doppler results in extremely poor performance for the GCC. In the next section, the effects of Doppler are successfully accounted for in the second of the two illustrative examples of traditional stationary methods of TDOA and FDOA determination, given sufficient SNR.

Finally, to further illustrate the breakdown of the GCC in modern signal environments, note the effect of introducing a single interfering SNOI with significant spatial, temporal and frequency overlap. The single SNOI is another BPSK signal with characteristics shown in the Appendix. The effects of this corruption on the estimate of

22

the TDOA of the SOI can be seen in Figure 2-6 (GCC-5). Note the SOI and SNOI have different center frequencies, bandwidths, keying rates and TDOA(s) which might distinguish them from one another quite well under other circumstances. However, in correlating the outputs of the two receivers, the combination of the partial overlap spatially, temporally, and spectrally produces a TDOA estimate that represents the true TDOA of neither emitter at 109 samples. In addition, though it is obvious that two signals are present, by the two peaks in the plot, even assuming the second peak at 29 samples is correct would lead to an incorrect estimate for the TDOA of the SOI. As a logical extension, it is obvious that the addition of poor SNR (and consequently even worse SNIR) as well as Doppler for the SOI to this last situation would render the GCC completely ineffective.

While the CAF discussed in the next section accounts for Doppler, it too suffers from poor SNR environments. In addition, it will become evident that SNOI make TDOA (and FDOA) estimation difficult for both the GCC and CAF and can be handled only through different techniques like the exploitation of cyclostationarity.
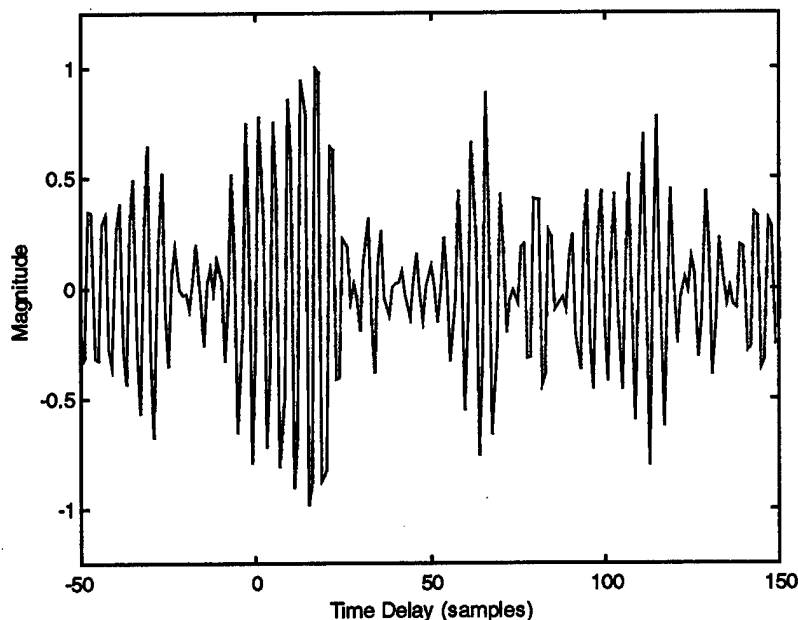

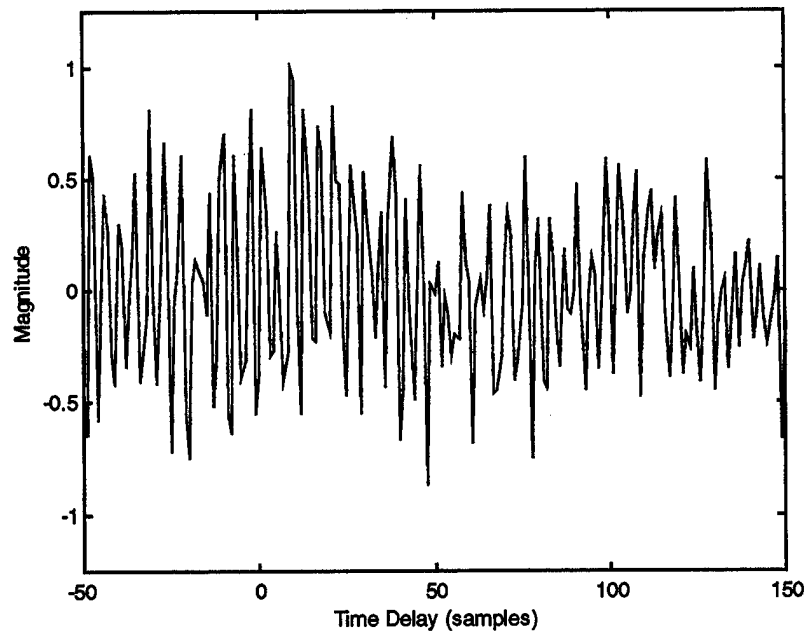Figure 2-4 – Plot of GCC output, high SNR and Doppler (GCC-3)

23
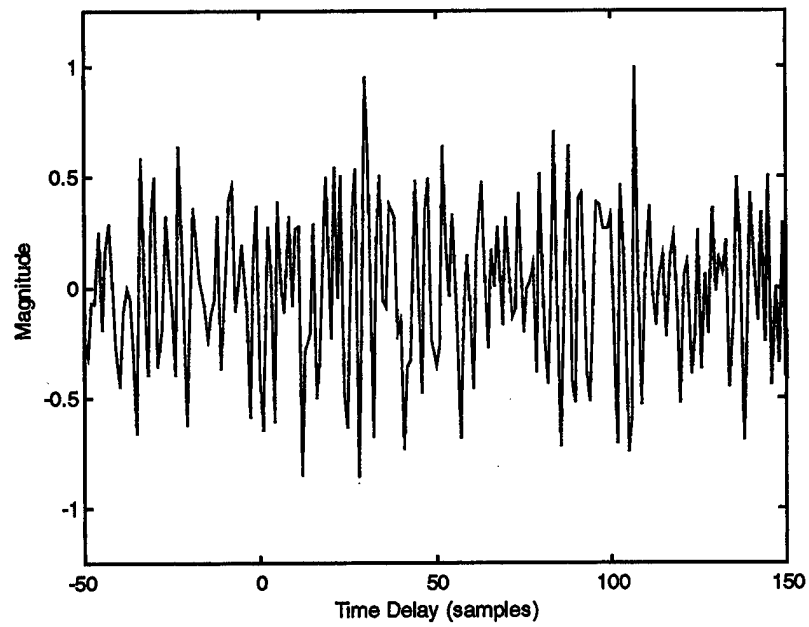
Figure 2-5 – Plot of GCC output, low SNR and Doppler (GCC-4)

Figure 2-6 – Plot of GCC output, high SNR and SNOI (GCC-5)

24

C. COMPLEX OR CROSS AMBIGUITY FUNCTION

1. Derivation

The complex ambiguity function (CAF), also known as the cross ambiguity function or the radar function can be interpreted as an extension of the GCC for moving transmitters and/or receivers. Since the GCC function relies upon the correlation of the signals' characteristics in either the time or frequency domain. Naturally, if components of one of the received signals were shifted in frequency by some amount relative to the other received signal (Doppler), the correlation would surely be corrupted and may even be rendered useless. This characteristic of the GCC was illustrated in Figures 2-6 and 2-7 above.

In fact, Stein in [7], showed that in order to properly determine the TDOA between two receivers in the presence of a Doppler difference at each receiver, the spectrum of one of the signals first must be translated in frequency by an amount f_d equal to the Doppler difference (FDOA) measured between the observers. In order to show this, a Doppler shift is introduced into Model B to obtain Model C. Equations (2-1) and (2-2) can now be written as

$$x(t) = s(t) + n_x(t) \tag{2-19}$$

$$y(t) = A_r s(t - D) e^{j2\pi f_d t} + n_y(t) \tag{2-20}$$

where the addition of f_d is the FDOA of the SOI as measured between receivers 1 and 2.

In place of calculating TDOA with the two dimensional GCC (time and magnitude of the correlation) from (2-16), which in the presence of significant Doppler, could peak at a value that does not truly correspond to the TDOA, it is necessary to calculate the three dimensional (time, frequency and magnitude of the correlation) CAF given by

$$A(D, f_d) = \int_0^T x(t)y^*(t-D)e^{-j2\pi f_d t} dt \qquad (2\text{-}21)$$

A block diagram of the CAF operation in the time domain appears in Figure 2-7.
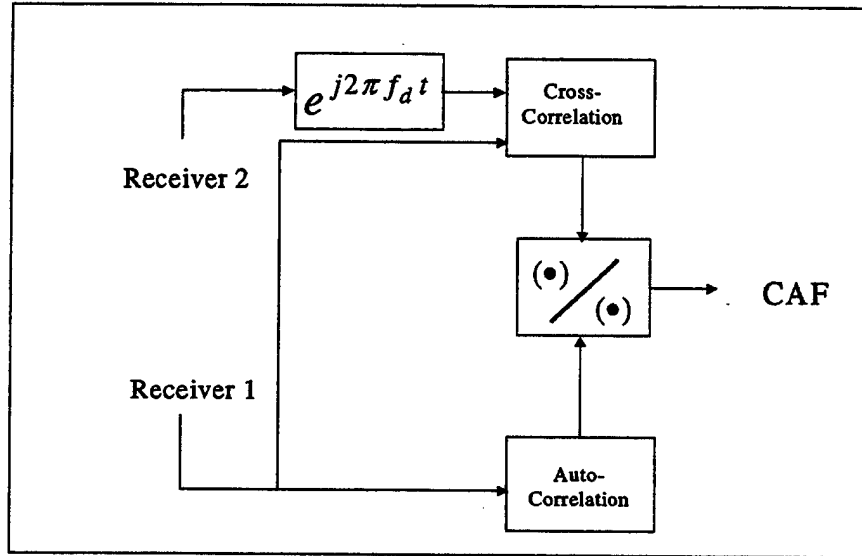
Figure 2-7 – CAF block diagram

The simultaneous determination of the TDOA, D and the Doppler shift, f_d, causes $|A(D, f_d)|$ to peak. At $f_d = 0$, the CAF reduces to a GCC problem as outlined above. For $f_d \neq 0$, the CAF may be thought of as a GCC performed after frequency shifting the spectrum of $y(t)$ up or down as necessary by an amount equal to f_d.

2. Estimation Variances

The three-dimensional width of the correlation lobe in (2-20) is directly proportional to the accuracy of the estimates of TDOA and FDOA. Stein further points out in [7] that the variance of the estimate for each parameter can be related to the noise bandwidth, the signal bandwidth, the integration time and the effective input signal to noise ratio as follows

$$\sigma_{TDOA} = \frac{1}{\beta} \frac{1}{\sqrt{BT\gamma}} \qquad (2\text{-}22)$$

$$\sigma_{FDOA} = \frac{1}{T_e} \frac{1}{\sqrt{BT\gamma}} \qquad (2\text{-}23)$$

where

B = noise bandwidth at the input of both receivers

$$\beta \overset{\Delta}{=} 2\pi \left[\frac{\int\limits_{-\infty}^{+\infty} f^2 W_s(f) df}{\int W_s(f) df} \right]^{\frac{1}{2}} \qquad (2\text{-}24)$$

where $W_s(f)$ is the spectral density of the signal as shaped by the receiver.

T_e = rms integration time

$$\frac{1}{\gamma} = \frac{1}{2} \left[\frac{1}{\gamma_1} + \frac{1}{\gamma_2} + \frac{1}{\gamma_1 \gamma_2} \right] \qquad (2\text{-}25)$$

where $\frac{1}{\gamma_1}$ and $\frac{1}{\gamma_2}$ are the SNR(s) for each receiver respectively as in (2-18) above.

3.   Binary Phase Shift Keying Example Extended

For ease of comparison, the following five examples apply the CAF to the precisely the same situations represented by the five GCC plots from the previous section. (Reference the Appendix for the characteristics of the SOI and the SNOI.)

In the first two sets of CAF plots, Figures 2-8 (CAF-1) and 2-9 (CAF-2) show three plots each. The first plot is the three dimensional CAF plot while the remaining two

are plots of the maximum values along lines of time delay and frequency delay respectfully. Figure 2-8 represents performance in a high SNR environment with no Doppler and Figure 2-9 illustrates the degradation in a low SNR environment. Note that because the CAF reduces to the GCC in this case only the three-dimensional rendering and slight differences in the plotting of the time delay distinguish these plots from Figures 2-2 and 2-3.

Furthering the CAF example, introduce the same FDOA of 20 KHz used in the GCC-3 and GCC-4 cases above. Here, in the high SNR environment, the CAF successfully estimates both the TDOA and FDOA in Figure 2-10 (CAF-3). However, the low SNR environment deteriorates the accuracy of both estimates which may be seen in Figure 2-11 (CAF-4). No single feature dominates the estimation of either TDOA or FDOA and in fact, the maximum values along each axis are incorrect estimates for the actual TDOA and FDOA of the SOI.

Finally, the introduction of the BPSK SNOI in Figure 2-12 has a similar effect on the CAF as it has on the GCC. Note that the SNOI signal has been modified to contain an FDOA of -11.7 kHz to help in the illustration of the effect of the SNOI on the FDOA estimate as well. As was true with case GCC-5 above, the addition of a strong SNOI spectrally, temporally and spatially close to the SOI masks the peak of the SOI in the CAF. The dominant feature in Figure 2-12 is actually attributable to the SNOI energy, making the accurate determination of the TDOA and FDOA of the SOI impossible without some pre-filtering like that performed by the weighting functions of the GCC.

Low SNR and overlapping SNOI make both the GCC and CAF much less effective in the successful estimation of the parameters of TDOA and FDOA for a single SOI in the collection bandwidth. The GCC's inability to account for Doppler shifts and both the methods' inability to distinguish the parameters of the SOI from overlapping SNOI motivate the pursuit of methods that support the accurate estimation of signal parameters, such as TDOA and FDOA, in the presence of poor SNR environments riddled with SNOI.
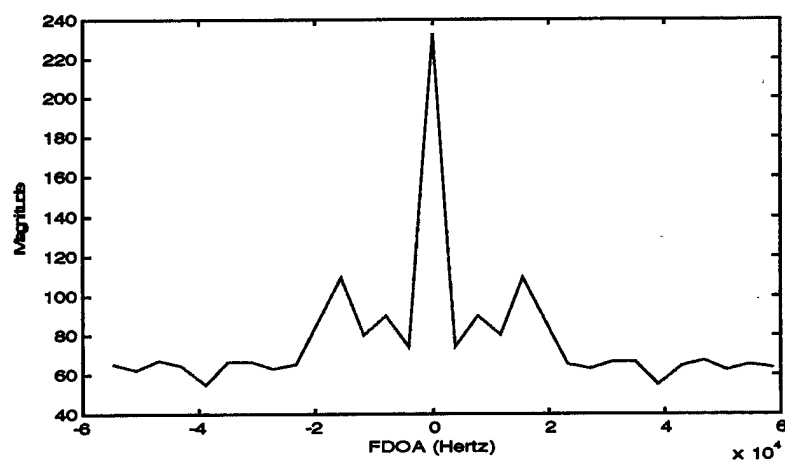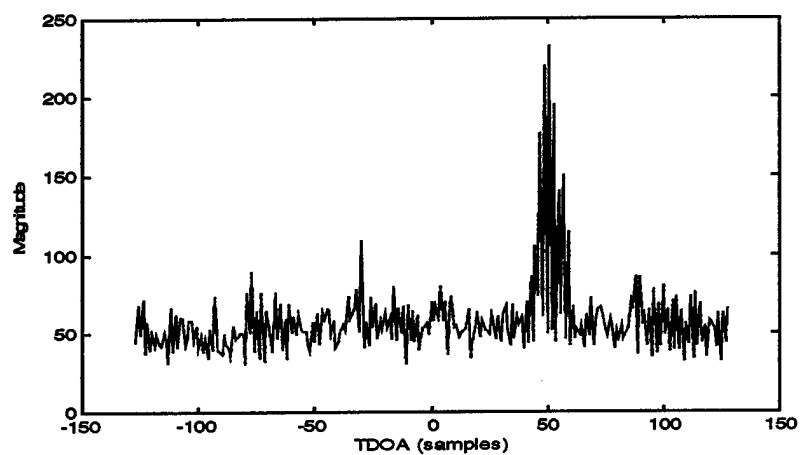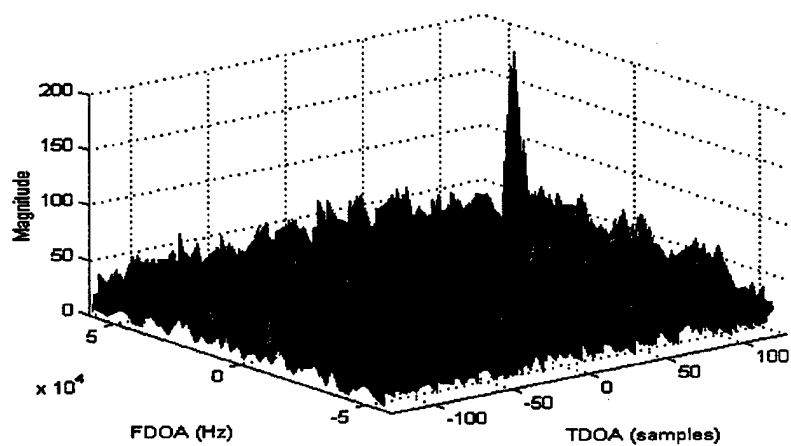
Figure 2-8 – Plots of CAF output, SNR = 3 dB and no Doppler (CAF-1)
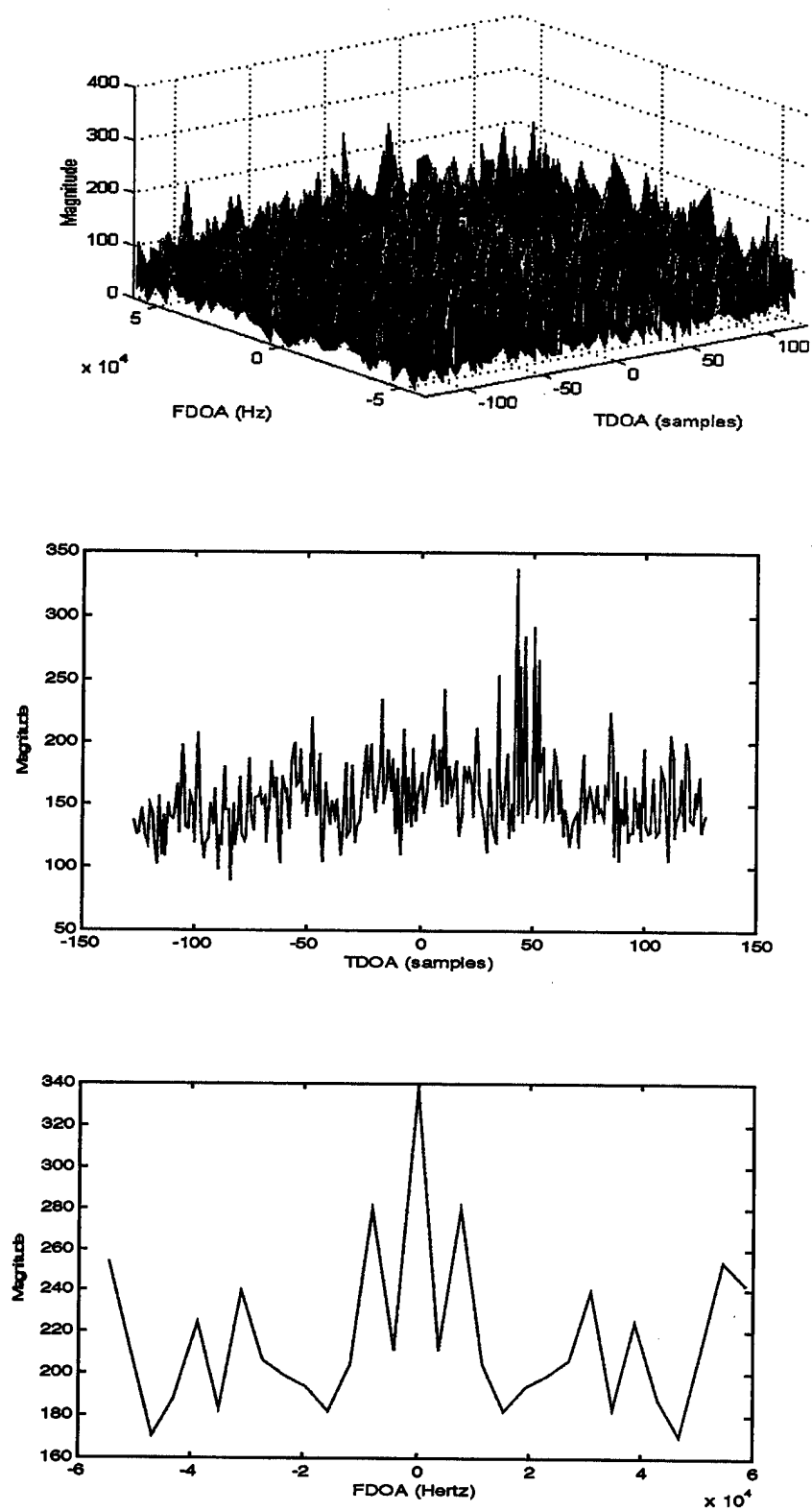
Figure 2-9 – Plots of CAF output, SNR = -10 dB and no Doppler (CAF-2)
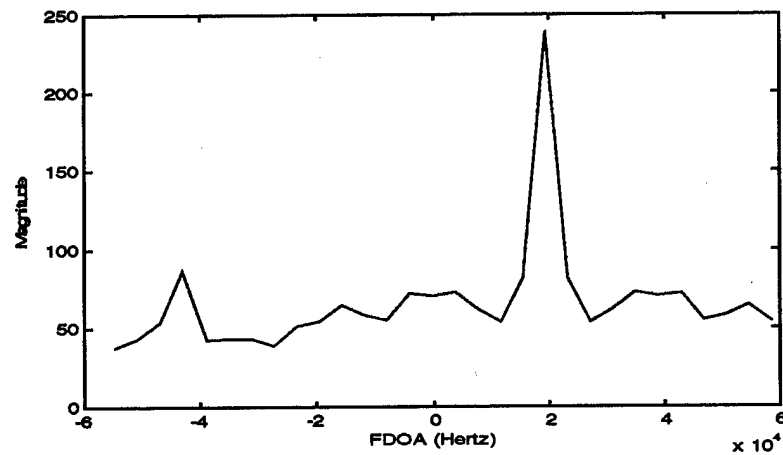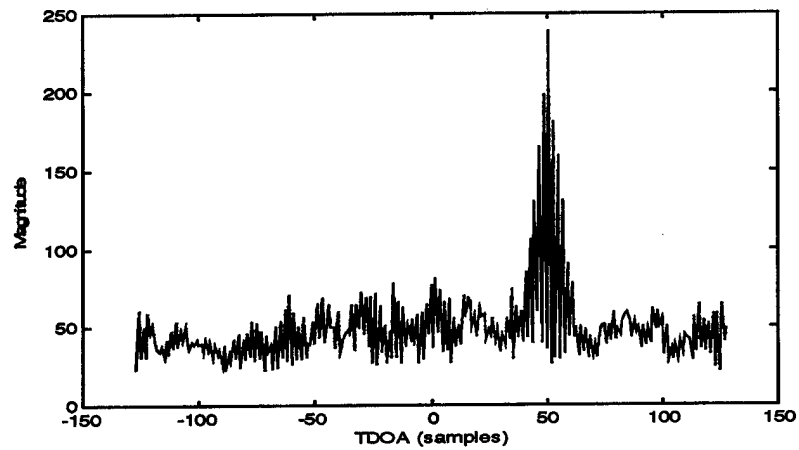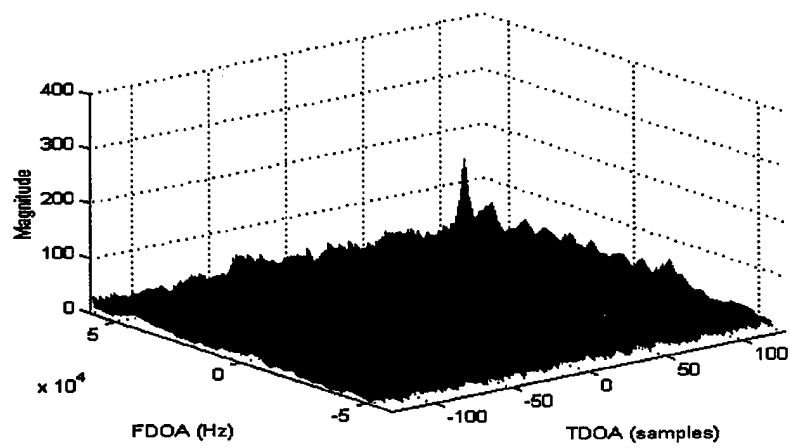
Figure 2-10 – Plot of CAF output, SNR = 3 dB and Doppler = 20 kHz (CAF-3)
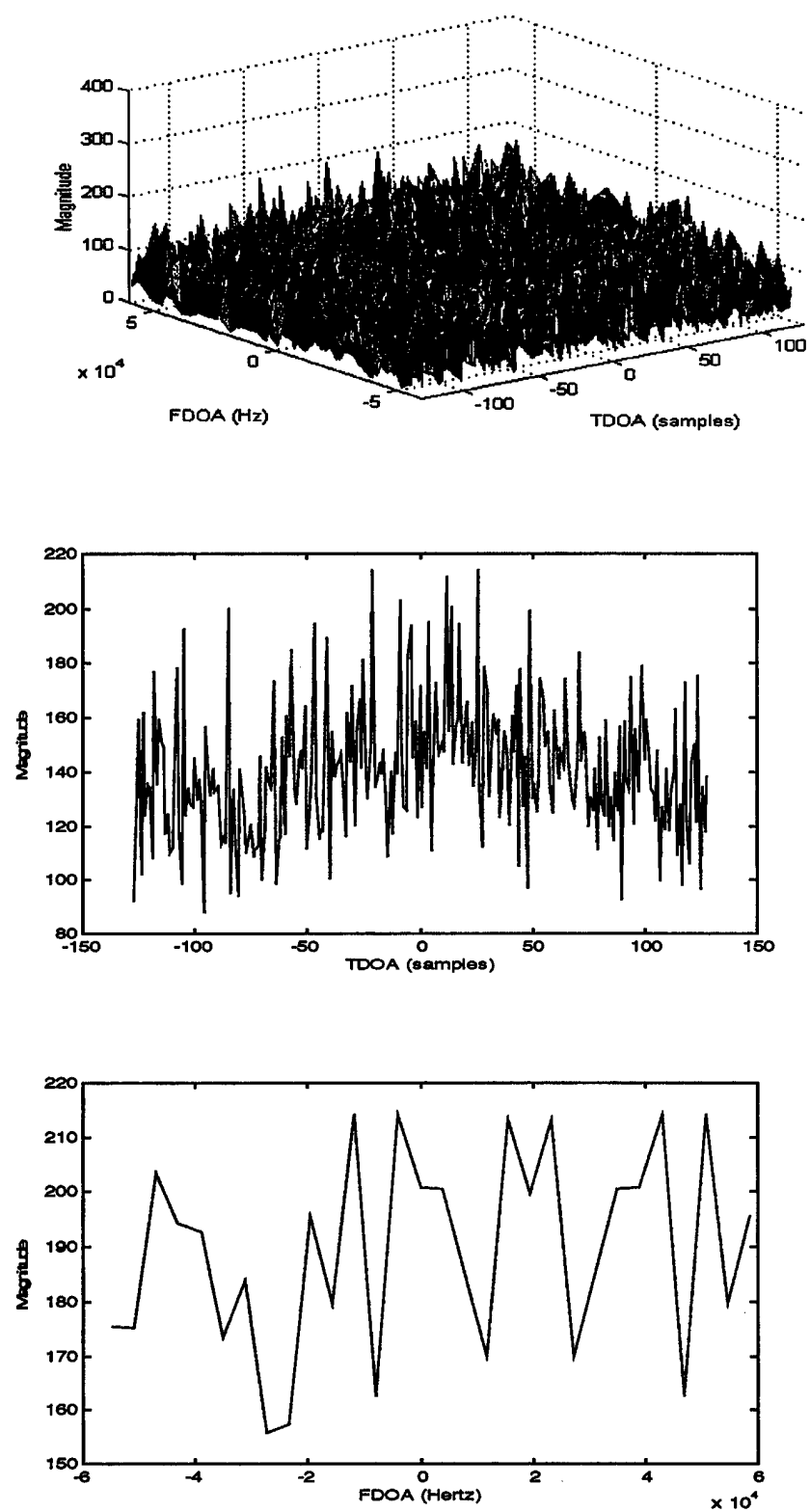
Figure 2-11 – Plots of CAF output, SNR = -10 dB and Doppler = 20 kHz (CAF-4)
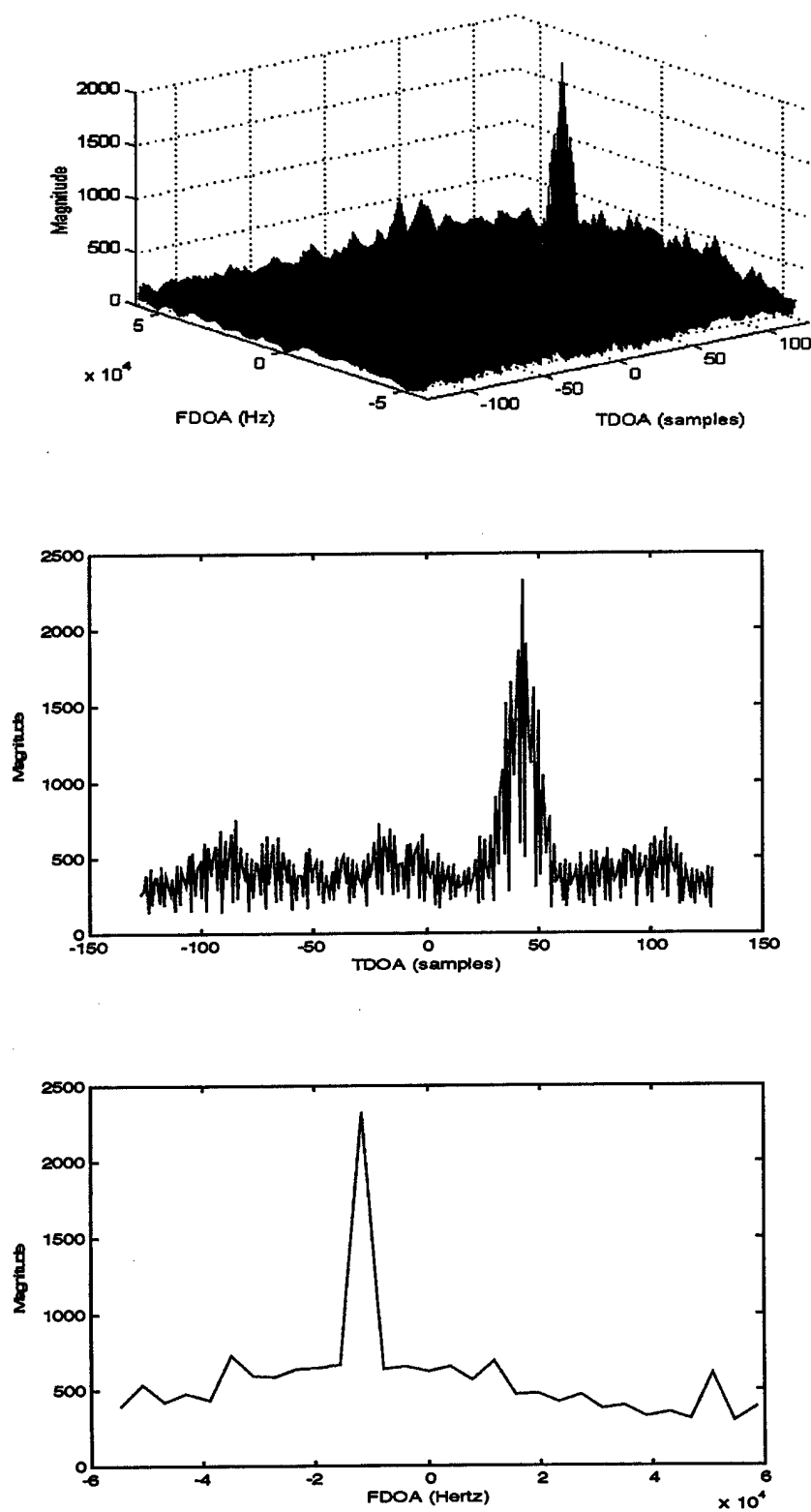
Figure 2-12 – Plots of CAF output, SINR = -13 dB, Doppler = 20 kHz, SNOI (CAF-5)

33

The exploitation of cyclostationarity in these signals makes possible the accurate estimation of signal parameters both in poor SNR situations as well as in the presence of many spectrally, temporally and spatially overlapping SNOI. In the next two chapters first the general theory of cyclostationarity and then past work on its specific application to TDOA and FDOA estimation is documented. In this, the noise tolerant, signal selective characteristics of these techniques will be evident.

III. CYCLOSTATIONARY THEORY

A. BACKGROUND

1. Basic Concept

The concepts of cyclostationarity have been examined in theory for well over two decades. Beginning in the late 1960's, Dr. Lewis Franks of the University of Massachusetts at Amhurst and Dr. William Gardner of the University of California at Davis (UCD) began extensive research in the area of cyclostationary signal processing. Dr. Gardner has since produced a plethora of publications in all aspects of the field. His paper on the general theory of cyclostationary signal processing, published in the April 1991 edition of the IEEE Signal Processing Magazine [13], stands as the key reference for most aspects of the basic theory. As is always the case when one individual has contributed so much to an important engineering development, much of the theory and examples presented here follow Dr. Gardner's work closely.

As previously noted, most modern signal processing techniques associated with communications applications treat SOI(s) as stationary random processes. However, because most manmade signals are generated through some repetitive, periodic process such as the amplitude, frequency or phase modulation of a sinusoidal carrier, the encoding of data or the encryption of a message, their statistics inevitably vary periodically with time. While in many instances, receivers may successfully ignore the underlying periodicity of a manmade signal, often the detection of the signal and the estimation of its parameters is more successfully accomplished by modeling the signal as cyclostationary instead of stationary.

As stated before, a process with statistics that vary periodically with time is termed cyclostationary. A stationary random message such as digital data or analog voice is modulated, clocked or framed by a periodic communications process through some nonlinear system and a cyclostationary signal results.

35

From a strictly mathematical point of view, a cyclostationary signal of order **n** is one that will have additive sine-wave components that result in spectral lines in some n^{th} order nonlinear transformation of the signal. In the case of **n** = 2, a signal is said to be second order cyclostationary if a quadratic transformation produces additive sine-wave components that generate spectral lines. This characteristic may be thought of as akin to a process being considered wide sense stationary or stationary through order 2.

To continue the case of **n** = 2 more specifically, a signal $x(t)$ is cyclostationary with cycle frequency α if and only if some of its delay products $y(t) = x(t)x(t - \tau)$ produce a spectral line at frequency α. If not all cycle frequencies α for which $x(t)$ exhibits cyclostationarity are harmonics of a single fundamental frequency, then $x(t)$ is *polycyclostationary* [14]. Polycyclostationarity implies the existence of more than one periodicity in the statistics of a signal. This in turn implies more than one source of periodicity such as the case when clocked-digital-data phase modulates a sinusoidal carrier in an M-ary phase shift keying scheme [14].

To further illustrate the concept, consider a signal $x(t)$ that contains an additive sine-wave component at frequency α and is of the form

$$x(t) = a\cos(2\alpha t + \theta) \qquad \text{with } \alpha \neq 0 \qquad \text{(3-1)}$$

The Fourier coefficient defined as

$$M_x^\alpha = \left\langle x(t)e^{-j2\pi\alpha t} \right\rangle \qquad \text{(3-2)}$$

where $\langle \bullet \rangle$ denotes time-averaging, will be non-zero. Note that this is of the form of the common representation of the Power Spectral Density (PSD) of $x(t)$ with a spectral line at $+\alpha$ and its mirror at $-\alpha$. In simple terms, $x(t)$ contains first-order periodicity at frequency α given by

$$\left|M_x^\alpha\right|^2 \left[\delta(f - \alpha) + \delta(f + \alpha)\right] \qquad \text{(3-3)}$$

36

Now, considering contributions to $x(t)$ from other sources, the total signal may be represented as

$$x(t) = a\cos(2\pi\alpha t + \theta) + n(t) \qquad (3\text{-}4)$$

where $n(t)$ can be thought of as the random energy outside that of the SOI. If $n(t)$ is strong in comparison to the SOI such that it masks the sine-wave components in $x(t)$ from detection during casual inspection of the waveform, then $x(t)$ can be thought of as possessing hidden periodicity. This hidden periodicity can still be exploited by using signal processing techniques such as the PSD function as noted above. However more powerful cyclostationary signal processing techniques are more sophisticated and can unmask periodicities in signals that are hidden even from common traditional techniques like the PSD function.

2. Philosophies on the Estimation of Parameters

Central to the results presented as part of this work is the theoretical basis for the models used to estimate the parameters of TDOA and FDOA. At the center of that theory are the two different schools of thought related to the estimation of those parameters from time-series. At first glance, the approaches may appear to be philosophical in nature only. However, the two approaches diverge considerably in their application to practical problems. In fact, one approach turns out to be more intuitive than the other and thus more easily applied to processing actual signal data.

Traditionally, the probabilistic theory of statistical inference treats a single time-series as merely one of an infinite number of sample paths in the ensemble of the assumed cyclostationary stochastic-process model. The ensemble is infinite in both numbers of paths (down the ensemble) and in time (across the ensemble). Both these facts, while strictly mathematical creations are necessary in the stochastic process model and as outlined in more detail below, cause difficulties in their application to practical problem

solving. Reliability in parameter estimations made from just a single time-series in this ensemble is hinged upon obtaining the same values for estimates regardless of the sample path chosen. This reliance upon reliability down the ensemble in the presence of merely a single time-series of actual data again causes some practical problems in obtaining empirical evidence of such reliability.

This stochastic-process model approach is empowered by great tradition and familiarity and enjoys the vast historic underpinnings of the extensive study of random phenomena. The principles and underlying elementary mathematics are well known and provide a strong basis for the stochastic-process model approach. In addition, the stochastic-process model fits well with many engineering and science problems where infinite ensembles are perfectly acceptable constructs.

On the other hand, it does not lend itself intuitively, as readily, to the development of techniques for the analysis of much of the actual signal data processed regularly. Its abstractions, like the expectation operator, and reliance upon infinite (in both dimensions) ensembles tends to make the method detached from the practical study of common signal processing problems found in everyday work. For instance, many communications signals are inherently single-sample-path phenomena (even in instances where time, frequency and spatial diversity deliberately appear. Thus, these types of problems derive no practical value from the stochastic process approach that requires assumptions of infinite ensembles when but one sample path is possible in any one experiment without some very high level generalizations that in the end, would remove most of the fidelity. In addition, in the real-time or near real-time signal processing problems of these single-sample-path time-series, there lies a danger in incorrectly assuming the underlying model in the stochastic approach. Often these mistakes prove fatal to the solution in practice. Nonetheless, the stochastic-process model for cyclostationarity offers some advantage in that for theoretical work, the probabilistic method is often easier to manipulate. Thus the development of this approach, while ultimately not used here, is not without merit.

A random process is defined as first order cyclostationary with period T if its probability density function can be characterized by

$$f_x\{x(t)\} = f_x\{x(t+nT)\} \tag{3-5}$$

where t is real and n is an integer. First order periodicity, of course, implies that the mean of the function is periodic with period T

$$E\{x(t) = E\{x(t+nT)\}\} \tag{3-6}$$

Given a periodic mean, the expected value can be represented in terms of a Fourier series with the form

$$E\{x(t)\} = \sum_{l=-\infty}^{\infty} m_l e^{j2\pi\left(\frac{l}{T}\right)t} \tag{3-7}$$

where the Fourier coefficient m_l can be written as

$$m_l = \frac{1}{T} \int_{-T_o/2}^{T_o/2} E\{x(t)\} e^{-j2\pi\left(\frac{l}{T}\right)t} \, dt \tag{3-8}$$

Equation 3-8 represents the cyclic mean and is the manifestation of first-order periodicity in x(t). It can also be considered the *probabilistic* cyclic mean.

A random process is said to be second order cyclostationary if

$$E\{x(t_1)x(t_2)\} = f_x\{x(t_1+nT), x(t_2+nT)\} \tag{3-9}$$

where t_1 and t_2 are real, n is an integer and T is the period. From (3-9) it can be seen that the autocorrelation function of a second-order cyclostationary process contains is periodic with period T and can be written

$$E\{x(t)x(t+\tau)\} = R_{xx}(t+nT,\tau) \tag{3-10}$$

and is considered cyclostationary in the wide-sense. In this instance, the Fourier coefficients derived from this periodicity are

$$R_{xx}^{\alpha} \overset{\Delta}{=} \frac{1}{T} \int_{-T_o/2}^{T_o/2} E\{x(t)x(t+\tau)\}e^{-j2\pi\alpha t}dt \tag{3-11}$$

and are referred to collectively as the *probabilistic* cyclic autocorrelation function.

In addition, the *probabilistic* spectral correlation density (SCD) function is defined simply as the Fourier transform of (3-11)

$$S_{xx}^{\alpha}(f) \overset{\Delta}{=} \Im\{R_{xx}^{\alpha}\} \tag{3-12}$$

Note that a more rigorous approach can be found in Gardner, [14]. The simple derivation above provides a basis for comparison with the non-probabilistic approach preferred for the work contained herein and for which the derivation appears in much greater detail below.

Given the shortcomings of the stochastic approach, an alternative that better addresses the needs of single-sample-path signal processing problems is needed. For this, the time-series approach evolved. Treating the time-series as a fraction of an infinitely long single sample path avoids many of the abstractions associated with forcing the idea of an ensemble from a stochastic process model onto measured signal samples. Reliability of estimates in this approach relies only on the ability to obtain approximately the same values independently of the fraction of time of the infinite time-series used to obtain the estimate. Inherently, this process model applies well to the types of problems described as troublesome for the stochastic-process approach, provided that the time-series approach can account for the necessary statistical inference and decision theory needed to develop

and evaluate signal processing algorithms within this framework. Fortunately this has proven true.

Essentially, rather than assuming an infinite replication of the experiment to form an ensemble, the time-series approach presumes a time-invariance that allows the signal data to be extended in both directions without bound. Then, the process model is directly related to the data in the limit as the data approaches infinity. This naturally leads to the theory of fraction–of-time (FOT) probability where the statistics are related to the fraction of time the data can be expected to behave in a measured manner.

Gardner in [15] proposes that the theory of statistical inference and decision in the FOT model is isomorphic to that of the stochastic-process model. To that end, the goal of statistical inference and decision theory within the FOT framework remains consistent with that of the stochastic-process: to draw conclusions with regard to the infinitely long time-series from parameters measured from finite-length observations (a theoretical subset of the infinite series). Within this framework it is possible to calculate bias, variance and other measures of reliability and therefore pursue optimizations as well. Optimization of an algorithm to estimate both time and frequency differences of arrival is the core of the research presented here and thus relies heavily upon the statistical inference and decision theory developed in [7], [14] and [15] for its foundation.

To that end, the remaining sections in this Chapter more rigorously develop the cyclostationary theory within the FOT model approach. In addition, to aid in comparison to the GCC and CAF and prepare for specific cyclostationary TDOA and FDOA algorithms, digital implementation issues for cyclostationary calculations follow. This sets the stage for Chapter IV, a survey of existing cyclostationary TDOA and FDOA algorithms.

B. CYCLIC CORRELATION FUNCTIONS

1. Continuous-Time Cyclic Correlation Functions

Traditionally, a common second order, time-domain statistic used in signal processing is the autocorrelation function given by the quadratic transformation

$$R_{xx}(\tau) = \langle x(t)x(t-\tau) \rangle \qquad (3\text{-}13)$$

In the case of a signal that can be modeled as cyclostationary, this transform will produce spectral lines at non-zero frequencies α such that

$$M_y^\alpha = \langle y(t)e^{-j2\pi\alpha t} \rangle \neq 0 \qquad (3\text{-}14)$$

where

$$y(t) = x(t)x(t-\tau) \qquad (3\text{-}15)$$

This signal $x(t)$ as noted above contains second order periodicity manifested in the PSD of the delay product given in equation (3-15) above. Transforming (3-15) into a symmetric delay product and accommodating complex signals as well gives

$$y(t) = x\left(t+\frac{\tau}{2}\right)x^*\left(t-\frac{\tau}{2}\right) \qquad (3\text{-}16)$$

which forms the basis for the fundamental second order cyclic moment known as the FOT continuous-time (CT) cyclic autocorrelation function:

$$R_{xx}^\alpha(\tau) \overset{\Delta}{=} \left\langle x\left(t+\frac{\tau}{2}\right)x^*\left(t-\frac{\tau}{2}\right)e^{-j2\pi\alpha t} \right\rangle \qquad (3\text{-}17)$$

Of note, the CT cyclic autocorrelation function (drop the FOT as all further development remains within that framework) assumes the form of the Fourier coefficients of the additive sine-wave components produced by the periodicity of the delay product in (3-16). Also note that (3-17) is the time-average equivalent of (3-7) from the probabilistic approach.

The CT cyclic cross-correlation function is a natural extension of (3-17) to the case of two signals. The simple substitution of $y^*(t)$ for $x^*(t)$ yields

$$R_{xy}^{\alpha}(\tau) \stackrel{\Delta}{=} \left\langle x\left(t+\frac{\tau}{2}\right) y^*\left(t-\frac{\tau}{2}\right) e^{-j2\pi\alpha t} \right\rangle \qquad (3\text{-}18)$$

which serves as the definition for the cyclic cross-correlation function.

Another interpretation of (3-17) is as the traditional stationary autocorrelation function multiplied by a kernel $e^{-j2\pi\alpha t}$ that produces spectral lines at frequencies where the stationary autocorrelation function contains additive sine-wave components indicative of its periodicity. Consequently, for either interpretation, at $\alpha = 0$, the cyclic autocorrelation function (drop the CT as the argument apples equally to either the continuous or discrete time versions – see below) reduces to the traditional autocorrelation function.

A final interpretation of the cyclic autocorrelation function can be seen by defining first

$$u(t) = x(t)e^{-j\pi\alpha t} \qquad (3\text{-}19)$$

and

$$v(t) = x(t)e^{+j\pi\alpha t} \qquad (3\text{-}20)$$

so that $u(t)$ and $v(t)$ are frequency shifted versions of x(t). Now $R_x^{\alpha}(\tau)$ can be written

$$R_x^\alpha(\tau) = \left\langle u\left(t+\frac{\tau}{2}\right)v^*\left(t+\frac{\tau}{2}\right)\right\rangle = R_{uv}(\tau) \qquad (3\text{-}21)$$

which is the cross-correlation of the two versions of $x(t)$ shifted up and down by frequency $\alpha/2$. In other words, the cyclic autocorrelation function may be viewed as the correlation in the time domain between two values of $x(t)$ separated in frequency by α.

Consider as an example, a generalized Binary Phase Shift Keyed (BPSK) signal, not unlike the specific signal used throughout Chapter II,

$$s(t) = A_c d(t)\cos(2\pi f_c t + \phi) \qquad (3\text{-}22)$$

where $d(t)$ is the binary modulating wave form consisting of positive and negative rectangular pulses given by

$$d(t) = \sum_{n=-\infty}^{\infty} d_n q(t - t_o - nT_b) \qquad (3\text{-}23)$$

Approximated as a random binary wave, it contains no first order periodicity and thus no spectral lines in its PSD. Consequently, the PSD of the BPSK signal $s(t)$ is a scaled sinc squared function and will also contain no spectral lines, as is evident its expression

$$S_{\text{BPSK}}(f) = A_c^2 T_b\left(\frac{\sin \pi f_c T_b}{\pi f_c T}\right)^2 \qquad (3\text{-}24)$$

Multiplying the conventional autocorrelation function by the cyclic kernel $e^{-j2\pi\alpha t}$, the cyclic autocorrelation function follows as

$$R_s^\alpha = \frac{1}{2T_b} r_q^\alpha(\tau) \cos(2\pi f_c \tau) e^{-j2\pi\alpha\tau_o}$$

$$+ \frac{1}{4T_b} \left[r_q^{\alpha+2f_c}(\tau) e^{-j2\pi[\alpha+2f_c]\tau_o} + r_q^{\alpha-2f_c}(\tau) e^{-j2\pi[\alpha-2f_c]\tau_o} \right] \tag{3-25}$$

where

$$r_q^\alpha(\tau) = \int_{-\infty}^{\infty} q\left(t + \frac{\tau}{2}\right) q\left(t - \frac{\tau}{2}\right) e^{-j2\pi\alpha t} dt \tag{3-26}$$

Equation (3-25) clearly shows additive sine-wave components at $\alpha = \pm 2 f_c \pm R_b$ and $\alpha = \pm R_b$[16]. Thus, the quadratic transform that is the cyclic autocorrelation function unmasks hidden periodicity in this simple BPSK signal and proves it polycyclostationary in the process.

2.   Discrete-Time Cyclic Correlation Functions

As Gardner notes in [14], the concepts presented above apply transparently to either the CT or discrete-time (DT) case. Instead of the CT signal representations and the CT-averaging operation

$$\langle \bullet \rangle \overset{\Delta}{=} \lim_{Z \to \infty} \frac{1}{2Z} \int_{-Z}^{Z} (\bullet)\, dt \tag{3-27}$$

use DT representations of the signals and the DT counterpart to (3-27)

$$\langle \bullet \rangle \overset{\Delta}{=} \lim_{Z \to \infty} \frac{1}{2Z+1} \sum_{t=-Z}^{Z} (\bullet) \tag{3-28}$$

In this manner it is possible to produce the DT cyclic correlation functions. For the general case of a complex signal, the DT cyclic autocorrelation function

45

$$R_{xx}^{\alpha}(\tau) \overset{\Delta}{=} \lim_{Z \to \infty} \frac{1}{2Z+1} \sum_{t=-Z}^{Z} x\left(t+\frac{\tau}{2}\right) x^*\left(t-\frac{\tau}{2}\right) e^{-j2\pi\alpha t} \tag{3-29}$$

which follows directly from (3-17) using (3-28). Consequently, the DT cyclic cross-correlation function

$$R_{xy}^{\alpha}(\tau) \overset{\Delta}{=} \lim_{Z \to \infty} \frac{1}{2Z+1} \sum_{t=-Z}^{Z} x\left(t+\frac{\tau}{2}\right) y^*\left(t-\frac{\tau}{2}\right) e^{-j2\pi\alpha t} \tag{3-30}$$

is the result of a simple substitution of $y^*(t)$ for $x^*(t)$.

C.   SPECTRAL CORRELATION DENSITY FUNCTIONS

1.   Continuous-Time Spectral Correlation Density Functions

The frequency domain equivalent for the CT cyclic autocorrelation function is the CT spectral correlation density (SCD) function. Gardner takes two approaches in [14] to define the SCD. In the first, he points out that the SCD is simply an extension of the process by which the power spectral density (PSD) is estimated. This process involves passing the SOI through a bank of bandpass filters, measuring the power in each band at the output of the filters. These filters constitute the traditional bins associated with spectrum analysis. The result of the process is the isolation of signal power in specific frequency bins. This situation that may be summarized mathematically as

$$S(f) \overset{\Delta}{=} \lim_{B \to 0} \frac{1}{B} \left\langle \left| h_B^f(t) \otimes x(t) \right|^2 \right\rangle \tag{3-31}$$

46

where $h_B^f(t)$ is the impulse response of the one-sided bandpass filter with center frequency f and bandwidth B.

The transition to the SCD definition is a simple matter of frequency shifting the SOI up and down by $\alpha/2$, channelizing and correlating. The frequency shifting operation is the same that occurs in the final interpretation of the cyclic correlation function and results in $u(t)$ and $v(t)$ identical to (3-18) and (3-19). Gardner in [14] defines one channel of the SCD estimation process as

$$S_x^\alpha(f) \overset{\Delta}{=} \lim_{B \to 0} \frac{1}{B} \left\langle \left[h_B^f(t) \otimes u(t) \right] \left[h_B^f(t) \otimes v(t) \right]^* \right\rangle \qquad (3\text{-}32)$$

the time-correlation of frequency shifted, channelized segments of the SOI.

As a second definition, note that is can be shown that the SCD is the Fourier Transform of the cyclic correlation function [9]. Consequently the SCD follows directly from (3-17) and has the form

$$S_X^\alpha(f) = \int_{-\infty}^{\infty} R_x^\alpha(\tau) e^{-j2\pi f\tau} d\tau \qquad (3\text{-}33)$$

More commonly used in cyclostationary signal processing, the CT SCD reduces to the conventional PSD at $\alpha = 0$ just as the CT cyclic autocorrelation function reduced to the conventional autocorrelation function at $\alpha = 0$. Note that (3-33) represents the time-average equivalent of (3-8), the probabilistic spectral correlation function.

In addition, the CT spectral cross-correlation function follows directly from (3-32) and (3-33) with the appropriate substitution. It has the forms

$$S_{xy}^\alpha(f) \overset{\Delta}{=} \lim_{B \to 0} \frac{1}{B} \left\langle \left[h_B^f(t) \otimes u(t) \right] \left[h_B^f(t) \otimes v(t) \right]^* \right\rangle \qquad (3\text{-}34)$$

$$S_{xy}^\alpha(f) = \int_{-\infty}^{\infty} R_{xy}^\alpha(\tau) e^{-j2\pi f\tau} d\tau \qquad (3\text{-}35)$$

47

where $v(t)$ now becomes a frequency shifted version of $y(t)$ in (3-34) and $R_{xy}^\alpha(\tau)$ replaces $R_x^\alpha(\tau)$ in (3-33) to obtain (3-35).

Continuing the BPSK example from above, the SCD can be found directly from (3-33). It has the form

$$S_x^\alpha(f) = \frac{1}{4T_b}\left[Q\left(f+f_o+\frac{\alpha}{2}\right)Q^*\left(f+f_o-\frac{\alpha}{2}\right) \right.$$
$$\left. + Q\left(f-f_o+\frac{\alpha}{2}\right)Q^*\left(f-f_o-\frac{\alpha}{2}\right)\right]e^{-j2\pi\alpha t_o}$$

for $\alpha = n/T_b$ and $\quad$ (3-36)

$$S_x^\alpha(f) = \frac{1}{4T_b}\left[Q\left(f+f_o+\frac{\alpha}{2}\right)Q^*\left(f-f_o-\frac{\alpha}{2}\right)e^{-j2\pi[\alpha+2f_c]t_o} \right.$$
$$\left. + Q\left(f+f_o+\frac{\alpha}{2}\right)Q^*\left(f-f_o-\frac{\alpha}{2}\right)e^{-j2\pi[\alpha-2f_c]t_o}\right]$$

for $\alpha = \pm 2f_c \pm n/T_b$ with $Q(f)$ being the Fourier transform of the keying envelope $q(t)$ [14].

The SCD is so named as it is in fact a correlation of the SOI in the frequency domain. The SCD at frequency f_o and cyclic frequency α_o is merely the correlation of two values of the signal in the frequency domain separated in frequency by α_o and centered at frequency f_o. Figure 3-1 shows this process concept graphically.

The SCD is plotted on what is called the bi-frequency plane. The plane is defined along one axis as spectral frequency f and along the opposing axis as cyclic frequency α.
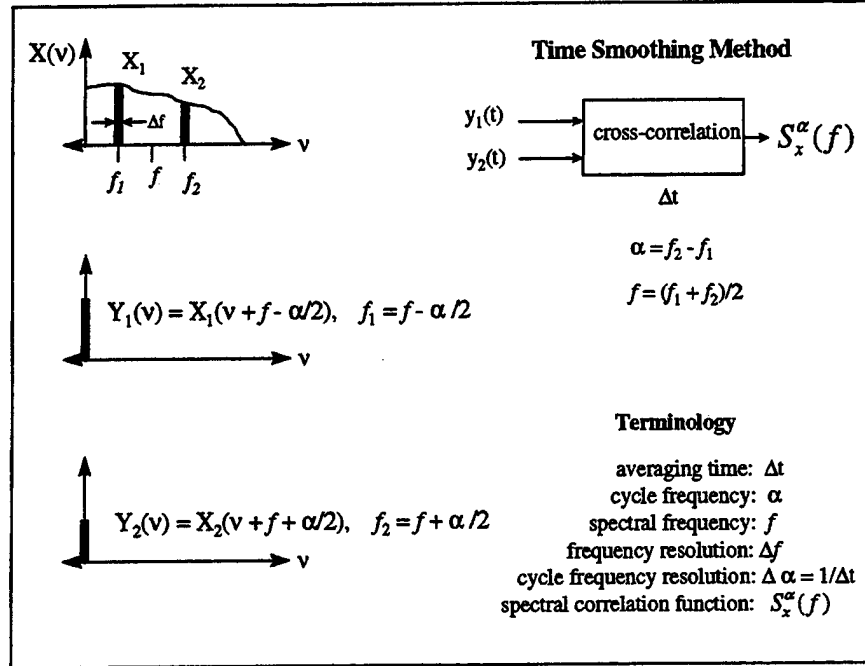
Figure 3-1 - Spectral Correlation Function illustrated, from [17]

Figure 3-2 illustrates this point. The magnitude of the SCD corresponds to a height above the bi-frequency plane and is often plotted in that fashion. Because α corresponds to the separation distance between correlated values in the frequency domain and the values for spectral frequency f naturally range from $-f_s/2$ to $f_s/2$, the values for α range from $-f_s$ to f_s.

2. Discrete-Time Spectral Correlation Functions

As is the case with the cyclic correlation functions, the theory presented above for the CT SCD functions can be applied equally well to the DT SCD functions. The DT SCD functions take the form

$$S_x^\alpha(f) \stackrel{\Delta}{=} \sum_{\tau=-\infty}^{\infty} R_x^\alpha(\tau)e^{-j2\pi f\tau} \qquad (3\text{-}37)$$

and

49

$$S_{xy}^{\alpha}(f) \stackrel{\Delta}{=} \sum_{\tau=-\infty}^{\infty} R_{xy}^{\alpha}(\tau)e^{-j2\pi f\tau} \tag{3-38}$$
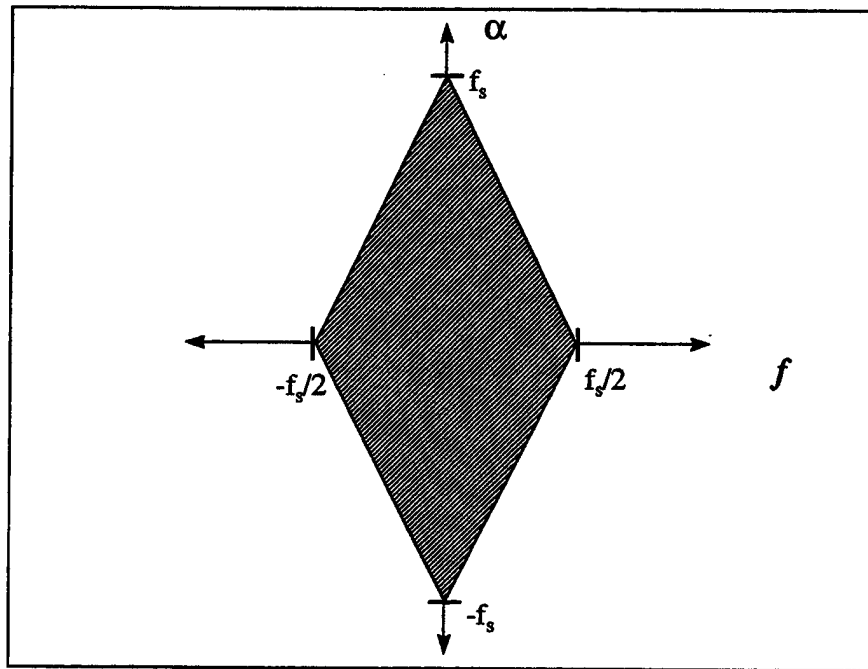

Figure 3-2 - Bi-frequency plane

D.   DIGITAL COMPUTATION OF THE SCD

1.   Introduction

The SCD computation can be computationally complex and demanding on any processor. For that reason, the development of computationally efficient algorithms is crucial to the practical application of the theory. These computational algorithms fall into either frequency-smoothing or time-smoothing categories. Roberts, Brown and Loomis in

50

[20] noted that the frequency-smoothing algorithms were most efficient when estimating the cyclic spectrum for few values of α or when calculating the cyclic spectrum for small time-frequency resolution.

The time-smoothing algorithms prove more efficient for the general case of calculating the entire cyclic spectrum of two complex signals. Specifically, two algorithms were developed in [20] with an exhaustive evaluation of the complexity of each. The Fast Fourier Transform Accumulation Method (FAM) and the Strip Spectral Correlation Analyzer (SSCA) both simplify and thereby accelerate the computation of the SCD. Because cyclostationary TDOA/FDOA algorithms typically require some a priori knowledge of the parameters of the signal of interest and calculating the SCF of a data set directly from (3-37) is prohibitively expensive in terms of computations required, digital techniques that approximate (3-37) closely without the computational burden are a necessity. Because of this, FAM and SSCA play an important role in this work, providing one method of measuring cycle frequencies in the received data sets without extensive computation time. In [20], Roberts, Brown and Loomis concluded that the SSCA was in fact the most efficient of the two methods for calculating the entire bi-frequency plane and thus it is used extensively in the research here. For that reason and as an excellent illustration of the compromise between performance and computational efficiency, it is presented in more detail below.

2. Strip Spectral Correlation Analyzer

Directly from its definition, (3-37), the SCD can be computed using a traditional time-smoothing approach as depicted in Figure 3-3. While this approach provides the most accurate estimate of the SCD, it proves prohibitively time consuming and inappropriate for most applications [18].

The SSCA algorithm, a modification of this standard time-smoothing method, provides an excellent combination of accurate estimation of cycle frequencies of interest and computational efficiency [18]. By eliminating one of the band-pass filters in Figure 3-

6 and using a Fourier transformer at the input and output, SSCA computes the SCD along diagonal strips of the bi-frequency plane as depicted in Figure 3-4.

While the SSCA does manage to compute the SCD in the most efficient manner developed thus far, it makes some compromises. The output SNR suffers slightly as a result of the efficiency that is gained by the elimination of the filter and the use of the Fourier transform. In addition, the strips cause the computation of the SCD to be off-center with respect to the alpha axis, thus distorting the graphical depiction of the SCD. However, the computational savings gained far outweigh the minor degradation in signal power to noise power at the output of the analyzer and the inconvenience of the graphical distortion.

Figure 3-5 illustrates the SSCA architecture. The input filter consists of a sliding, Hamming-windowed, coarse FFT of length N'. Each of these N' length segments is essentially the output of a band-pass filter with a bandwidth of $1/N'$. This band-pass output is then downconverted to baseband by a complex exponential multiplication. These products are termed the complex demodulates of the input signal and appear in
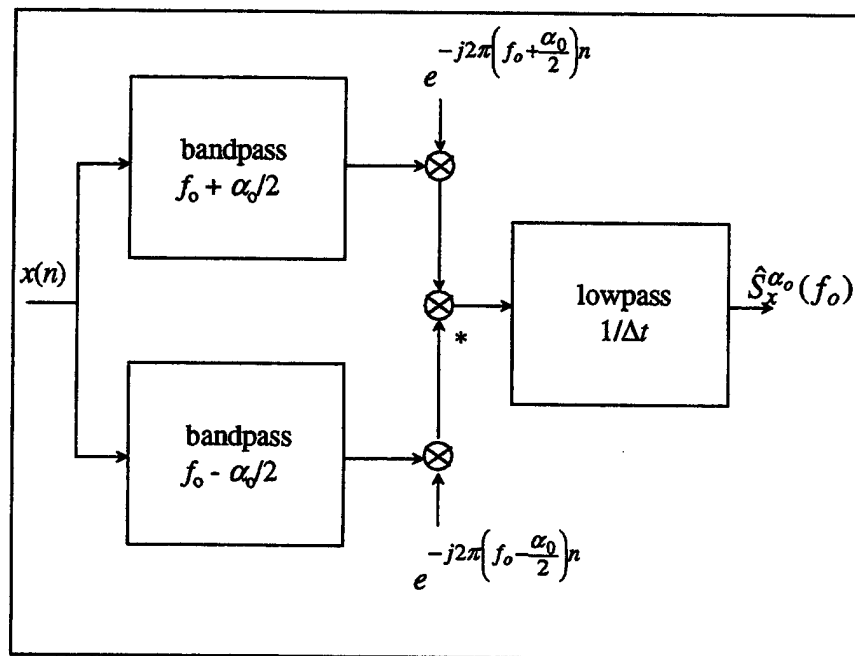

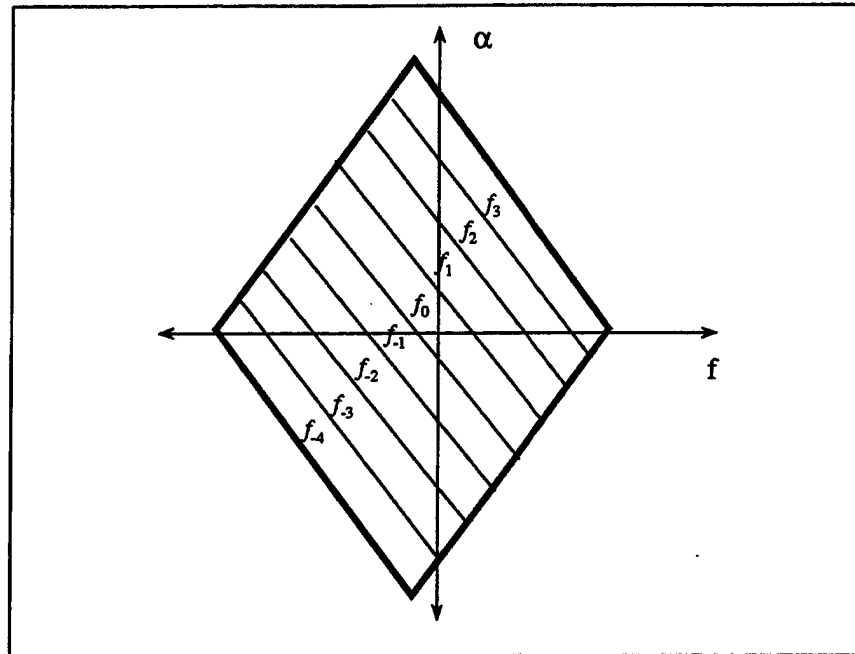Figure 3-3 - Time-smoothing spectral correlation analyzer [19]

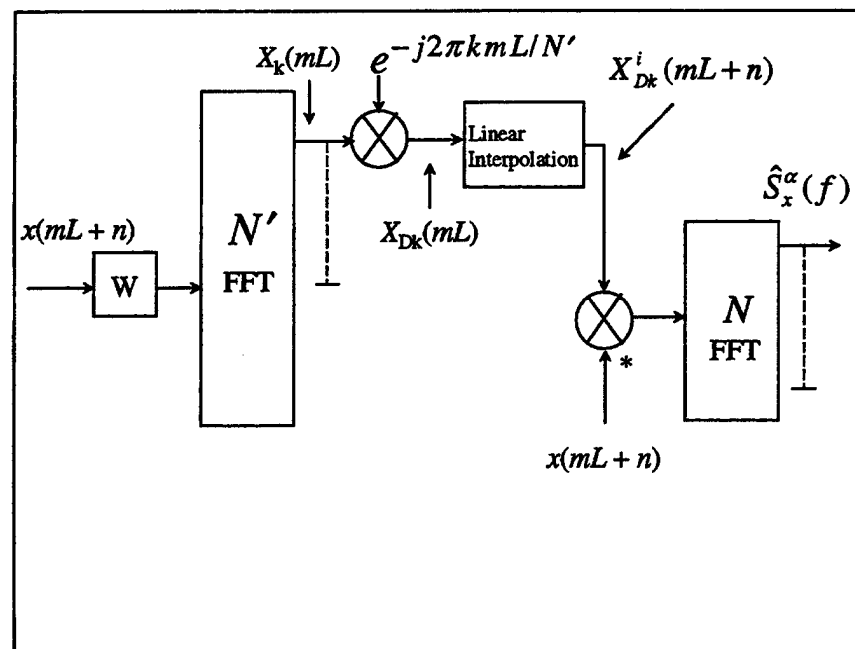Figure 3-4 - SSCA computation in the bi-frequency plane, $N' = 8$, from [19]

Figure 3-5 - SSCA architecture, from [19]

greater detail in Figure 3-6. As can be seen, the process of windowing and sliding at the input filter essentially decimates the input sequence. Brown and Loomis found that the most appropriate value for the decimation factor or subsampling parameter L was $N'/4$ [19].
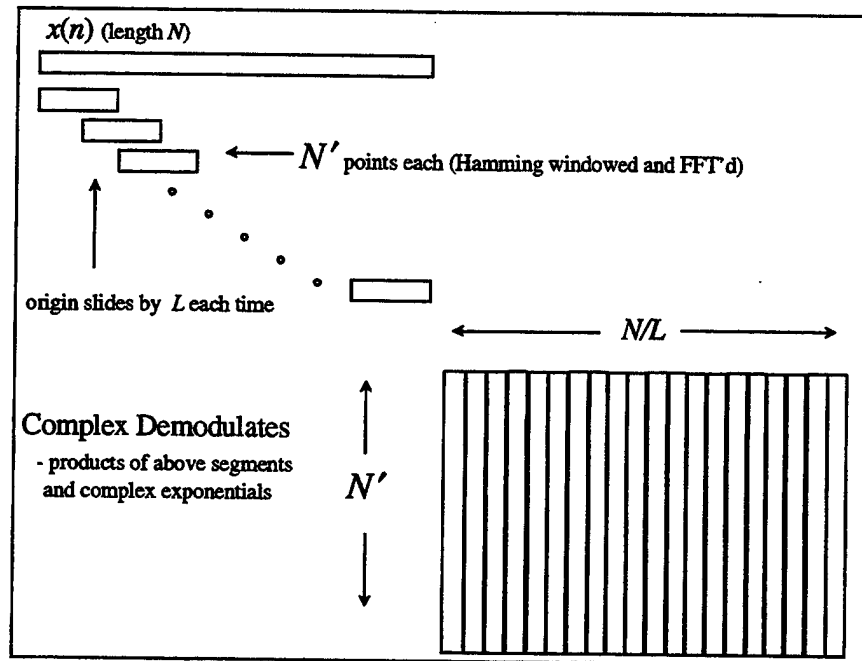

Figure 3-6 - Detail of the computation of complex demodulates

Because these complex demodulates are multiplied by the original sequence before the final FFT, they must be interpolated to the original sampling rate. In [19] and [20] Loomis and Brown use a simple hold operation. Linear interpolation induces less high frequency error and adds little in computational complexity. It is used here in place of the first order sample and hold interpolation. Finally, the interpolated complex demodulates and the original sequence are complex multiplied and the product Fourier transformed by a full length, unwindowed FFT. The relationship of the output to the bi-frequency plane appears in Figure 3-7. Each row of output represents one of the N' diagonal strips in the bi-frequency plane as depicted in Figure 3-4. Each column represents the values of the

SCD along the diagonal lines. The resolution along lines of f is coarse at $1/N'$ as a byproduct of the computational savings. However, the resolution in α, at $1/N$, is much higher which accommodates the characterization nicely.
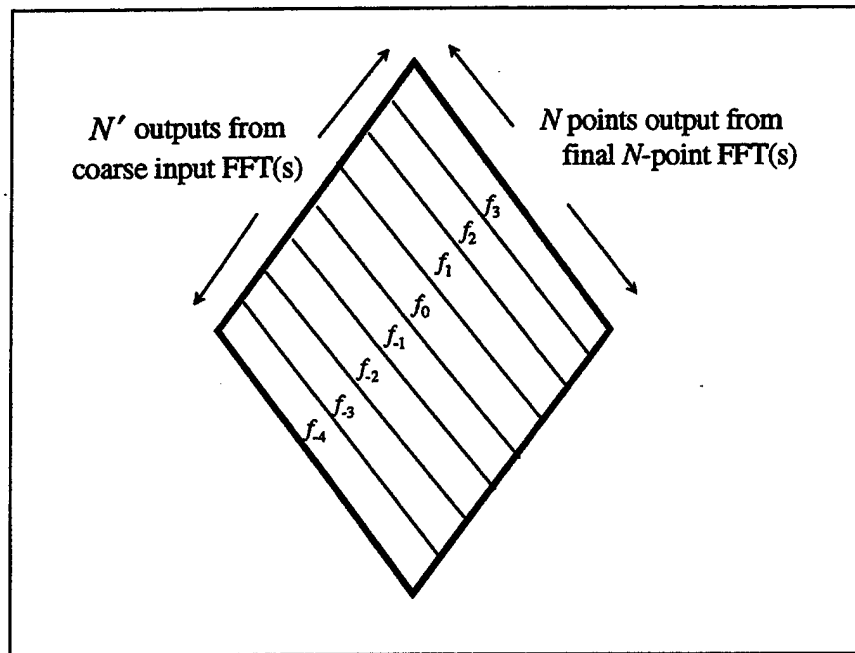

Figure 3-7 - Block form of SSCA output

Given that the majority of operations in the SSCA can be implemented as vector or matrix operations, its implementation in any vector processing language such as Matlab® is fairly simple. The psuedocode for the algorithm appears in Figure 3-8. The output of the SSCA when implemented is a matrix with N' rows corresponding to the N' diagonal strips of the computation and columns corresponding to the SCD along the respective strips. Referring again to Figures 3-4 and 3-6, these strips are not computed along lines of f and α and must therefore be transposed along those lines before plotting.

The transformation involves applying the relationship between the diagonal strip subscript k, the frequency f and the cyclic frequency α. Those relationships from [20] are

$$f_k = k\left(\frac{f_s}{N'}\right), \qquad \frac{-N'}{2} \leq k \leq \frac{N'}{2} - 1 \tag{3-39}$$

$$\alpha = 2f_k - 2f \tag{3-40}$$

While cyclostationary signal processing techniques provide powerful tools for use in poor signal environments, those tools are used at the expense of computational complexity. The SSCA strives to reduce that complexity without serious degradation in the SNR of the output. In the next chapter, specific applications of cyclostationary signal-selectivity to the estimation of TDOA are surveyed. In this section, it will become even more clear the value that computationally efficient digital implementations have in the practical employment of some of the cyclostationary techniques.

```
/* Compute Complex Demodulates of x */
Do p := 0 to P-1
  Compute xT(pL,fk) = FFT[a(r)x(pL+r)]
  Do k := -N'/2 to N'/2-1
    Compute XT(pL, fk) = xT(pL, fk)exp{-j2πpLk/N'}
  end
end
/* Interpolate XT(pL, fk) */
Compute XT(pL,fk)   ⇒  X̃T(n, fk)

/* Compute and Smooth Product Waveforms
Do k := -N'/2 to N'/2-1
  Compute Sxyʸᶠᵏ(n, fk) = y*(n)X̃T(n, fk)
  Compute Sxyʸᵅ⁰(n, fk)Δt = FFT{g(n)Sxyʸᶠᵏ(n, fk)}
end
```

Figure 3-8 - Psuedocode for SSCA computation, from [19]

56

IV. CYCLOSTATIONARY TDOA AND FDOA ESTIMATION

A. CYCLOSTATIONARY TIME DIFFERENCE OF ARRIVAL

1. Cyclostationary TDOA Signal Model

The signal model used to develop cyclostationary TDOA algorithms is Model B and identical to that presented in Chapter II. Recall the signals received at two spatially separated observers can be given by (2-1) and (2-2) and are repeated below for clarity

$$x(t) = s(t) + n_1(t) \qquad (4\text{-}1)$$

and

$$y(t) = A_r \cdot s(t - D) + n_2(t) \qquad (4\text{-}2)$$

The difference between the two models lies in the temporal and spectral relationships between $s(t)$, $n_1(t)$ and $n_2(t)$. In Chapter II, $n_1(t)$ and $n_2(t)$ were assumed to have no components that temporally and spectrally overlap the SOI, $s(t)$. In the cyclostationary TDOA signal model, $n_1(t)$ and $n_2(t)$ represent all SNOI(s) and noise present at the respective observers. They may or may not contain co-channel interferers in reality, however for purposes of this work, they are assumed to contain interference that in fact spectrally overlaps the SOI.

Given this model, the cyclic auto and cross-correlation functions in general can be written as

$$R_x^\alpha(\tau) = R_s^\alpha(\tau) + R_{n_1}^\alpha(\tau) \qquad (4\text{-}3)$$

$$R_y^\alpha(\tau) = |A_r|^2 R_s^\alpha(\tau) e^{-j2\pi\alpha D} + R_{n_2}^\alpha(\tau) \qquad (4\text{-}4)$$

$$R_{yx}^{\alpha}(\tau) = A_r R_s^{\alpha}(\tau - \text{D})e^{-j\pi\alpha\text{D}} + R_{n_1 n_2}^{\alpha}(\tau) \qquad (4\text{-}5)$$

just as (2-3) - (2-5) represented the conventional auto and cross-correlation functions. In addition, as with (2-6) - (2-8), the spectral correlation functions are

$$S_x^{\alpha}(f) = S_s^{\alpha}(f) + S_{n_1}^{\alpha}(f) \qquad (4\text{-}6)$$

$$S_y^{\alpha}(f) = \left|A_r\right|^2 S_s^{\alpha}(f)e^{-j2\pi\alpha\text{D}} + S_{n_2}^{\alpha}(f) \qquad (4\text{-}7)$$

$$S_{yx}^{\alpha}(f) = A_r S_s^{\alpha}(f)e^{-j2\pi(f+\alpha/2)\text{D}} + S_{n_1 n_2}^{\alpha}(f) \qquad (4\text{-}8)$$

The cross-SCD(s) for the SOI and the noise are omitted because they are identically zero with the assumption that the SOI and the noise are independent. This assumption is not made for any SNOI contained in the noise terms. They are assumed to be correlated and thus the cross-SCD for the noise terms at each receiver appears in (4-8).

Though (4-6) - (4-8) contain the TDOA, D, this parameter is now masked by the spectrally overlapping components of $n_1(t)$ and $n_2(t)$. Thus, any attempt to estimate D with traditional methods that compute the above equations at $\alpha = 0$, like those illustrated in Chapter II, would result in a corrupted value. However, if $s(t)$ contains some cycle frequency, α_o, for which the cyclic cross-correlation between $n_1(t)$ and $n_2(t)$ is zero, then cyclostationary techniques can determine the TDOA, D of the SOI, $s(t)$ even in the presence of strong contributions from $n_1(t)$ and $n_2(t)$ that would otherwise corrupt the estimate. Essentially this eliminates the SNOI(s), resulting in (4-6), (4-7) and (4-8) being rewritten for the use of α_o as

$$S_x^{\alpha_o}(f) = S_s^{\alpha_o}(f) \qquad (4\text{-}9)$$

$$S_y^{\alpha_o}(f) = \left|A_r\right|^2 S_s^{\alpha_o}(f)e^{-j2\pi\alpha_o\text{D}} \qquad (4\text{-}10)$$

$$S_{yx}^{\alpha_o}(f) = A_r S_s^{\alpha_o}(f)e^{-j2\pi(f+\alpha_o/2)D} \qquad (4\text{-}11)$$

Thus a reliable estimate of D is possible even in highly corrupt environments provided a unique α_o exists for the SOI.

2. Current Cyclostationary TDOA Determination Algorithms

In [16], Gardner and Chen outlined no less than seven different cyclostationary TDOA algorithms. The algorithms range in complexity from simple cyclic modifications to the GCC to more complicated minimum least squares approaches, each with its strengths and weaknesses. The three algorithms of this group that most thoroughly represent the range of techniques developed in [16] are described below.

The Cyclic Cross-Correlation (CCC) method is the result of the simple substitution of the cyclic cross-correlation function for the limit auto-correlation function in the CC TDOA method from above, yielding the following relation from (49) in [16]

$$a_\alpha(\tau) \stackrel{\Delta}{=} \left|R_{yx}^\alpha(\tau)\right| = |A|\left|R_s^\alpha(\tau-D)\right| \qquad (4\text{-}12)$$

Note that the inclusion of the cyclic cross-correlation function in the solution injects the inherent signal selectivity of cyclostationary signal processing into the CC-like TDOA determination, significantly mitigating the nagging problem of co-channel, co-temporal interference outlined with the CC and CAF above. Gardner and Chen found that although the peak of $\left|R_s^\alpha(u)\right|$ does not occur at $u = 0$ for all signals, since it is an even function of u, in those situations lacking a single peak at $u = 0$, usually a pair of peaks straddle $u = 0$ thereby identifying the TDOA unambiguously [16].

Gardner and Chen further point out that the performance of the CCC can be significantly improved using cyclic versions of the same methods employed in the

construction of the GCC. The direct cyclic counterpart of the GCC in (2-15) can be written as the estimate $\hat{b}_\alpha(\tau)$ of the ideal measurement

$$b_\alpha(\tau) \overset{\Delta}{=} \left| \int_{\|f|-f_\alpha|<B_\alpha/2} \frac{S_{yx}^\alpha(f)}{S_x^\alpha(f)} e^{i2\pi f\tau} df \right| \tag{4-13}$$

which is (56a) in [16] and always produces a peak at the TDOA value. Because it is essentially the ratio of cyclic cross spectrum to the cyclic auto-spectrum at a selected cycle frequency, this method is known as the Spectral Correlation Ratio (SPECCORR).

A significant difference between this cyclic version of the GCC and the traditional GCC is the phase content of the weighting functions used in SPECCORR. The weighting functions seen in Table 2-1 above merely emphasize or de-emphasize certain spectral bands essentially operating effectively only at $\alpha = 0$.. The weighting functions in SPECCORR also contribute to the band selection along that $\alpha = 0$ line in the cyclic plane. However, the phase content contained in the complex values of these cyclic weighting functions also serve to pre-filter further in the cyclic plane to eliminate interference and emphasize features at cycle frequencies other than $\alpha = 0$. Herein lies the performance gain.

The third estimator in [16], Spectral Coherence Alignment (SPECCOA) was developed and presented as the solution to an ad hoc minimum least squares (MLS) approach. Because it has proven an excellent performer in a broad range of environments, more emphasis will be placed on its development here.

Using equations (4-3) - (4-5), and the assumption that $s(t)$ contains a unique α_0, it can be seen that

$$R_{yx}^\alpha(u) = CR_x^\alpha(u-D)e^{-j\pi\alpha D} \tag{4-14}$$

The cross-correlation term for $n_1(t)$ and $n_2(t)$ is eliminated by the use of a cycle frequency unique to the SOI. An estimate of the TDOA, $\hat{D}$ that minimizes the magnitude of the sum

60

of the square errors between the measured value of the left side of (4-14), R_{yx}^{α} and the measurement of the right side of (4-14), R_x^{α} (with $\hat{D}$ substituted) yields the minimum-least-squares-optimized value for the TDOA.

Mathematically, from [16],

$$\hat{D} \overset{\Delta}{=} \underset{\hat{c},\tau}{\arg\min}\left\{\hat{c}_{\alpha}(\tau)\right\} \tag{4-15}$$

where $\hat{c}_{\alpha}(\tau)$ is the estimate of the MLS function. It was further shown in [16], that the solution of the MLS problem is of the form

$$\hat{D} \overset{\Delta}{=} \underset{\tau}{\arg\max}\left\{\hat{c}_{\alpha}(\tau)\right\} \tag{4-16}$$

where

$$\hat{c}_{\alpha}'(\tau) \overset{\Delta}{=} \left| \int R_{yx}^{\alpha}(u) R_x^{\alpha}(u-\tau)^* du \right| \tag{4-17}$$

$$= \left| \int S_{yx}^{\alpha}(f) S_x^{\alpha}(f)^* e^{j2\pi f\tau} df \right| \tag{4-18}$$

where (4-18) derives from (4-17) through Parseval's relation. Gardner and Chen go on to further prove that (4-18) does indeed peak at $\tau = D$.

SPECCOA derives its name from the fact that the peak in (4-18) occurs by maximizing the correlation in f of the two *spectral correlation* functions through the *alignment* of the phases of the respective functions.

In [4], Spooner and Gardner derive two additional cyclostationary TDOA algorithms, both considerably more computationally complex than the three outlined above. The first is a more extensive generalized version of SPECCOA termed G-SPECCOA and the second, Maximum Likelihood (ML), is the result of a maximum likelihood development.

61

The generalization of G-SPECCOA adds seven additional terms to the estimator taking into account multiple cycle frequencies and both conjugate and non-conjugate cyclostationarity. It includes the products of the cross-spectral correlation and the auto spectral correlation which are referred to as the auto-cross terms. In addition, G-SPECCOA includes products of cross spectral correlations and cross spectral correlations (cross-cross terms) and products of auto spectral correlations and auto spectral correlations (auto-auto terms). The result is an eight term algorithm that has the form

$$
\hat{d} = \underset{d}{\mathrm{argmax}} \left\{ \mathrm{Re} \left\{ \sum_{\alpha} \begin{bmatrix} \int_{-\infty}^{\infty} \hat{S}_{xy}^{\alpha}(f)\hat{S}_{yx}^{\alpha}(f)^{*} e^{j4\pi fd} \mathrm{d}f \\[2mm] + \int_{-\infty}^{\infty} \hat{S}_{xy}^{\alpha}(f)\hat{S}_{yy}^{\alpha}(f)^{*} e^{j2\pi\left(f+\alpha/2\right)d} \mathrm{d}f \\[2mm] + \int_{-\infty}^{\infty} \hat{S}_{xy}^{\alpha}(f)\hat{S}_{xx}^{\alpha}(f)^{*} e^{j2\pi\left(f-\alpha/2\right)d} \mathrm{d}f \\[2mm] + \int_{-\infty}^{\infty} \hat{S}_{yy}^{\alpha}(f)\hat{S}_{xx}^{\alpha}(f)^{*} e^{-j2\pi\alpha d} \mathrm{d}f \end{bmatrix} + \sum_{\beta} \begin{bmatrix} \int_{-\infty}^{\infty} \hat{S}_{xy^*}^{\beta}(f)\hat{S}_{yx^*}^{\beta}(f)^{*} e^{j4\pi fd} \mathrm{d}f \\[2mm] + \int_{-\infty}^{\infty} \hat{S}_{xy^*}^{\beta}(f)\hat{S}_{yy^*}^{\beta}(f)^{*} e^{j2\pi\left(f+\beta/2\right)d} \mathrm{d}f \\[2mm] + \int_{-\infty}^{\infty} \hat{S}_{xy^*}^{\beta}(f)\hat{S}_{xx^*}^{\beta}(f)^{*} e^{j2\pi\left(f-\beta/2\right)d} \mathrm{d}f \\[2mm] + \int_{-\infty}^{\infty} \hat{S}_{yy^*}^{\beta}(f)\hat{S}_{xx^*}^{\beta}(f)^{*} e^{-j2\pi\beta d} \mathrm{d}f \end{bmatrix} \right\} \right\} \tag{4-19}
$$

Finally, Spooner and Gardner's ML algorithm is derived for Model B modified to include complex constants received signals. Through a complex series of steps and simplifications, some of which are utilized in the ML derivation in Chapter V, Spooner and

Gardner derive an asymptotically ML estimator for TDOA that also has eight terms and a computational complexity similar to that of G-SPECCOA.

Like G-SPECCOA, the algorithm includes auto-cross terms, cross-cross terms and auto-auto terms. In its ideal ML form, the algorithm is expressed as a function of the receiver data records and the SOI waveform. As complete knowledge of the SOI is usually not available, this algorithm is considered an ideal ML TDOA estimator. Substituting for the terms that contain the SOI with approximations that contain only the data records, converts this ideal algorithm into one that is implementable. An infinite number of substitutions are possible so Spooner and Gardner propose several approximations in [4] to create practical estimators. The original ML algorithm, equation (101) in [4] appears below as (4-20).

$$
P_z(r|A,B,D) \propto \mathrm{Re}
\begin{bmatrix}
|A|^2 \sum_\alpha \int_{-\infty}^{+\infty} \hat{S}_{x_T}^\alpha(f)^* S_s^\alpha(f) df \\[2ex]
+A^2 \sum_\beta \int_{-\infty}^{+\infty} \hat{S}_{xx_T^*}^\beta(f)^* S_{ss^*}^\beta(f) df \\[2ex]
+|B|^2 \sum_\alpha \int_{-\infty}^{+\infty} \hat{S}_{y_T}^\alpha(f)^* S_s^\alpha(f) e^{-j2\pi\alpha D} df \\[2ex]
+B^2 \sum_\beta \int_{-\infty}^{+\infty} \hat{S}_{yy_T^*}^\beta(f)^* S_{ss^*}^\beta(f) e^{-j2\pi\beta D} df \\[2ex]
+A^*B \sum_\alpha \int_{-\infty}^{+\infty} \hat{S}_{yx_T}^\alpha(f) S_s^\alpha(f) e^{-j2\pi fD} e^{-j\pi\alpha D} df \\[2ex]
+AB \sum_\beta \int_{-\infty}^{+\infty} \hat{S}_{yx_T^*}^\beta(f)^* S_{ss^*}^\beta(f) e^{-j2\pi fD} e^{-j\pi\beta D} df \\[2ex]
+AB^* \sum_\alpha \int_{-\infty}^{+\infty} \hat{S}_{xy_T}^\alpha(f)^* S_s^\alpha(f) e^{j2\pi fD} e^{-j\pi\alpha D} df \\[2ex]
+AB \sum_\beta \int_{-\infty}^{+\infty} \hat{S}_{xy_T^*}^\beta(f)^* S_{ss^*}^\beta(f) e^{j2\pi fD} e^{-j\pi\beta D} df
\end{bmatrix}
\qquad (4-20)
$$

V. NEW MAXIMUM-LIKELIHOOD ESTIMATORS

A. BACKGROUND

1. Signal Model

The ultimate goal of this work is to find the ML estimators for the TDOA and FDOA of a weak cyclostationary signal in white Gaussian noise. To that end, an appropriate signal model must be used both to accurately reflect the signal environment of interest and to make the derivation mathematically tractable. Signal Model C is chosen to most accurately depict the case of two receivers collecting a single SOI in white Gaussian noise while maintaining some degree of mathematical tractability. One change made to the model is the elimination of the arbitrary gain and phase mismatch between the receivers. This complex constant scaling the output of receiver #2 represents a mismatch that is an unnecessary distraction in this derivation for several reasons. First, gain mismatch is easily accommodated with some form of normalization if such a procedure is even necessary. Second, modern collections systems enjoy the benefits of digital technology, GPS and fine frequency standards and thus take advantage of excellent coherence in both timing and frequency. Finally, the inclusion of such a complex constant in a maximum likelihood derivation would involve a maximum likelihood estimate of its own, taking away from the original intent of the research. Thus, to concentrate on a joint ML estimate for TDOA and FDOA, the gain and phase mismatch can be dropped here.

The new model for the derivation of the MLE is a simplified Doppler signal model similar to Model C but expressed in discrete time and lacking the complex constant in the second receiver equation:

$$x(n) = s(n) + m_x(n) \qquad\qquad (5\text{-}1)$$

$$y(n) = s(n - D)e^{+j2\pi f_d n} + m_y(n) \tag{5-2}$$

for $n = 1, 2, \ldots, N$ and all but n, D and f_d are complex-valued.

2.   Mathematical Model

To find ML estimates for D and f_d, it is necessary to maximize a likelihood function conditioned on only those parameters. In order to do so, a likelihood function for an equivalent complex-valued model conditioned on all the unknown parameters, including but not limited to D and f_d can be formed [4]. In due course, the conditioning on the unknown parameters not of interest are removed to leave the likelihood function needed for the estimates of D and f_d. The equivalent complex-valued model is

$$\mathbf{z} = \mathbf{v} + \mathbf{w} \tag{5-3}$$

where

$$\mathbf{z} = \begin{bmatrix} x(n) \\ y(n) \end{bmatrix}, \quad \mathbf{v} = \begin{bmatrix} s(n) \\ s(n-D)e^{+j2\pi f_d n} \end{bmatrix} \quad \text{and} \quad \mathbf{w} = \begin{bmatrix} m_x(n) \\ m_y(n) \end{bmatrix} \tag{5-4}$$

and the dimensions of each vector set at $2N \times 1$.

For the conditioning on the unknown parameters, let $\mathbf{b}$ and θ denote the random and nonrandom conditioning parameters respectively. To find the likelihood function, the probability density function (pdf) of $\mathbf{z}$ is needed specifically conditioned on $\mathbf{b}$ and θ or equivalently, conditioned on φ with

$$\varphi = \begin{bmatrix} \mathbf{b} & \theta \end{bmatrix} \tag{5-5}$$

66

where

$$\theta = \begin{bmatrix} D & f_d \end{bmatrix}$$ (5-6)

Thus, the equivalent complex valued mathematical model and the vector of conditioning parameters contain all the information about the signal model needed to develop a likelihood function that will produce maximum likelihood estimates for the two parameters of interest D and f_d.

B. DERIVATION

Of key importance in the formation of this likelihood function is the statistics of the noise. First, the only knowledge of the system's statistics is the definition of the noise at each receiver as zero-mean, additive white Gaussian noise. Second, the noise terms are assumed to be uncorrelated and thus to contain not SNOI. Thus the noise pdf, conditioned on the signal parameters completely describes the system. Expressing the noise, $m_x(n)$ and $m_y(n)$, contained in the vector w, in terms of its signal and receiver components produces a pdf with receiver terms, $x(n)$ and $y(n)$ contained in the vector z, and signal terms, $s(n)$ and its time-delayed and shifted version contained in the vector v, conditioned on all the unknown random and non-random parameters. It takes the form of a discrete jointly Gaussian pdf

$$P_w(w|\varphi) = \frac{1}{(2\pi)^{2N}|R_{z-v}|} \exp\left[-(z-v)^{*T}(R_{z-v})^{-1}(z-v)\right]$$ (5-7)

where again $w = z - v$ [21].

Now because the noise is zero-mean Gaussian, some simplifications can be made. Specifically, substituting

$$|R_{z-v}| = N_0^{2N}$$ (5-8)

67

and

$$(\mathbf{R}_{z-v})^{-1} = \frac{1}{N_o} \mathbf{I}_{2Nx2N} \qquad (5\text{-}9)$$

produces the following changes to the likelihood function,

$$P_w(\mathbf{w}|\varphi) = \frac{1}{(2\pi N_o)^{2N}} \exp\left[-\frac{1}{N_o}(\mathbf{z}-\mathbf{v})^{*T} \mathbf{I}_{2Nx2N}(\mathbf{z}-\mathbf{v}) \right] \qquad (5\text{-}10)$$

which in turn simplifies to

$$P_w(\mathbf{w}|\varphi) = \frac{1}{(2\pi N_o)^{2N}} \exp\left[-\frac{1}{N_o}(\mathbf{z}-\mathbf{v})^{*T}(\mathbf{z}-\mathbf{v}) \right] \qquad (5\text{-}11)$$

Finally, when expanded within the exponential, the expression becomes

$$P_w(\mathbf{w}|\varphi) = \frac{1}{(2\pi N_o)^{2N}} \exp\left[-\frac{1}{N_o}\left(\mathbf{z}^{*T}\mathbf{z} - \mathbf{v}^{*T}\mathbf{z} - \mathbf{z}^{*T}\mathbf{v} + \mathbf{v}^{*T}\mathbf{v} \right) \right] \qquad (5\text{-}12)$$

Though highly relevant to an hardware and system implementation problem where thresholds and amplifier gains are major issues, the constant of proportionality does not depend upon the variables of concern here and is merely a DC offset in any effort to maximize an equation derived from the remainder of the expression above. Thus it is dropped for convenience. Hence, the likelihood function now becomes,

$$P_w(\mathbf{w}|\varphi) \propto \exp\left(\frac{-\mathbf{z}^{*T}\mathbf{z}}{N_o} \right) \exp\left(\frac{\mathbf{v}^{*T}\mathbf{z}}{N_o} \right) \exp\left(\frac{\mathbf{z}^{*T}\mathbf{v}}{N_o} \right) \exp\left(\frac{-\mathbf{v}^{*T}\mathbf{v}}{N_o} \right) \qquad (5\text{-}13)$$

The weak signal assumption allows the expansion of the exponential expressions into Taylor series as follows

$$\exp\left(\frac{-z^{*T}z}{N_o}\right) = 1 - \frac{z^{*T}z}{N_o} + \frac{\left(z^{*T}z\right)^2}{2N_o} \tag{5-14}$$

$$\exp\left(\frac{v^{*T}z}{N_o}\right) = 1 + \frac{v^{*T}z}{N_o} + \frac{\left(v^{*T}z\right)^2}{2N_o} \tag{5-15}$$

$$\exp\left(\frac{z^{*T}v}{N_o}\right) = 1 + \frac{z^{*T}v}{N_o} + \frac{\left(z^{*T}v\right)^2}{2N_o} \tag{5-16}$$

$$\exp\left(\frac{-v^{*T}v}{N_o}\right) = 1 - \frac{v^{*T}v}{N_o} + \frac{\left(v^{*T}v\right)^2}{2N_o} \tag{5-17}$$

and substituting the four expressions into the pdf gives us a straight-forward but tedious problem.

$$P_w(w|\phi) \propto \left(1 - \frac{z^{*T}z}{N_o} + \frac{\left(z^{*T}z\right)^2}{2N_o}\right)\left(1 + \frac{v^{*T}z}{N_o} + \frac{\left(v^{*T}z\right)^2}{2N_o}\right)\left(1 + \frac{z^{*T}v}{N_o} + \frac{\left(z^{*T}v\right)^2}{2N_o}\right)\left(1 - \frac{v^{*T}v}{N_o} + \frac{\left(v^{*T}v\right)^2}{2N_o}\right)$$

$$\tag{5-18}$$

Expanding the quadratic and retaining only fourth or lower order terms, the expression becomes a sum of fourteen products

$$P_w(w|\phi) \propto \left\{ \begin{array}{l} 1 - \dfrac{z^{*T}z}{N_0} + \dfrac{\left(z^{*T}z\right)^2}{2N_0^2} + \dfrac{z^{*T}v}{N_0} + \dfrac{\left(z^{*T}v\right)^2}{2N_0^2} \\[2mm] - \dfrac{z^{*T}zz^{*T}v}{N_0^2} - \dfrac{z^{*T}zv^{*T}z}{N_0^2} + \dfrac{z^{*T}zv^{*T}v}{N_0^2} \\[2mm] + \dfrac{z^{*T}vv^{*T}z}{N_0^2} + \dfrac{z^{*T}vv^{*T}v}{N_0^2} - \dfrac{v^{*T}zz^{*T}z}{N_0^2} \\[2mm] + \dfrac{v^{*T}z}{N_0} + \dfrac{\left(v^{*T}z\right)^2}{2N_0^2} - \dfrac{v^{*T}v}{N_0} + \dfrac{\left(v^{*T}v\right)^2}{2N_0^2} \end{array} \right. \tag{5-19}$$

which are numbered P_1 to P_{14} (for product 1, product 2, ...) from left to right, top to bottom, discounting the leading constant.

Without loss of generality, if the sample rate is greater than the Nyquist rate to ensure perfect reconstruction of the analog signal, the transformation of the fourteen expressions above into continuous-time integrals is possible. The terms now are numbered CP_1 to CP_{14}, for continuous-time products 1 to 14. At the same time, the substitution of the original system and signal terms back into the expressions gives us an initial insight into the content of the terms. To avoid the additional clutter associated with the addition of the time-delay variable D and frequency shift complex exponential, the variable $s_d(t)$ represents the time-delayed and frequency shifted version of pure signal that is measured at receiver 2. The transformed terms appear below:

CP_1:
$$-\frac{1}{N_0}\left[\int_0^T\!\!\int_0^T x^*(t)x(t)\,\mathrm{d}t + \int_0^T\!\!\int_0^T y^*(t)y(t)\,\mathrm{d}t \right] \tag{5-20}$$

CP$_2$:

$$+\frac{1}{2N_0^2}\left[\begin{array}{l}\int_0^T\int_0^T x^*(t_1)x(t_1)x^*(t_2)x(t_2)dt_1dt_2+\int_0^T\int_0^T x^*(t_1)x(t_1)y^*(t_2)y(t_2)dt_1dt_2\\[2mm]+\int_0^T\int_0^T y^*(t_1)y(t_1)x^*(t_2)x(t_2)dt_1dt_2+\int_0^T\int_0^T y^*(t_1)y(t_1)y^*(t_2)y(t_2)dt_1dt_2\end{array}\right]\qquad(5\text{-}21)$$

CP$_3$:

$$+\frac{1}{N_o}\left[\int_0^T\int_0^T x^*(t)s(t)dt+\int_0^T\int_0^T y^*(t)s_d(t)dt\right]\qquad(5\text{-}22)$$

CP$_4$:
$$+\frac{1}{2N_0^2}\left[\begin{array}{l}\int_0^T\int_0^T x^*(t_1)s(t_1)x^*(t_2)s(t_2)dt_1dt_2+\int_0^T\int_0^T x^*(t_1)s(t_1)y^*(t_2)s_d(t_2)dt_1dt_2\\[2mm]+\int_0^T\int_0^T y^*(t_1)s_d(t_1)x^*(t_2)s(t_2)dt_1dt_2+\int_0^T\int_0^T y^*(t_1)s_d(t_1)y^*(t_2)s_d(t_2)dt_1dt_2\end{array}\right]\qquad(5\text{-}23)$$

CP$_5$:

$$-\frac{1}{N_0^2}\left[\begin{array}{l}\int_0^T\int_0^T x^*(t_1)x(t_1)x^*(t_2)s(t_2)dt_1dt_2+\int_0^T\int_0^T x^*(t_1)x(t_1)y^*(t_2)s_d(t_2)dt_1dt_2\\[2mm]+\int_0^T\int_0^T y^*(t_1)y(t_1)x^*(t_2)s(t_2)dt_1dt_2+\int_0^T\int_0^T y^*(t_1)y(t_1)y^*(t_2)s_d(t_2)dt_1dt_2\end{array}\right]\qquad(5\text{-}24)$$

CP$_6$:

$$-\frac{1}{N_0^2}\left[\begin{array}{l}\int_0^T\int_0^T x^*(t_1)x(t_1)s^*(t_2)x(t_2)dt_1dt_2+\int_0^T\int_0^T x^*(t_1)s(t_1)s_d^{\ *}(t_2)y(t_2)dt_1dt_2\\[2mm]+\int_0^T\int_0^T y^*(t_1)y(t_1)s^*(t_2)x(t_2)dt_1dt_2+\int_0^T\int_0^T y^*(t_1)y(t_1)s_d^{\ *}(t_2)y(t_2)dt_1dt_2\end{array}\right]\qquad(5\text{-}25)$$

CP$_7$:

$$+\frac{1}{N_o^2}\left[\begin{array}{l}\int\limits_0^T\int\limits_0^T s^*(t_1)x(t_1)x^*(t_2)s(t_2)dt_1dt_2+\int\limits_0^T\int\limits_0^T s^*(t_1)x(t_1)y^*(t_2)s_d(t_2)dt_1dt_2\\[4mm]+\int\limits_0^T\int\limits_0^T s_d^{\ *}(t_1)y(t_1)x^*(t_2)s(t_2)dt_1dt_2+\int\limits_0^T\int\limits_0^T s_d^{\ *}(t_1)y(t_1)y^*(t_2)s_d(t_2)dt_1dt_2\end{array}\right]\quad(5\text{-}26)$$

CP$_8$:

$$+\frac{1}{N_o^2}\left[\begin{array}{l}\int\limits_0^T\int\limits_0^T x^*(t_1)s(t_1)s^*(t_2)x(t_2)dt_1dt_2+\int\limits_0^T\int\limits_0^T x^*(t_1)s(t_1)s_d^{\ *}(t_2)y(t_2)dt_1dt_2\\[4mm]+\int\limits_0^T\int\limits_0^T y^*(t_1)s_d(t_1)s^*(t_2)x(t_2)dt_1dt_2+\int\limits_0^T\int\limits_0^T y^*(t_1)s_d(t_1)s_d^{\ *}(t_2)y(t_2)dt_1dt_2\end{array}\right]\quad(5\text{-}27)$$

CP$_9$:

$$-\frac{1}{N_o^2}\left[\begin{array}{l}\int\limits_0^T\int\limits_0^T x^*(t_1)s(t_1)s^*(t_2)s(t_2)dt_1dt_2+\int\limits_0^T\int\limits_0^T x^*(t_1)s(t_1)s_d^{\ *}(t_2)s_d(t_2)dt_1dt_2\\[4mm]+\int\limits_0^T\int\limits_0^T y^*(t_1)s_d(t_1)s^*(t_2)s(t_2)dt_1dt_2+\int\limits_0^T\int\limits_0^T y^*(t_1)s_d(t_1)s_d^{\ *}(t_2)s_d(t_2)dt_1dt_2\end{array}\right]\quad(5\text{-}28)$$

CP$_{10}$:

$$-\frac{1}{N_o^2}\left[\begin{array}{l}\int\limits_0^T\int\limits_0^T s^*(t_1)x(t_1)x^*(t_2)x(t_2)dt_1dt_2+\int\limits_0^T\int\limits_0^T s^*(t_1)x(t_1)y^*(t_2)y(t_2)dt_1dt_2\\[4mm]+\int\limits_0^T\int\limits_0^T s_d^{\ *}(t_1)y(t_1)x^*(t_2)x(t_2)dt_1dt_2+\int\limits_0^T\int\limits_0^T s_d^{\ *}(t_1)y(t_1)y^*(t_2)y(t_2)dt_1dt_2\end{array}\right]\quad(5\text{-}29)$$

CP$_{11}$:

$$+\frac{1}{N_o}\left[\int\limits_0^T\int\limits_0^T s^*(t)x(t)dt+\int\limits_0^T\int\limits_0^T s_d^{\ *}(t)y(t)dt\right]\quad(5\text{-}30)$$

$$CP_{12}: +\frac{1}{2N_o^2}\left[\begin{array}{l}\int\limits_0^T\int\limits_0^T s^*(t_1)x(t_1)s^*(t_2)x(t_2)dt_1dt_2 + \int\limits_0^T\int\limits_0^T s^*(t_1)x(t_1)s_d{}^*(t_2)y(t_2)dt_1dt_2 \\ +\int\limits_0^T\int\limits_0^T s_d{}^*(t_1)y(t_1)s^*(t_2)x(t_2)dt_1dt_2 + \int\limits_0^T\int\limits_0^T s_d{}^*(t_1)y(t_1)s_d{}^*(t_2)y(t_2)dt_1dt_2\end{array}\right] \quad (5\text{-}31)$$

$$CP_{13}: \qquad -\frac{1}{N_o}\left[\int\limits_0^T\int\limits_0^T s^*(t)s(t)dt + \int\limits_0^T\int\limits_0^T s_d{}^*(t)s_d(t)dt\right] \qquad (5\text{-}32)$$

$CP_{14}:$

$$+\frac{1}{2N_o}\left[\begin{array}{l}\int\limits_0^T\int\limits_0^T s^*(t_1)s(t_1)s^*(t_2)s(t_2)dt_1dt_2 + \int\limits_0^T\int\limits_0^T s^*(t_1)s(t_1)s_d{}^*(t_2)s_d(t_2)dt_1dt_2 \\ +\int\limits_0^T\int\limits_0^T s_d{}^*(t_1)s_d(t_1)s^*(t_2)s(t_2)dt_1dt_2 + \int\limits_0^T\int\limits_0^T s_d{}^*(t_1)s_d(t_1)s_d{}^*(t_2)s_d(t_2)dt_1dt_2\end{array}\right] \quad (5\text{-}33)$$

Next, the weak signal assumption eliminates term CP_2 because contribution to the MLE of TDOA and FDOA for this term will be very small given that the signal content in term CP_2 is small compared to the noise content. The same is true for the contribution of the fourth-order signal term CP_{14}. It too can be dropped because the weak signal assumption causes fourth-order terms to become very small [4].

Finally, writing terms CP_1 and CP_{13} as

$$\frac{1}{N_o}\int_0^T \|x\|^2 dt + \frac{1}{N_o}\int_0^T \|y\|^2 dt \qquad (5\text{-}34)$$

and

$$\frac{1}{N_o}\int_0^T \|s\|^2 dt + \frac{1}{N_o}\int_0^T \|s_d\|^2 dt \qquad (5\text{-}35)$$

reveal they are essentially power terms. If T is sufficiently large, these terms converge to scaled average powers of the received waveforms, the SOI and the delayed and Doppler-shifted SOI. These average powers do not depend on the TDOA, D or the FDOA, f_d. Consequently, they are dropped as contributing little to the MLE [4].

Following that simplification, the next step should remove the conditioning on the random parameter vector $\mathbf{b}$. For nearly all digital communications signals, the only contribution to this random conditioning vector comes from the bit or symbol sequence of the message [4]. To that end, if the expected value of the signal $s(t)$ is zero, as is the case in almost every man-made digital signal, carrying out the expectation over $\mathbf{b}$ causes any term with an odd power of signal components to go identically to zero. This eliminates terms CP_3, CP_5, CP_6, CP_9, CP_{10} and CP_{11}.

This leaves terms CP_4, CP_7, CP_8 and CP_{12} which will collapse using the complex conjugate relationships, $CP_{12} = CP_4^*$ and $CP_7 = CP_8^*$, into two new terms T_1 and T_2 with the following relationship to the original 14 CP terms:

$$T_1 = CP_4 + CP_{12} = 2\,\mathrm{Re}\{CP_4\} \qquad (5\text{-}36)$$

$$T_2 = CP_7 + CP_8 = 2\,\mathrm{Re}\{CP_8\} \qquad (5\text{-}37)$$

with the constant out front dropped as merely a bias term. The new terms are now

T_1:

$$\frac{\mathrm{Re}}{N_o^2}\left[E_b\left\{ \begin{array}{l} \int_0^T\!\!\int_0^T x^*(t_1)s(t_1)x^*(t_2)s(t_2)\,dt_1dt_2 + \int_0^T\!\!\int_0^T x^*(t_1)s(t_1)y^*(t_2)s_d(t_2)\,dt_1dt_2 \\[2mm] +\int_0^T\!\!\int_0^T y^*(t_1)s_d(t_1)x^*(t_2)s(t_2)\,dt_1dt_2 + \int_0^T\!\!\int_0^T y^*(t_1)s_d(t_1)y^*(t_2)s_d(t_2)\,dt_1dt_2 \end{array} \right\} \right] \quad (5\text{-}38)$$

74

T_2:

$$\frac{2\,\mathrm{Re}}{N_0^2}\left[E_b\left\{\begin{array}{l}\displaystyle\int_0^T\!\!\int_0^T x^*(t_1)s(t_1)s^*(t_2)x(t_2)\,dt_1dt_2 + \int_0^T\!\!\int_0^T x^*(t_1)s(t_1)s_d^*(t_2)y(t_2)\,dt_1dt_2 \\[2ex] +\displaystyle\int_0^T\!\!\int_0^T y^*(t_1)s_d(t_1)s^*(t_2)x(t_2)\,dt_1dt_2 + \int_0^T\!\!\int_0^T y^*(t_1)s_d(t_1)s_d^*(t_2)y(t_2)\,dt_1dt_2\end{array}\right\}\right] \quad (5\text{-}39)$$

Note that the first integral in T_1 does not contain either parameter of interest. The same is true for the first integral in T_2. Therefore, these two integrals are removed from the estimator. Now, carrying out the expectation with the remaining terms, enables the expression of the sum of products in terms of the cyclic correlation functions. The expectation operator allows the treatment of the signal terms as random variables and the receiver terms as non-random constants, forming the probabilistic auto- and cross-correlation functions according to

$$R_{pq}(t_1,t_2)\overset{\Delta}{=}\mathrm{E}\left\{p(t_1)q^*(t_2)\right\} \quad (5\text{-}40)$$

where $p(\cdot)$ and $q(\cdot)$ each represent one of the signals $\left\{s(\cdot),\, s^*(\cdot),\, s_d(\cdot),\, s_d^*(\cdot)\right\}$.

Following that, the remaining pieces comprise the finite-time-averaged auto- and cross-correlation functions for various combinations of the received waveforms, for example,

$$\hat{R}_{x y_T}^{\alpha}(\tau)\overset{\Delta}{=}\int_0^T x_T\!\left(t+\tfrac{\tau}{2}\right)y_T^*\!\left(t-\tfrac{\tau}{2}\right)e^{-j2\pi\alpha t}\,dt \quad (5\text{-}41)$$

where

$$\begin{aligned}x_T(t)&\overset{\Delta}{=}u_T\!\left(t-\tfrac{T}{2}\right)x(t) \\ y_T(t)&\overset{\Delta}{=}u_T\!\left(t-\tfrac{T}{2}\right)y(t)\end{aligned} \quad (5\text{-}42)$$

75

with $u(t)$ defined as the unit step function

$$u_T(t) \overset{\Delta}{=} \begin{cases} 1 & |t| < T/2 \\ \\ 0 & \text{otherwise} \end{cases} \tag{5-43}$$

or

$$\hat{R}^{\alpha}_{xy_T}(\tau) \overset{\Delta}{=} \begin{cases} \displaystyle\int_{|\tau|/2}^{T-|\tau|/2} x\left(t+\tau/2\right)y^*\left(t-\tau/2\right)e^{-j2\pi\alpha t}\,dt & \text{for } |\tau| \leq T, \\ \\ 0 & \text{for } |\tau| > T \end{cases} \tag{5-44}$$

Finally, the cyclic correlation functions follow using the following relationship below

$$R_{pq}(t_1, t_2) = \sum_{\alpha} R^{\alpha}_{pq}(t_1 - t_2)e^{j2\pi\alpha(t_1 + t_2)} \tag{5-45}$$

where $p(t)$ and $q(t)$ again represent one of the signals, $\left\{s(\cdot), s^*(\cdot), s_d(\cdot), s_d^*(\cdot)\right\}$.

Thus, the likelihood function may now be expressed as products of the cyclic auto- and cross-correlation functions of the receiver and signal variables. The expression now has the form

76

$$\propto \frac{\text{Re}}{N_0^2 T}
\begin{bmatrix}
\sum\limits_{\beta} \int\limits_{-\infty}^{+\infty} \hat{R}_{yx_T^*}^{\beta}(\tau) R_{s_d s^*}^{\beta}(\tau)^* d\tau \\[2ex]
+\sum\limits_{\beta} \int\limits_{-\infty}^{+\infty} \hat{R}_{xy_T^*}^{\beta}(\tau) R_{ss_d^*}^{\beta}(\tau)^* d\tau \\[2ex]
+\sum\limits_{\beta} \int\limits_{-\infty}^{+\infty} \hat{R}_{yy_T^*}^{\beta}(\tau) R_{s_d s_d^*}^{\beta}(\tau)^* d\tau \\[2ex]
+2\sum\limits_{\alpha} \int\limits_{-\infty}^{+\infty} \hat{R}_{xy_T}^{\alpha}(\tau) R_{ss_d}^{\alpha}(\tau)^* d\tau \\[2ex]
+2\sum\limits_{\alpha} \int\limits_{-\infty}^{+\infty} \hat{R}_{yx_T}^{\alpha}(\tau) R_{s_d s}^{\alpha}(\tau)^* d\tau \\[2ex]
+2\sum\limits_{\alpha} \int\limits_{-\infty}^{+\infty} \hat{R}_{yy_T}^{\alpha}(\tau) R_{s_d s_d}^{\alpha}(\tau)^* d\tau
\end{bmatrix}
\tag{5-46}$$

Next, a final substitution of $s(t)$ for $s_d(t)$ expresses the estimator in terms of the received waveforms $x(t)$ and $y(t)$ and the limit cyclic correlation functions of $s(t)$. This is the Ideal Two-Dimensional Maximum Likelihood Estimator (I2DMLE).

$$\propto \frac{\text{Re}}{N_0^2 T}
\begin{bmatrix}
\sum\limits_{\beta} \int\limits_{-\infty}^{+\infty} \hat{R}_{yx_T^*}^{\beta}(\tau) \hat{R}_{ss^*}^{\beta+f_d}(\tau-D)^* e^{-j\pi(\beta+f_d)D} e^{-j\pi f_d \tau} d\tau \\[2ex]
+\sum\limits_{\beta} \int\limits_{-\infty}^{+\infty} \hat{R}_{xy_T^*}^{\beta}(\tau) \hat{R}_{ss^*}^{\beta+f_d}(\tau+D)^* e^{-j\pi(\beta+f_d)D} e^{+j\pi f_d \tau} d\tau \\[2ex]
+\sum\limits_{\beta} \int\limits_{-\infty}^{+\infty} \hat{R}_{yy_T^*}^{\beta}(\tau) \hat{R}_{ss^*}^{\beta+2f_d}(\tau)^* e^{-j\pi(\beta+2f_d)D} e^{-j2\pi f_d \tau} d\tau \\[2ex]
+2\sum\limits_{\alpha} \int\limits_{-\infty}^{+\infty} \hat{R}_{xy_T}^{\alpha}(\tau) \hat{R}_{ss}^{\alpha+f_d}(\tau+D)^* e^{-j\pi(\alpha+f_d)D} e^{+j\pi f_d \tau} d\tau \\[2ex]
+2\sum\limits_{\alpha} \int\limits_{-\infty}^{+\infty} \hat{R}_{yx_T}^{\alpha}(\tau) \hat{R}_{ss}^{\alpha+f_d}(\tau-D)^* e^{-j\pi(\alpha+f_d)D} e^{-j\pi f_d \tau} d\tau \\[2ex]
+2\sum\limits_{\alpha} \int\limits_{-\infty}^{+\infty} \hat{R}_{yy_T}^{\alpha}(\tau) \hat{R}_{ss}^{\alpha}(\tau)^* e^{-j2\pi\alpha D} e^{-j2\pi f_d \tau} d\tau
\end{bmatrix}
\tag{5-47}$$

where the expression to be maximized simultaneously over D and f_d to obtain cyclostationary ML estimates for TDOA and FDOA.

Note that I2DMLE is in fact ideal because it requires knowledge of the ideal cyclic auto-correlation function of the SOI a priori. In practice this cyclic correlation function is not available thus requiring the ideal caveat. Nonetheless, this is the first of three cyclostationary TDOA/FDOA estimators implemented and tested here. The performance of this ideal algorithm is instructive in assessing the loss in performance due to the approximations made in order to realize the next two algorithms outlined below. In addition, should an acceptable extension of the Cramer-Rao Lower Bound be found for the cyclostationary TDOA/FDOA case, the extent to which the ideal algorithm approaches this bound as the collect length increases will be a valuable investigation as well.

Finally, in order to more easily implement I2DMLE, the expression can be written in terms of the spectral correlation functions by using Parseval's relation. I2DMLE in the frequency domain, still with maximization over D and f_d, assumes the form

$$
\propto \frac{Re}{N_0^2 T}
\begin{bmatrix}
\displaystyle\sum_{\beta}\int_{-\infty}^{+\infty} \hat{S}^{\beta}_{yx_T^*}(f)\, S^{\beta+f_d}_{ss^*}\left(f+\frac{f_d}{2}\right)^* e^{-j\pi(\beta+f_d)D}\, e^{+j2\pi f D}\, df \\[2.5ex]
+\displaystyle\sum_{\beta}\int_{-\infty}^{+\infty} \hat{S}^{\beta}_{xy_T^*}(f)\, S^{\beta+f_d}_{ss^*}\left(f-\frac{f_d}{2}\right)^* e^{-j\pi(\beta+f_d)D}\, e^{-j2\pi f D}\, df \\[2.5ex]
+\displaystyle\sum_{\beta}\int_{-\infty}^{+\infty} \hat{S}^{\beta}_{yy_T^*}(f)\, S^{\beta+2f_d}_{ss^*}\left(f+f_d\right)^* e^{-j2\pi(\beta+2f_d)D}\, df \\[2.5ex]
+2\displaystyle\sum_{\alpha}\int_{-\infty}^{+\infty} \hat{S}^{\alpha}_{xy_T}(f)\, S^{\alpha+f_d}_{ss}\left(f-\frac{f_d}{2}\right)^* e^{-j\pi(\alpha+f_d)D}\, e^{-j2\pi f D}\, df \\[2.5ex]
+2\displaystyle\sum_{\alpha}\int_{-\infty}^{+\infty} \hat{S}^{\alpha}_{yx_T}(f)\, S^{\alpha+f_d}_{ss}\left(f+\frac{f_d}{2}\right)^* e^{-j\pi(\alpha+f_d)D}\, e^{+j2\pi f D}\, df \\[2.5ex]
+2\displaystyle\sum_{\alpha}\int_{-\infty}^{+\infty} \hat{S}^{\alpha}_{yy_T}(f)\, S^{\alpha}_{ss}\left(f+f_d\right)^* e^{-j2\pi\alpha D}\, df
\end{bmatrix} \qquad (5\text{-}48)
$$

C. ALGORITHMS

1. Approximated 2-Dimensional Maximum Likelihood Algorithm #1

To obtain the final two estimators, both approximations to the I2DMLE, we must substitute for the ideal cyclic auto-correlation function of the SOI with the cyclic correlation functions of the data record $x(t)$ and $y(t)$. This is possible and represents a plausible approximation because by modeling the received signals as cyclostationary and choosing SOI-unique cycle frequencies, in the limit as $T \rightarrow \infty$, the SOI spectral correlation function can be measured as accurately as desired. Note as an example, that the following is true

$$\lim_{T \to \infty} \hat{R}^{\alpha}_{xx}(\tau) = R^{\alpha}_{ss}(\tau), \quad \alpha \neq 0 \tag{5-49}$$

and

$$\lim_{T \to \infty} \hat{R}^{\beta}_{xx}(\tau) = R^{\beta}_{ss}(\tau) \tag{5-50}$$

Consequently, the simplest practical approximation to the ideal estimator is obtained by substituting $x(t)$ directly for $s(t)$ in the above expression to obtain the Approximated Two-dimensional Maximum Likelihood Estimator #1 (A2DMLE#1) which is maximized over D and f_d and takes the form

$$\propto \frac{\mathrm{Re}}{N_0^2 T} \begin{bmatrix} \displaystyle\sum_{\beta}\int_{-\infty}^{+\infty} \hat{R}_{yx_T^*}^{\beta}(\tau)\hat{R}_{xx_T^*}^{\beta+f_d}(\tau-D)^* e^{-j\pi(\beta+f_d)D}e^{-j\pi f_d \tau}\,d\tau \\[1.5em] +\displaystyle\sum_{\beta}\int_{-\infty}^{+\infty} \hat{R}_{xy_T^*}^{\beta}(\tau)\hat{R}_{xx_T^*}^{\beta+f_d}(\tau+D)^* e^{-j\pi(\beta+f_d)D}e^{+j\pi f_d \tau}\,d\tau \\[1.5em] +\displaystyle\sum_{\beta}\int_{-\infty}^{+\infty} \hat{R}_{yy_T^*}^{\beta}(\tau)\hat{R}_{xx_T^*}^{\beta+2f_d}(\tau)^* e^{-j\pi(\beta+2f_d)D}e^{-j2\pi f_d \tau}\,d\tau \\[1.5em] +2\displaystyle\sum_{\alpha}\int_{-\infty}^{+\infty} \hat{R}_{xy_T}^{\alpha}(\tau)\hat{R}_{xx_T}^{\alpha+f_d}(\tau+D)^* e^{-j\pi(\alpha+f_d)D}e^{+j\pi f_d \tau}\,d\tau,\ \alpha\neq 0 \\[1.5em] +2\displaystyle\sum_{\alpha}\int_{-\infty}^{+\infty} \hat{R}_{yx_T}^{\alpha}(\tau)\hat{R}_{xx_T}^{\alpha+f_d}(\tau-D)^* e^{-j\pi(\alpha+f_d)D}e^{-j\pi f_d \tau}\,d\tau,\ \alpha\neq 0 \\[1.5em] +2\displaystyle\sum_{\alpha}\int_{-\infty}^{+\infty} \hat{R}_{yy_T}^{\alpha}(\tau)\hat{R}_{xx_T}^{\alpha}(\tau)^* e^{-j2\pi\alpha D}e^{-j2\pi f_d \tau}\,d\tau,\ \alpha\neq 0 \end{bmatrix} \quad (5\text{-}51)$$

Note that A2DMLE#1 contains both conjugate and non-conjugate terms with cross-cross terms and auto-cross terms, resembling some portions of G-SPECCOA. Thus, it is expected that the resulting combination possess some of the strengths and weaknesses of this previously derived algorithm in some form.

In the frequency domain, A2DMLE#1 looks identical to I2DMLE with $x(t)$ substituted for $s(t)$ and still maximized over D and f_d.

$$\propto \frac{\mathrm{Re}}{N_0^2 T} \begin{bmatrix} \sum_\beta \int_{-\infty}^{+\infty} \hat{S}_{yx_T}^{\beta\,*}(f)\hat{S}_{xx_T}^{\beta+f_d\,*}\left(f+\frac{f_d}{2}\right)^* e^{-j\pi(\beta+f_d)D}e^{+j2\pi fD}\,df \\[2ex] +\sum_\beta \int_{-\infty}^{+\infty} \hat{S}_{xy_T}^{\beta\,*}(f)\hat{S}_{xx_T}^{\beta+f_d\,*}\left(f-\frac{f_d}{2}\right)^* e^{-j\pi(\beta+f_d)D}e^{-j2\pi fD}\,df \\[2ex] +\sum_\beta \int_{-\infty}^{+\infty} \hat{S}_{yy_T}^{\beta\,*}(f)\hat{S}_{xx_T}^{\beta+2f_d\,*}\left(f+f_d\right)^* e^{-j2\pi(\beta+2f_d)D}\,df \\[2ex] +2\sum_\alpha \int_{-\infty}^{+\infty} \hat{S}_{xy_T}^{\alpha}(f)\hat{S}_{xx_T}^{\alpha+f_d}\left(f-\frac{f_d}{2}\right)^* e^{-j\pi(\alpha+f_d)D}e^{-j2\pi fD}\,df,\,\alpha\neq 0 \\[2ex] +2\sum_\alpha \int_{-\infty}^{+\infty} \hat{S}_{yx_T}^{\alpha}(f)\hat{S}_{xx_T}^{\alpha+f_d}\left(f+\frac{f_d}{2}\right)^* e^{-j\pi(\alpha+f_d)D}e^{+j2\pi fD}\,df,\,\alpha\neq 0 \\[2ex] +2\sum_\alpha \int_{-\infty}^{+\infty} \hat{S}_{yy_T}^{\alpha}(f)\hat{S}_{xx_T}^{\alpha}\left(f+f_d\right)^* e^{-j2\pi\alpha D}\,df,\,\alpha\neq 0 \end{bmatrix} \tag{5-52}$$

2. Approximated 2-Dimensional Maximum Likelihood Algorithm #2

The second approximation to the I2DMLE is a logical extension of A2DMLE#1 above with three concurrent goals: (1) keep the strongest terms to maintain as much as possible the performance of A2DMLE#1, (2) maintain both the conjugate and non-conjugate cyclostationary exploitation and (3) minimize the computational burden by limiting the number of terms as much as possible. Observing first that the final summation depends little on the frequency parameter of interest f_d it can be eliminated from the second approximation. Also noting that the first and second summations, as well as the fourth and fifth summations, differ only in their first cross-correlation terms, only one of each of these pairs of terms is retained. Finally, to obtain another auto-cross term like SPECCOA, the third sum is converted into such a term by substituting for $R_{ss}^\alpha(\tau)$ with the following cyclic cross-correlation

$$R_{ss}^\alpha(\tau) = \hat{R}_{xy}^{\alpha-f_d}(\tau-D)e^{-j\pi(\alpha+f_d)D}e^{j\pi f_d\tau} \tag{5-53}$$

producing an auto-cross term which is theoretically a strong contributor to the MLE .

The result is Approximated Two-dimensional Maximum Likelihood Estimator #2 (A2DMLE#2), a three term algorithm whose performance should not deteriorate considerably from that of A2DMLE#1, still exploits both conjugate and non-conjugate cyclostationarity and is much more easily implemented with less computational burden. It retains the need for maximization over D and f_d and has the form

$$\propto \frac{\text{Re}}{N_0^2 T} \left[\begin{array}{l} \displaystyle\sum_\beta \int_{-\infty}^{+\infty} \hat{R}^\beta_{xy_T^*}(\tau)\hat{R}^{\beta+f_d}_{xx_T^*}(\tau+D)^* e^{-j\pi(\beta+f_d)D} e^{+j\pi f_d \tau} d\tau \\[4mm] \displaystyle +\sum_\beta \int_{-\infty}^{+\infty} \hat{R}^\beta_{yy_T^*}(\tau)\hat{R}^{\beta+f_d}_{xy}(\tau-D)^* e^{+j\pi(\beta+3f_d)D} e^{-j\pi f_d \tau} d\tau \\[4mm] \displaystyle +2\sum_\alpha \int_{-\infty}^{+\infty} \hat{R}^\alpha_{xy_T}(\tau)\hat{R}^{\alpha+f_d}_{xx}(\tau+D)^* e^{-j\pi(\alpha+f_d)D} e^{+j\pi f_d \tau} d\tau, \alpha \neq 0 \end{array} \right] \quad (5\text{-}54)$$

In the frequency domain, A2DMLE#2 is similar to A2DMLE#1 with the exception of the second term which has the cyclic cross-correlation substituted in place of the cyclic auto-correlation function. The entire expression in the frequency domain has the form

$$\propto \frac{\text{Re}}{N_0^2 T} \left[\begin{array}{l} \displaystyle\sum_\beta \int_{-\infty}^{+\infty} \hat{S}^\beta_{xy_T^*}(f)\hat{S}^{\beta+f_d}_{xx_T^*}\left(f-\frac{f_d}{2}\right)^* e^{-j\pi(\beta+f_d)D} e^{+j2\pi f D} df \\[4mm] \displaystyle +\sum_\beta \int_{-\infty}^{+\infty} \hat{S}^\beta_{yy_T^*}(f)\hat{S}^{\beta+f_d}_{xy_T^*}\left(f+\frac{f_d}{2}\right)^* e^{+j\pi(\beta+3f_d)D} e^{-j2\pi f D} df \\[4mm] \displaystyle +2\sum_\alpha \int_{-\infty}^{+\infty} \hat{S}^\alpha_{xy_T}(f)\hat{S}^{\alpha+f_d}_{xx}\left(f-\frac{f_d}{2}\right)^* e^{-j\pi(\alpha+f_d)D} e^{+j2\pi f D} df, \alpha \neq 0 \end{array} \right] \quad (5\text{-}55)$$

Now that three different original ML algorithms are derived, a method with which to measure and compare their performance is needed. In the next chapter, the details of the Monte Carlo testing provide a measure of the Root Mean Square Error in TDOA and FDOA estimation for each of the three algorithms. This performance measure is

calculated for a variety of signal environments and then compared to the performance of traditional techniques and previously derived cyclostationary TDOA algorithms.

VI. MONTE CARLO PERFORMANCE TESTING

A. OBJECTIVES

The Monte Carlo Testing (MCT) satisfies four objectives, two quantitative and two qualitative. The quantitative objectives for the MCT are: (1) provide a numerical measure of the performance of the three newly derived algorithms, I2DMLE, A2DMLE#1 and A2DMLE#2 and (2) provide a quantitative means of direct comparison to the performance of the CAF under identical circumstances. The qualitative objectives are: (1) provide a qualitative means of comparison to the performance of previously derived cyclostationary TDOA algorithms; and (2) provide a means of comparison to the stationary CRB.

Satisfying the first quantitative objective by empirically measuring the performance of the three algorithms allows specific conclusions to be drawn regarding the loss in performance due to each of the two approximations to the ideal algorithm. This in turn can lead to other more informed approximations in future work. The second quantitative objective allows the direct numerical comparison of three cyclostationary TDOA-FDOA estimators to the traditional, well-known CAF under the exact same conditions. This reveals to some degree the extent of the performance gain achieved by these cyclostationary techniques and also to some degree, under which circumstances cyclostationary techniques are superior or inferior to the traditional TDOA-FDOA estimation process.

The first qualitative objective is satisfied by intelligent comparison of the MCT results with those obtained in previously published work under similar but not identical testing scenarios. The relationship of the performance of these new estimators to the performance of those estimators that constitute the heritage for this work is important in understanding if in fact the TDOA estimates found here compare well with that previous work. Additionally, whether those estimates for TDOA were obtained in conjunction with comparable performance in FDOA estimation is an important consideration.

85

The second qualitative objective comes in the comparison of the stationary CRB on the performance of the CAF to the results of the MCT. Since the CRB represents the theoretical lower limit on the variance of the estimates obtained from the CAF, it is in a sense, the very best that a traditional TDOA-FDOA estimator can do. Though the CRB used here was derived using different assumptions than those that form the basis for the cyclostationary TDOA-FDOA estimators developed here, comparing the MCT results to its ultimate lower limit provides another piece of evidence in support of the added contribution that cyclostationary techniques make over and beyond even the ideal stationary estimator.

B.   TEST ENVIRONMENTS

1.   Introduction

In each case, the SOI is the BPSK signal introduced in Chapter II and detailed in the Appendix. Because this is the only modulation scheme investigated here it hardly represents an exhaustive examination of the performance of these algorithms. But, BPSK is a rich modulation scheme from a cyclostationary perspective, exhibiting both conjugate and non-conjugate features as well as features associated with the carrier frequency, the bit rate and several combinations of the two. Thus, it is considered an excellent subject for initial investigation with other modulation schemes saved for follow-on work.

Regardless of modulation scheme, three simple parameters dominate the performance of TDOA and FDOA estimators: the type of interference, the relative strength of that interference and the amount of data available to process. In a benign situation, slightly overlapping or no interference with high SINR and long collect lengths represent the best situation an estimator could encounter. On the contrary, completely co-channel and co-temporal, partially co-spatial interference with low SINR and short collect lengths represent the more realistic and decidedly poor situation. Therefore, in order to properly exercise these algorithms in pursuit of the first two objectives and allow for easy

comparison to previous work, two of the most stressing of environments are used: wideband interference and narrowband interference. These two environments represent similar scenarios used in [4] and [22] thus facilitating the comparison of the results.

2.   Wideband Interference Environment

Environment I tests the algorithms in a wideband interference environment. In this case, the bandwidth of the SNOI is nearly twice that of the SOI, ensuring complete spectral and temporal overlap as shown in Figure 6-1. Note that the presence of a second signal is not obvious in this plot of the spectral density of the received signal for receiver #1. In fact, the BPSK spectrum that appears in the plot is primarily due to the SNOI, not the SOI, with the only evidence of the SOI being the small amount of additional energy that causes the slight spreading toward the origin of the SNOI main lobe.
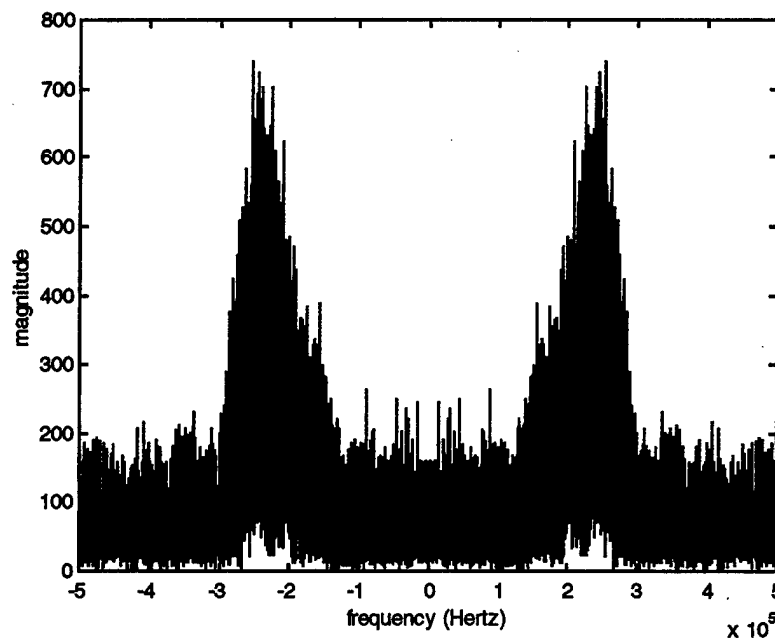
Figure 6-1 – Power spectral density of Environment I at SINR = -3 dB

87

In addition, the TDOA of the SOI and the SNOI are separated by only 8 samples, creating some spatial overlap, while their FDOA vary by $\frac{2}{256}$ f_s, making the separation of the parameters of these two signals difficult for traditional techniques as shown in Chapter II . Note as a further example, in Figure 6-2 that the CAF resolves both peaks in this case. However, the SNOI peak is dominant resulting in an incorrect estimate for both TDOA and FDOA for the SOI. As the SINR decreases, the SNOI peak dominates more, causing more consistent errors in the estimate. To assess the performance of the three new cyclostationary algorithms, the SNR is set throughout this environment at 0-dB while the SIR starts at 0-dB and decreases through -3 dB, -10 dB and -13 dB, representing an increasingly stronger interferer. This results in SINRs that cover - 3 dB, - 4.8 dB, -10.4 dB and - 13.2 dB.

There are seven collect lengths for which the algorithms are tested. Starting with 256 samples which represents 256 μs, the collect lengths increase by powers of 2 to 16384 samples, representing 16.384 ms.
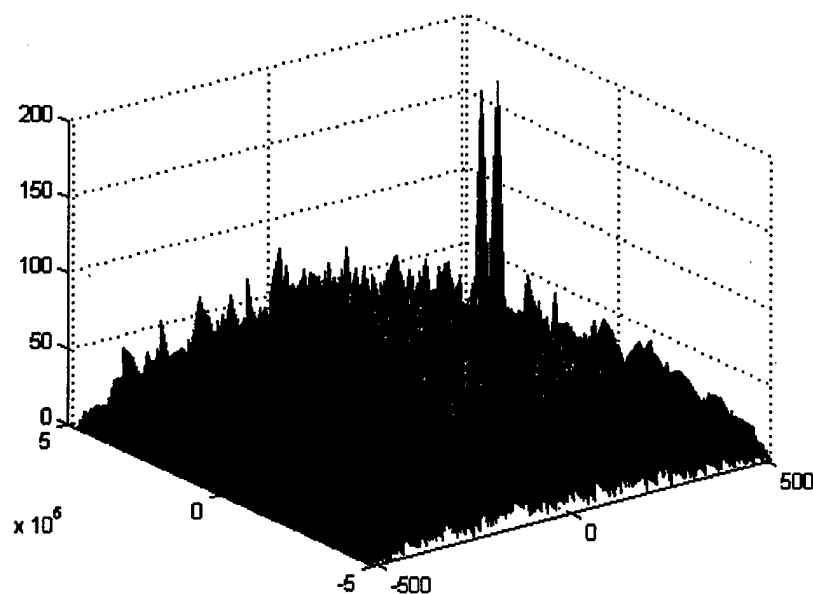
Figure 6-2 – CAF of Environment I, SINR = -3 dB with 512 samples

3. Narrowband Interference Environment

In Environment II, the interferer, a narrowband SNOI, has 10% of the bandwidth of the SOI. In this case, the ability of the algorithms to tolerate more focused interference can be seen. Rather than the complete spectral and temporal overlap of the wideband case, which results in some of the SNOI energy lying outside the bandwidth of the SOI, the energy of the narrowband SNOI lies completely within the bandwidth of the SOI. This creates a different type of problem for estimators seeking to measure the parameters of a weak SOI in the presence of a strong much more spectrally concentrated SNOI. In the wideband case, some of the energy of the SNOI can be eliminated by filtering the inputs to the algorithm with a bandpass filter whose center frequency is equal to the carrier of the SOI and with bandwidth equal to the bandwidth of the SOI. In the narrowband case, this is not possible. The effects of that energy concentration can be seen in Figures 6-3 and 6-4, the spectral density of the received signal and an example plot of the CAF for this environment.

In the spectral density plot, the narrowband SNOI is obvious as its main lobe is much narrower and rises significantly higher than the overlapping main lobe of the SOI. This however does not translate well to a separation in the peaks of the CAF. In fact, the peaks appear to combine even more in this case than the wideband case. At this point, the SNOI peak is again dominant, causing an incorrect estimate for the parameters of the SOI. This smearing worsens with lower SINR and eventually causes the estimator to report the presence of one signal instead of two. Additionally, the estimates often obtained are good for neither the SOI nor the SNOI due to the combination of the energy from each of the signals' CAF peaks.

The same SNR, SIR and SINR levels are used in the narrowband case as were found in the wideband case. This allows for a proper comparison of the performance of the algorithms in both cases. In addition, for the same reason, the collect lengths remain the same.
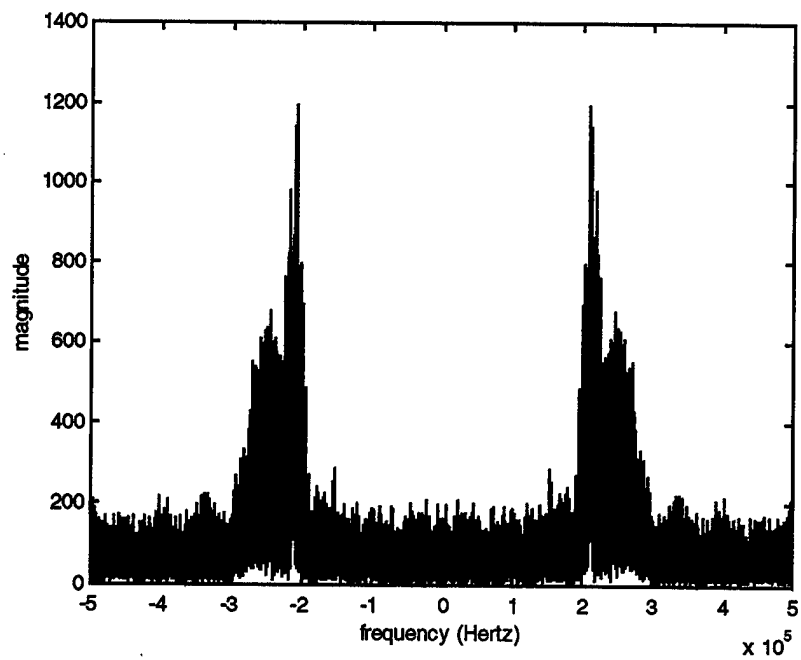
Figure 6-3 – Power spectral density of Environment II at SINR = -3 dB
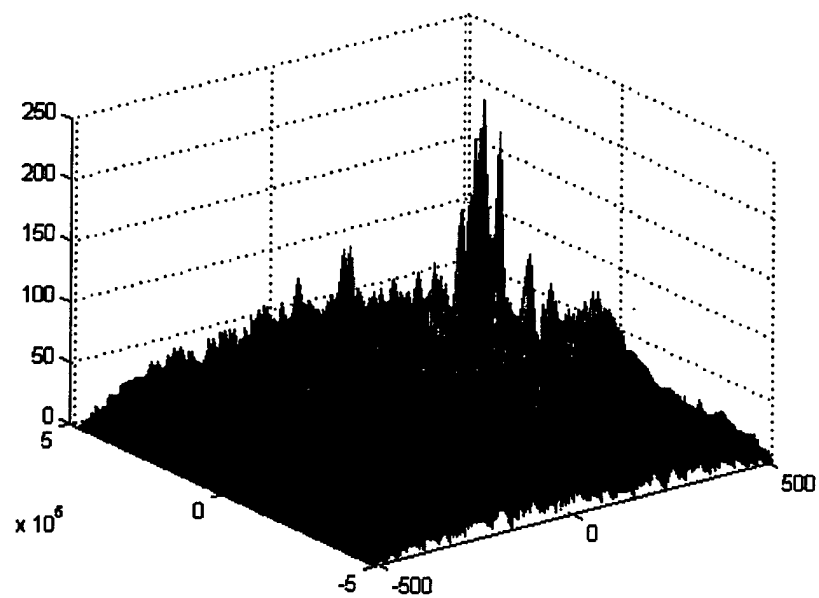
Figure 6-4 – CAF of Environment II, SINR = -3 dB with 512 samples

C. TESTING

1. Stability of Estimates

A key consideration in the design of the MCT was the number of trials per case needed. The driving factor in selecting that number is the degree of stability exhibited by the measure of the variance in the estimate for TDOA and FDOA, produced by averaging the error results over all the trials (see next section for discussion of averaging technique). Initially, 400 trials were used based upon testing conducted in [22]. Unfortunately and most likely due to the combination of more stressing environments and different algorithms tested, the 400 trials did not produce a stable estimate of the variance. This is obvious in the inadequately damped sinusoid of Figure 6-5, a plot of the cumulative sum of the square error over the trial number, versus the trial number. An adequate number of trials would produce little variation in the final few values on the plot (i.e. a well-damped sinusoidal function). For these algorithms, 400 trials was inadequate for such a curve.
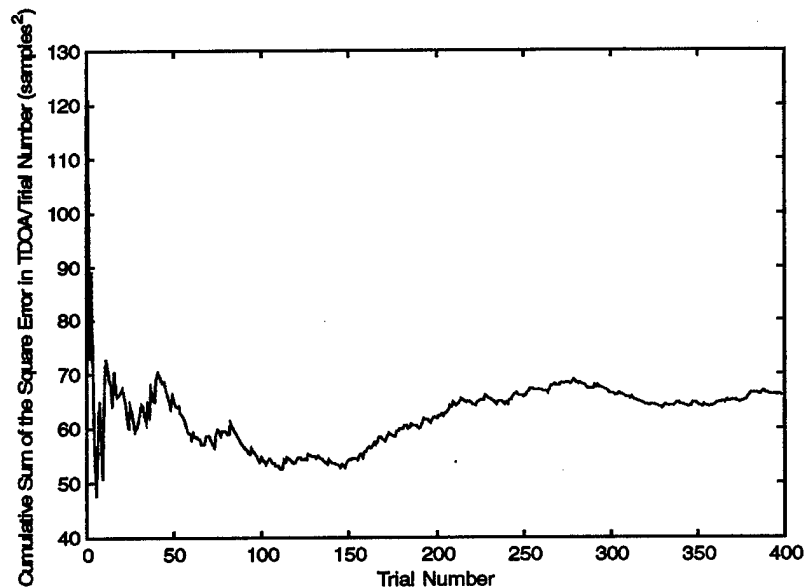
Figure 6-5 – Stability plot - TDOA, 400 trials, Env. I, SINR = -3 dB, 512 samples

Upon further investigation of [4], it appeared that 1000 trials produced stable estimates for algorithms similar to those developed here. Therefore with an additional 200 trials added to the 1000 for margin, the resulting stability was sufficient. At its worst, the variation in the average error is less than 2% for the TDOA estimate for the wideband interference case, SINR = -3 dB and 512 samples. At its best it is less than 0.25% for the estimate of FDOA for the wideband case, SINR = -3 dB and 1024 samples and several other cases. Both stability plots for these extremes can be seen in Figures 6-6 and 6-7 respectively. In all cases, the stability of the FDOA estimate exceeded that of the TDOA estimate by a factor of approximately two.
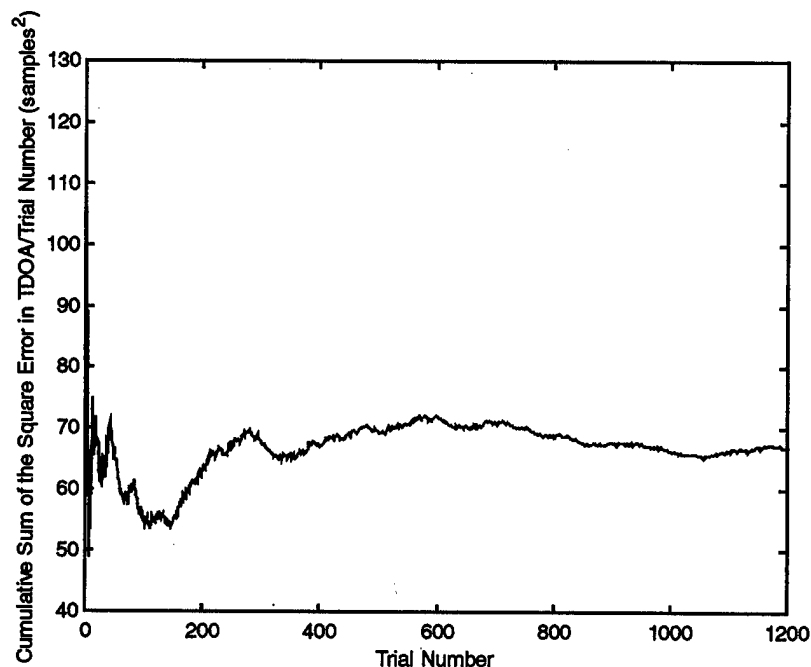
Figure 6-6 – Stability plot - TDOA, 1200 trials, Env. I, SINR = -3 dB, 512 samples
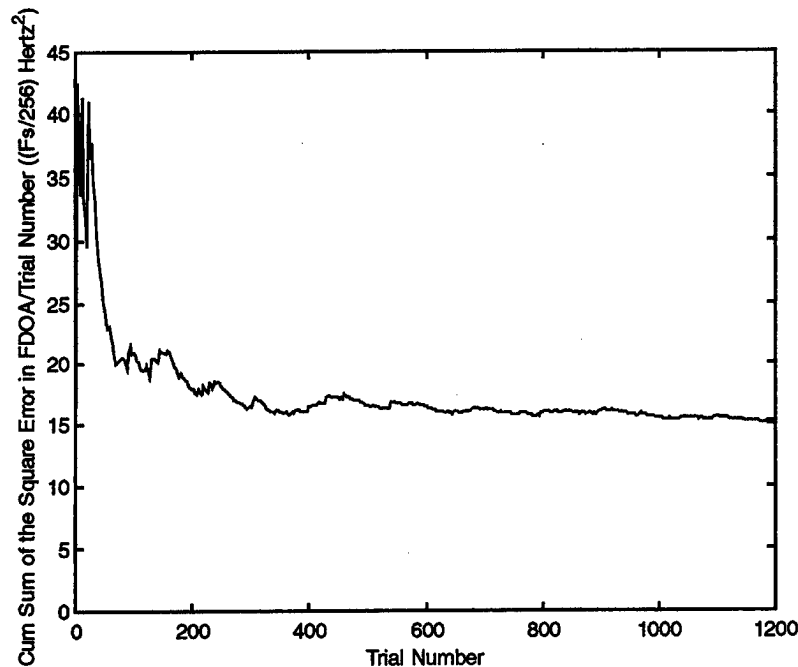
Figure 6-7 – Stability plot - FDOA, 1200 trials, Env. I, SINR = -3 dB, 1024 samples

2.   Products of Monte Carlo Testing

Ultimately, the MCT produces a measure of performance for each collect length of each of the eight cases, consisting of an environment and a SINR. To do so, each trial of the MCT produces three main products: a $D\text{-}f_d$ – plane, $\hat{D}$ and $\hat{f}_d$, the MLEs for TDOA and FDOA, ε_{TD} and ε_{FD}, the error in the TDOA and FDOA estimates. Each of the 1200 trials, that make up each case produces a $D\text{-}f_d$ - plane, similar to the CAF plane, that is the manifestation of the maximization of the cyclostationary TDOA-FDOA algorithm over time-delay, D and Doppler, f_d. Figure 6-8 shows an example of this plane. This plane peaks at a point that is indicative of the maximum likelihood estimates for the TDOA and FDOA for the SOI.

93
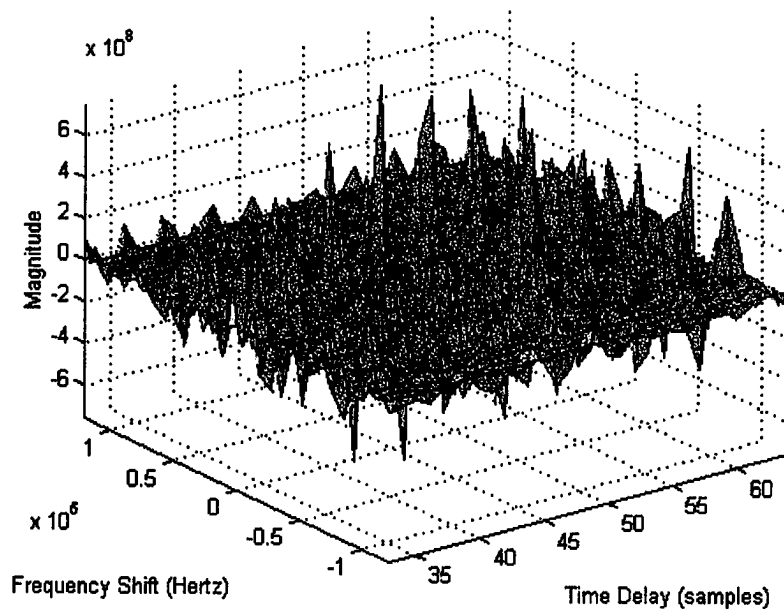
Figure 6-8 – Example of D-f_d – plane for Env. I, SINR = -3 dB, 1024 samples

The maximum likelihood estimates for TDOA and FDOA come from this plane as the value for D and f_d that produces the peak in the D-f_d – plane. In Figure 6-8, the MLE for TDOA can be seen as the value along the x-axis that corresponds to the peak in the plane, a TDOA of 47 samples or 47 μs in this case. The MLE for FDOA is similarly found as the value on the y-axis that corresponds to the peak in the plane - 19.53 kHz for this example. Figures 6-9 and 6-10 show the slices of the D_f_d – plane along lines of time delay and frequency shift that clearly illustrate the TDOA and FDOA respectively.

Finally, each trial produces a measurement of the error in the estimated TDOA and FDOA by finding the absolute value of the difference in the measured TDOA and FDOA versus the actual TDOA and FDOA. For the example begun in Figure 6-8 and continuing through Figures 6-9 and 6-10, those errors are ε_{TDOA} = 3 samples or 3 μs and ε_{FDOA} = 0 Hertz. Each trial thus produces a D-f_d – plane, from that, an MLE for both TDOA and FDOA and finally, from the MLEs, a quantitative measurement of the error in the estimate either in samples for TDOA or in Hertz for FDOA.

94
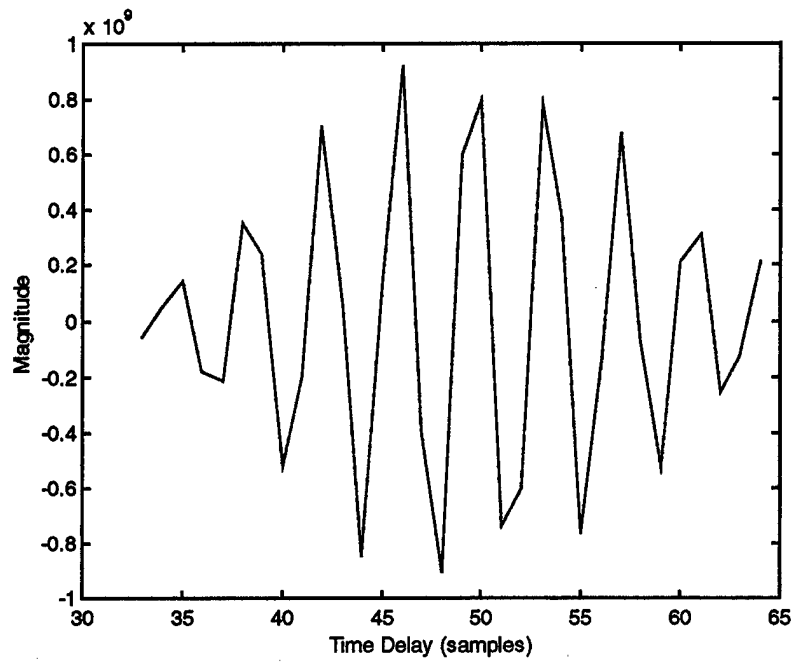
Figure 6-9 – Slice of D_f_d – plane along the x-axis to illustrate MLE of TDOA
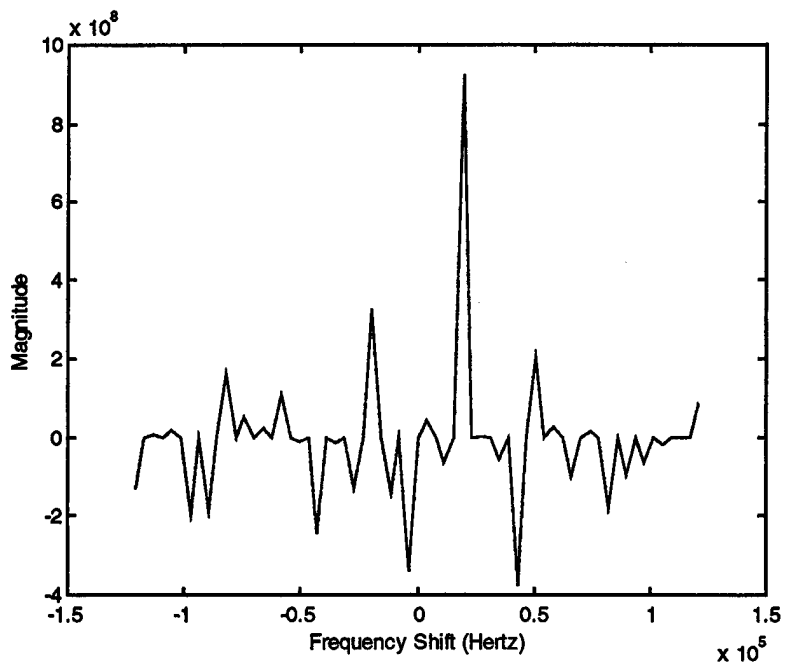
Figure 6-10 - Slice of D_f_d – plane along the y-axis to illustrate MLE of TDOA

Therefore, for each Environment/SINR case at each of the seven collect lengths, 1200 errors for TDOA and FDOA estimation are produced which in turn, form the basis for the Root Mean Square Error (RMSE). The RMSE is the ultimate product of the MCT and is the parameter used to compare the performance of the newly derived algorithms to that of the CAF and the stationary CRB. The comparison to previously derived cyclostationary TDOA algorithms is addressed in the next chapter through a normalization of the RMSE.

The RMSE for TDOA has the form of the standard Root Mean Square Error

$$\text{RMSE}_{\text{TDOA}}(s, dB) = 20 \log_{10}\left[\frac{1}{L}\sum_{l=1}^{L}\left[\left(D - \hat{D}_l\right)\right]^2\right]^{1/2} \qquad (6\text{-}1)$$

where L is the number of trials, D is the actual TDOA in seconds, and $\hat{D}_l$ is the MLE for the TDOA in the lth trial in seconds.

The performance parameter for FDOA, $\text{RMSE}_{\text{FDOA}}$ is similar to $\text{RMSE}_{\text{TDOA}}$ differing only in the units. $\text{RMSE}_{\text{FDOA}}$ has the form

$$\text{RMSE}_{\text{FDOA}}(Hz, dB) = 20 \log_{10}\left[\frac{1}{L}\sum_{l=1}^{L}\left[\left(f_d - \hat{f}_{d_l}\right)\right]^2\right]^{1/2} \qquad (6\text{-}2)$$

where again L is the number of trials, f_d is the actual FDOA in Hertz, and $\hat{f}_{d_l}$ is the MLE of the FDOA for the lth trial in Hertz.

Thus, with two Environments and four SINR levels per Environment creating eight distinctive cases, each with seven collect lengths tested, the results of the MCT consist of two plots for each case, one for $\text{RMSE}_{\text{TDOA}}$ and one for $\text{RMSE}_{\text{FDOA}}$. Each of these sixteen plots (eight for $\text{RMSE}_{\text{TDOA}}$ and eight for $\text{RMSE}_{\text{FDOA}}$) contains five series of seven points each. The five series represent the results for I2DMLE, A2DMLE#1, A2DMLE#2, CAF and stationary CRB with the seven points per series corresponding to the results obtained for the seven collect lengths for that case.

D. RESULTS

1. Performance in Environment I - Wideband Interference

Figures 6-11, 6-12, 6-13 and 6-14 show the results for RMSE$_{TDOA}$ Environment I,
SINR = -3 dB, SINR = -4.8 dB, SINR = -10.4 dB and SINR = -13.2 dB respectively.
Following that, Figures 6-15, 6-16, 6-17 and 6-18 illustrate the RMSE$_{FDOA}$ for
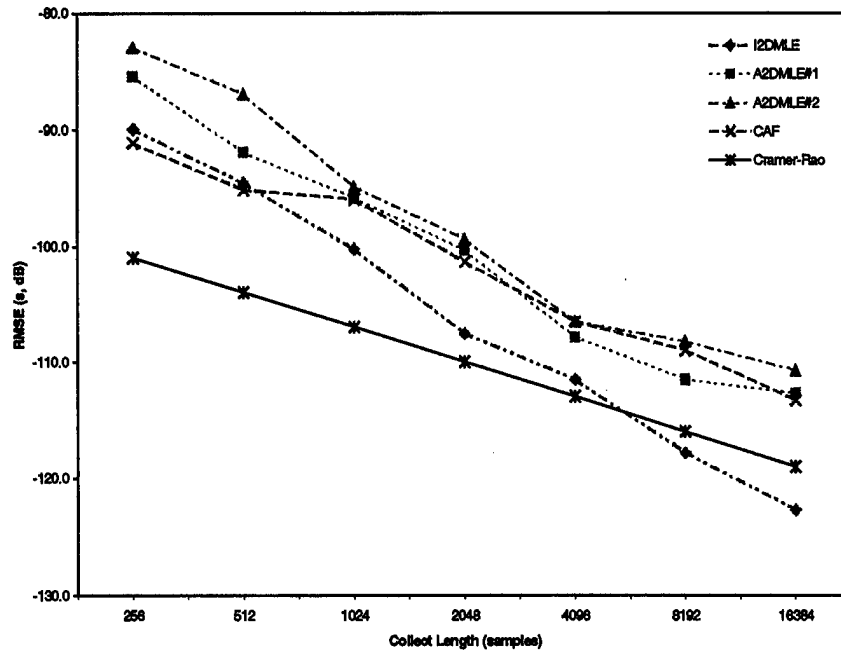Environment I, SINR = -3 dB, SINR = -4.8 dB, SINR = -10.4 dB and SINR = -13.2 dB
respectively. Note that the x-axis for all these plots is the collect length and is plotted as a
log$_2$-scaled axis to simplify the visualization of data taken at collect lengths that range
from 2^8 to 2^{14} samples.
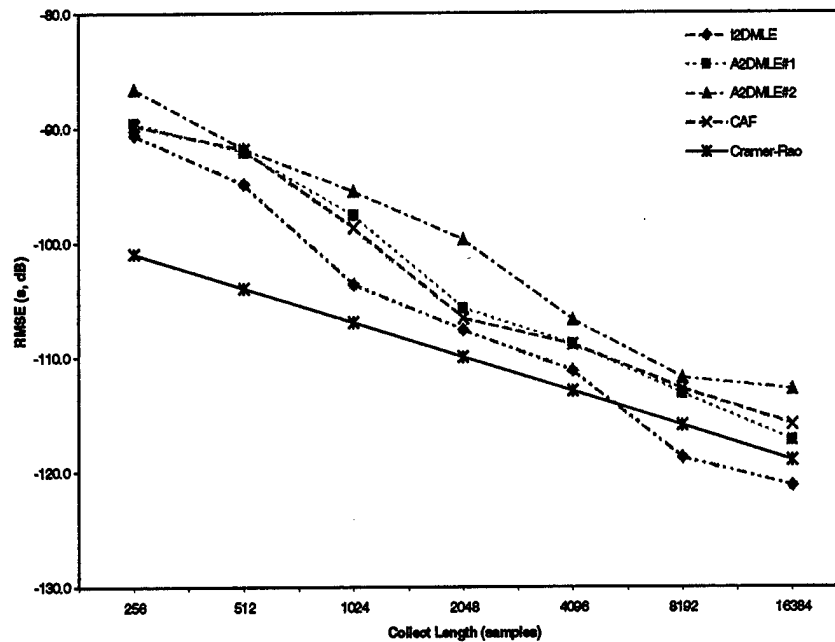
Figure 6-11 – RMSE$_{TDOA}$ – Environment I, SINR = -3 dB
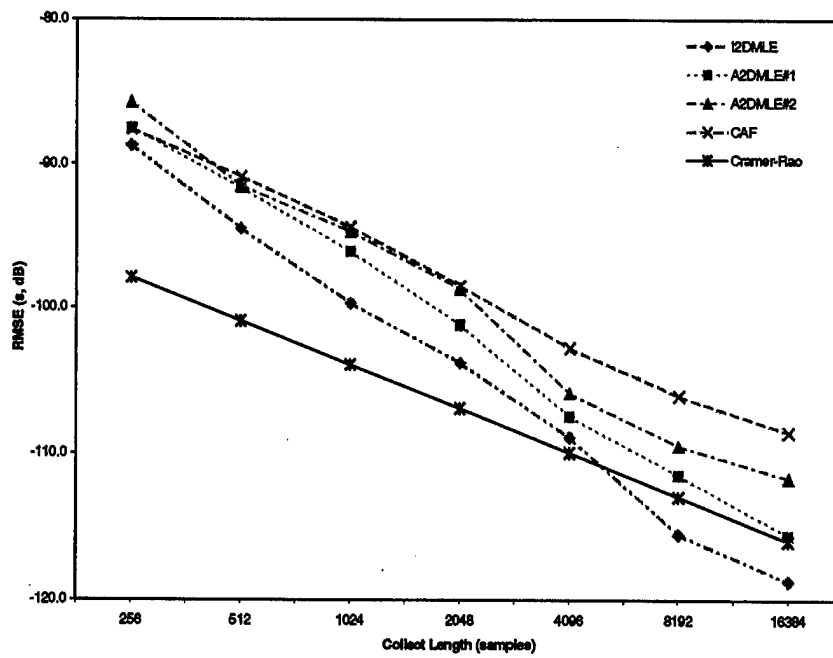
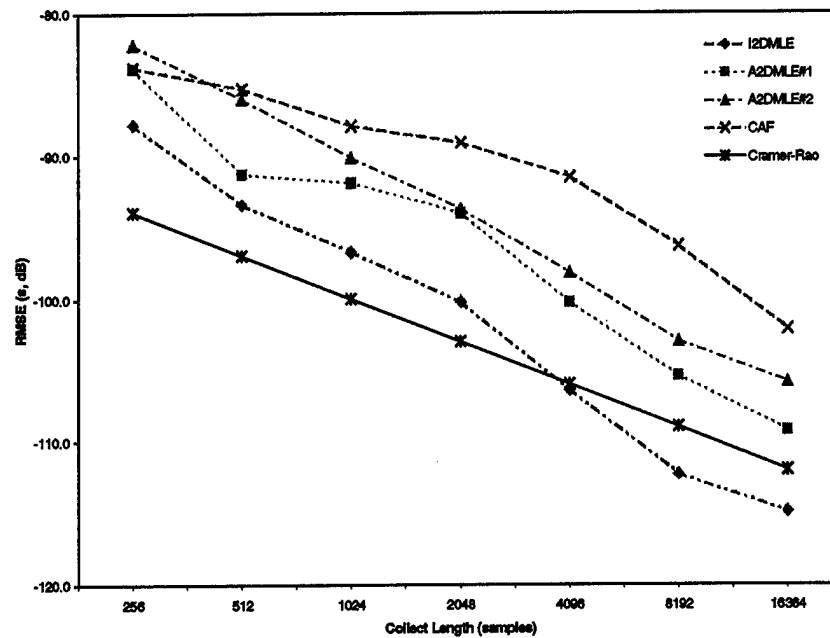Figure 6-12 – RMSE$_{TDOA}$ – Environment I, SINR = -4.8 dB
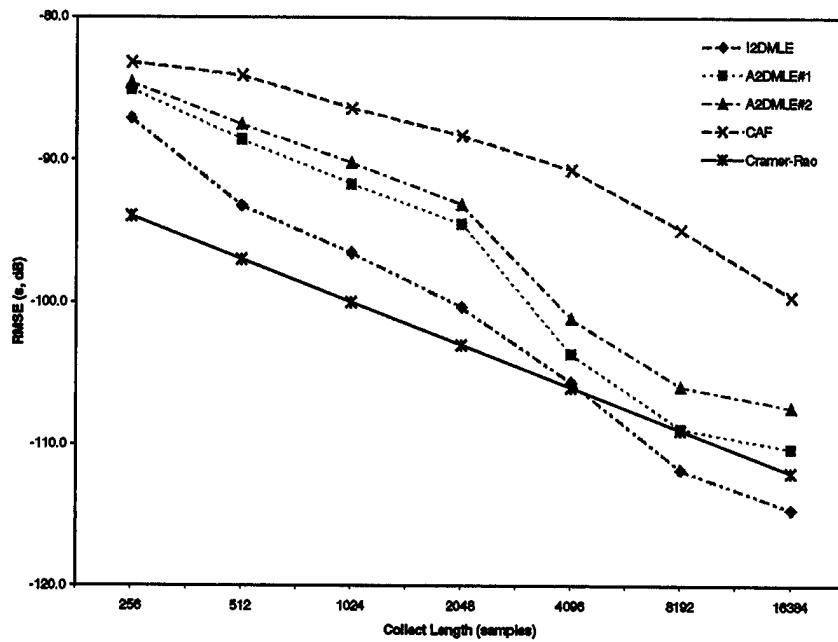
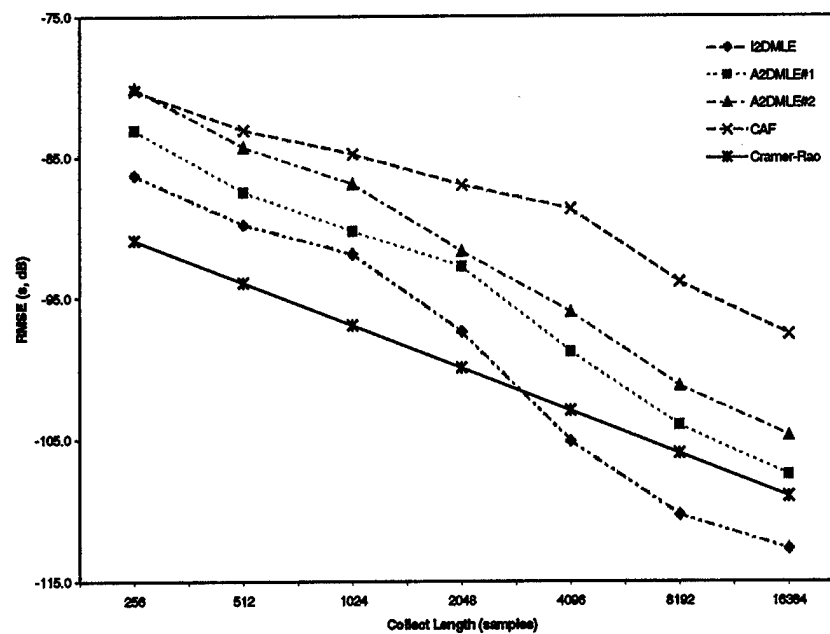Figure 6-13 – RMSE$_{TDOA}$ – Environment I, SINR = -10.4 dB

98
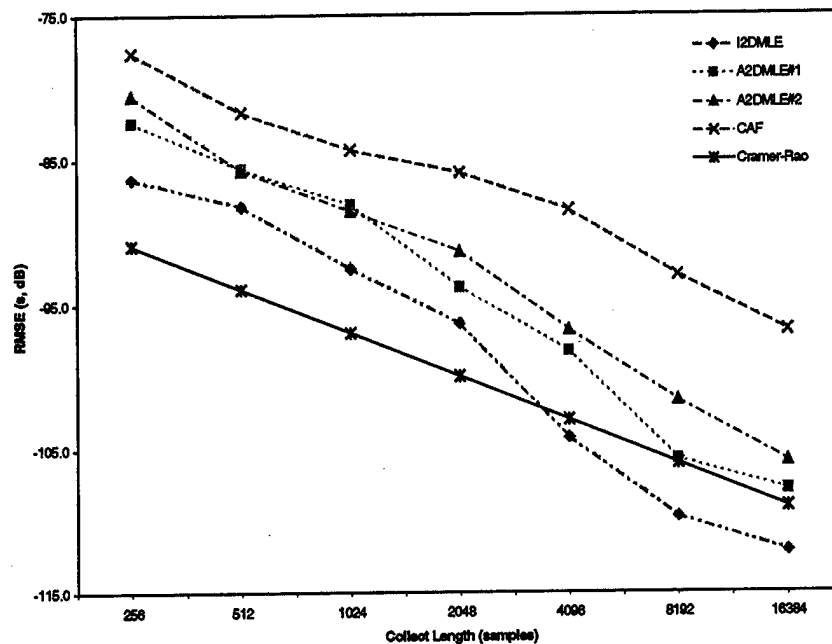
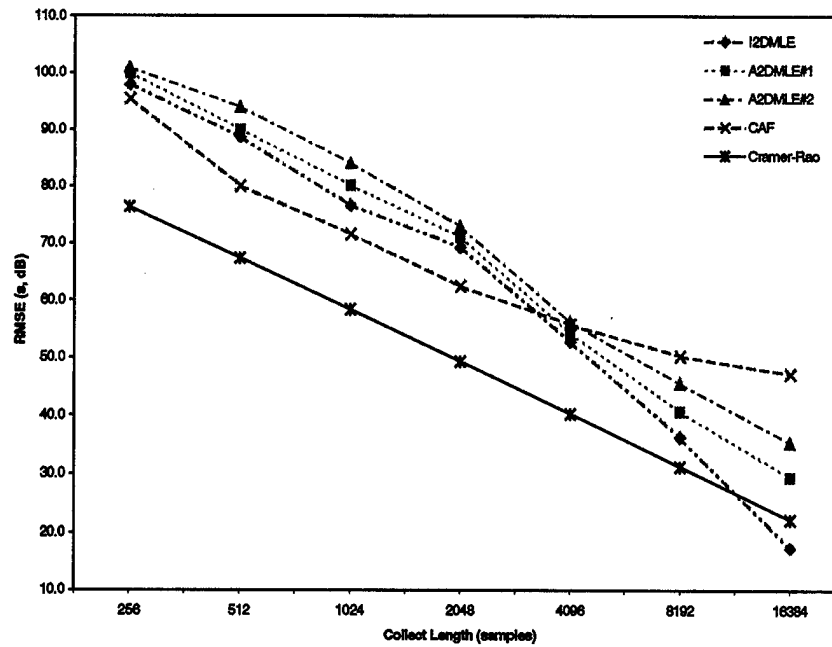Figure 6-14 – RMSE$_{TDOA}$ – Environment I, SINR = -13.2 dB
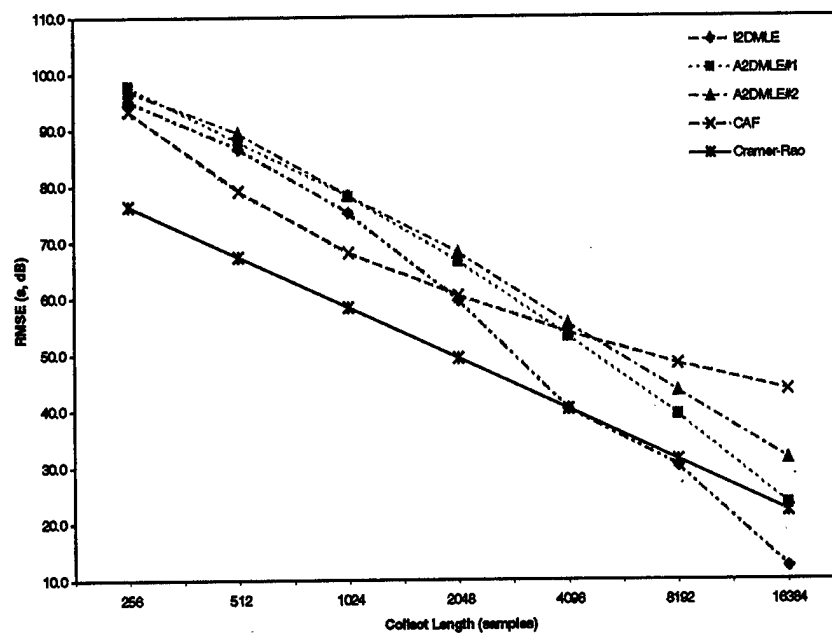
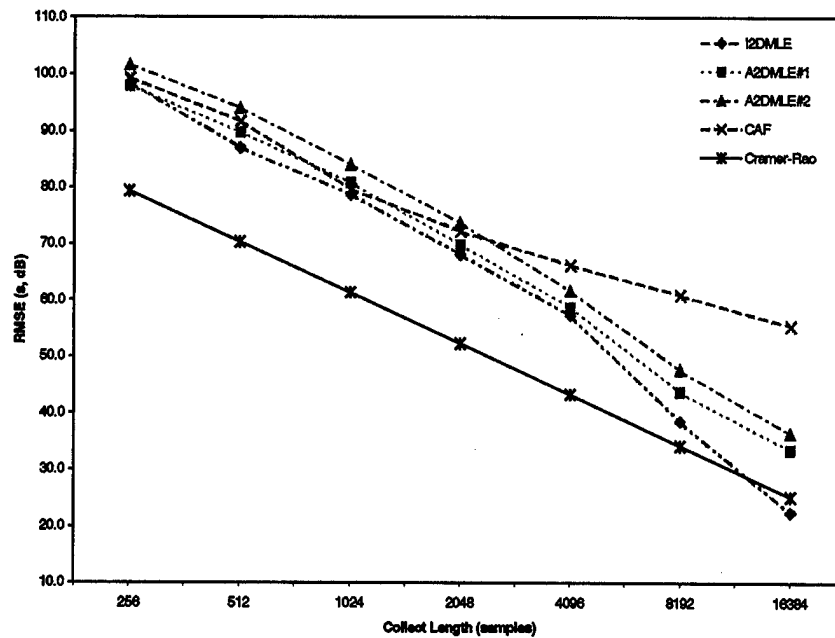Figure 6-15 – RMSE$_{FDOA}$ – Environment I, SINR = -3 dB
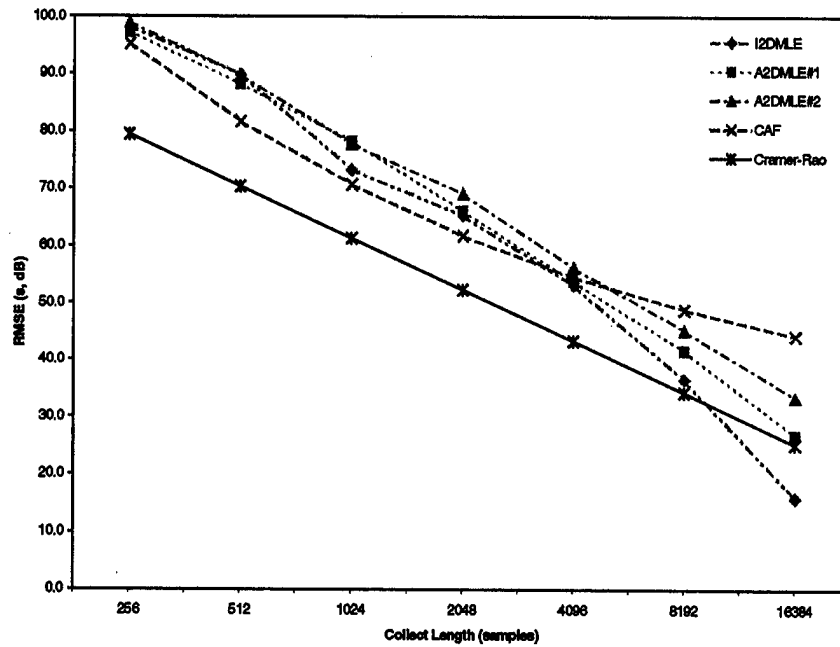
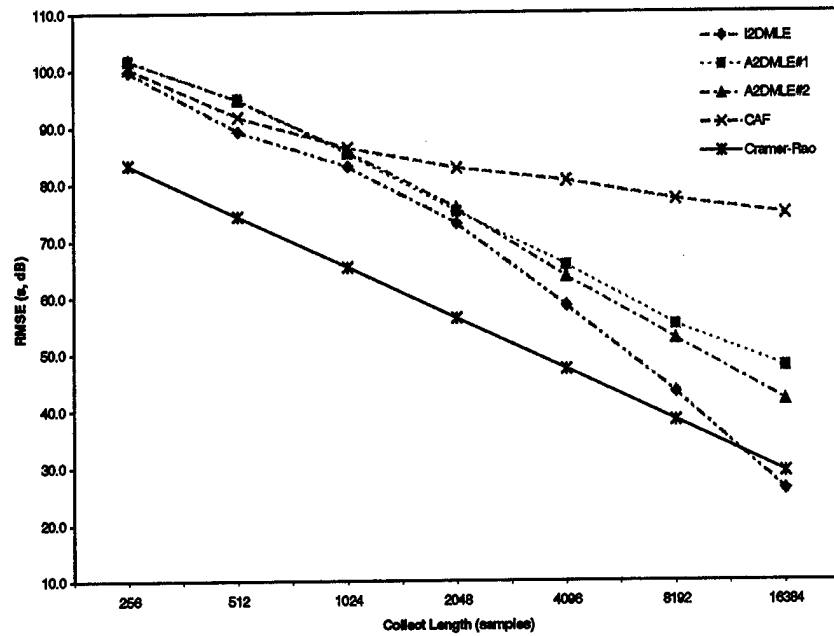Figure 6-16 – RMSE$_{FDOA}$ – Environment I, SINR = -4.8 dB
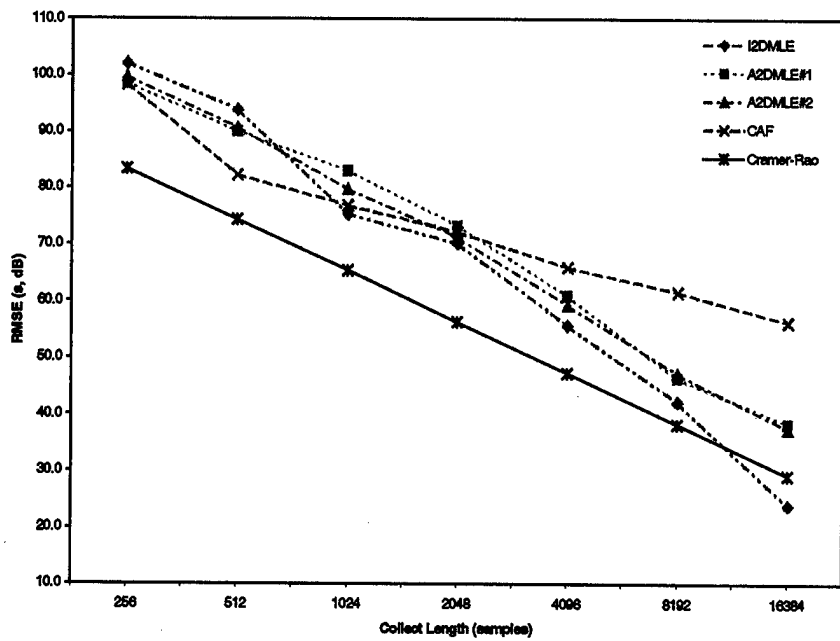
Figure 6-17 – RMSE$_{FDOA}$ – Environment I, SINR = -10.4 dB
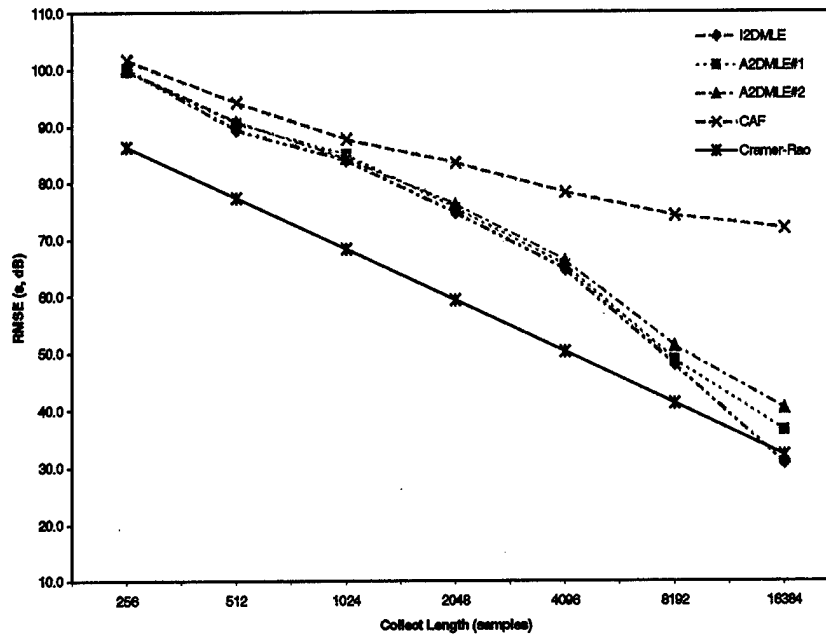
Figure 6-18 – RMSE$_{FDOA}$ – Environment I, SINR = -13.2 dB

Because the algorithms were interpolated on the frequency axis by a factor of 8 at each collect length, their performance is tied directly to the minimum frequency resolution that each collect length employed with the minimum ε_{FDOA} = 1*Δf per trial. Thus, the minimum ε_{FDOA} ranges from 1*Δf = 488 Hz at N = 256 to 1*Δf = 7.6 Hz at N = 16384. The level of interpolation is important as it affects the RMSE$_{FDOA}$ reported in the next section. With more interpolation in some cases it is possible to produce smaller errors in the estimate of FDOA and thus lower the RMSE. A factor of 8 was chosen as a compromise between accuracy and computational burden.

2. Performance in Environment II - Narrowband Interference

Figures 6-19, 6-20, 6-21 and 6-22 show the results for RMSE$_{TDOA}$ Environment II, SINR = -3 dB, SINR = -4.8 dB, SINR = -10.4 dB and SINR = -13.2 dB respectively. Finally, Figures 6-23, 6-24, 6-25 and 6-26 illustrate the RMSE$_{FDOA}$ for Environment II, SINR = -3 dB, SINR = -4.8 dB, SINR = -10.4 dB and SINR = -13.2 dB respectively.

101

Figure 6-19 – RMSE$_{TDOA}$ – Environment II, SINR = -3 dB
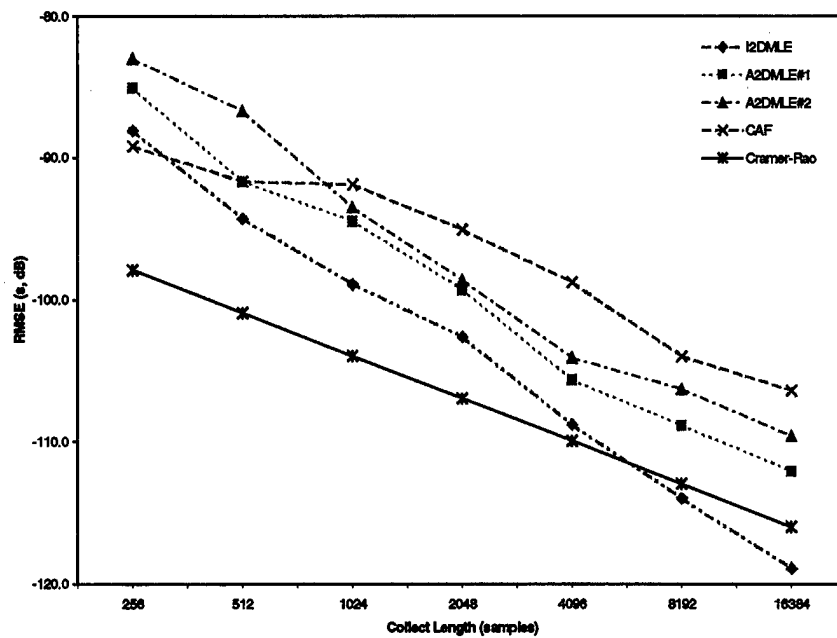
Figure 6-20 – RMSE$_{TDOA}$ – Environment II, SINR = -4.8 dB

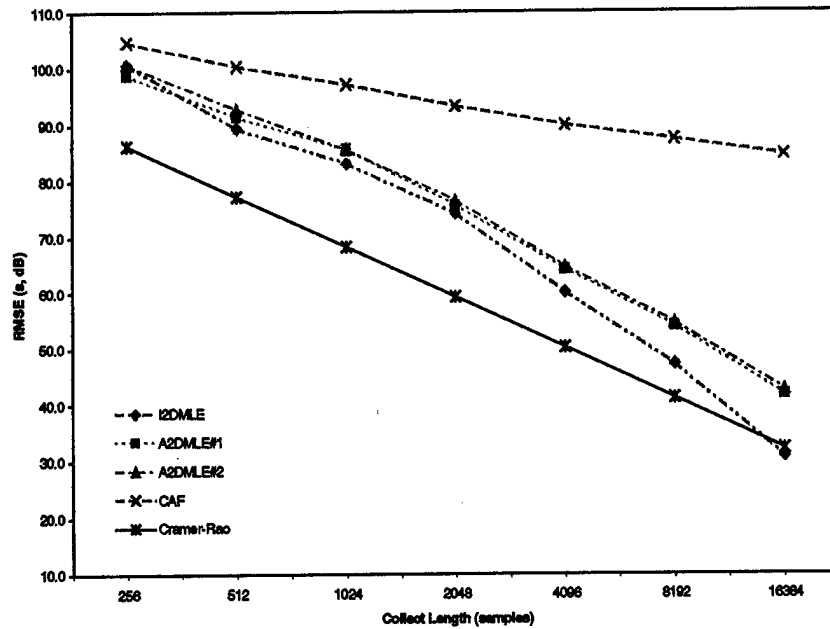Figure 6-21 – RMSE$_{TDOA}$ – Environment II, SINR = -10.4 dB

Figure 6-22 – RMSE$_{TDOA}$ – Environment II, SINR = -13.2 dB

103

Figure 6-23 – RMSE$_{FDOA}$ – Environment II, SINR = -3 dB

Figure 6-24 – RMSE$_{FDOA}$ – Environment II, SINR = -4.8 dB

Figure 6-25 – RMSE$_{FDOA}$ – Environment II, SINR = -10.4 dB

Figure 6-26 – RMSE$_{FDOA}$ – Environment II, SINR = -13.2 dB

105

VII. OBSERVATIONS AND CONCLUSIONS

A. COMMENTS ON MONTE CARLO RESULTS

1. Ideal vs. Approximation

I2DMLE represents the theoretical maximum likelihood algorithm while A2DMLE#1 and A2DMLE#2 are a close and more distant approximation respectively. Consequently, I2DMLE should consistently outperform the two approximations, which turns out to be the case in all instances. The main objective of the first approximation, A2DMLE#1 was to maintain all six terms from I2DMLE, substitute simply for the pure signal components and assess the performance hoping to mimic closely that of the ideal algorithm. A2DMLE#1 does in fact follow closely, the trends exhibited by the ideal algorithm hovering generally between 3 and 6 dB below the performance of I2DMLE in both TDOA and FDOA. The two obvious exceptions to this are first, in the higher SINR cases, the slope of A2DMLE#1 RMSE is flatter in the higher collect lengths for both TDOA and FDOA. This indicates its performance is still improving as N increases but to a lesser degree than I2DMLE. Second, in the narrowband case, A2DMLE#1 appears to loose more performance from the ideal than it does in the wideband case and suffers to a greater degree, degradation as the strength of the narrowband interference increases with increasing SINR. In general however, it is a very good, practical approximation to the ideal.

A2DMLE#2 has three main objectives in its development: (1) keep the strongest terms from A2DMLE#1 to maintain as much as possible the performance of A2DMLE#1, (2) maintain both the conjugate and non-conjugate cyclostationary exploitation for flexibility and (3) minimize the computational burden by limiting the number of terms as much as possible. With these dichotomous goals in mind the resulting three terms perform well with respect to A2DMLE#1 in most circumstances and reduce the computational burden by a factor of 2. Its performance in TDOA is more even than either the ideal or

107

the first approximation progressing with a near linear slope on the RMSE curves. It too slows its increase in performance as the collect length increases to 16384 samples as is evident by the increase in the slope of the performance line at the longest collect lengths. In the narrowband case for TDOA, it is surprisingly well behaved, with performance near or in excess of A2DMLE#1. Finally, in FDOA, the same trends found in TDOA continue but with an apparent threshold around SINR = -13 dB where it again rises back above the A2DMLE#1 line. In general, A2DMLE#2 is another good approximation resulting in reduced computational burden over A2DMLE#1 and appears to endure narrowband interference more successfully.

2.   New Cyclostationary Estimators and the Cross Ambiguity Function

Comparison with the CAF illustrates the value of cyclostationary techniques in these heavy interference environments. In general for TDOA, at shorter collect lengths and higher SINR, the CAF outperforms all but the ideal algorithm and in some cases, outperforms all three. But as collect length increases, all three cyclostationary algorithms begin to outperform the CAF until at the longest collect lengths, the difference in performance is as great as 15 to 16 dB (seconds) between I2DMLE and the CAF at SINR = -13 dB. Also, as SINR decreases, the CAF rapidly falls off, until at SINR = -13 dB, all three cyclostationary algorithms outperform the CAF at every collect length. There seemed a slight difference in the CAF performance between the wideband and the narrowband environments with the performance worse with narrowband interference.

For FDOA, the CAF actually performs better than all three cyclostationary algorithms for a longer period than was true for TDOA. At higher SINR in the wideband case, the CAF outperforms all three cyclostationary algorithms until I2DMLE crosses at N = 2048. Following that, the two approximations cross at N = 4096 and all three continue to outperform the CAF from that point. At higher SINR in the narrowband case, the CAF maintains superiority through N = 4096 when all three cyclostationary algorithms exceed it performance. Finally, for lower SINR in both the wideband and narrowband environments, the CAF performance deteriorates quickly to the point at which its results

are consistently in error and dominated completely by the parameters of the interfering signal. This is clear in the SINR = -13 dB cases where the CAF is significantly worse than all three cyclostationary algorithms.

3. New Cyclostationary Estimators and the Cramer-Rao Bounds

The three new cyclostationary algorithms perform well in comparison to the lower bound predicted by the stationary CRB. Because it is derived under the assumption that the environment is pure Gaussian and stationary in nature and because cyclostationary theory actually requires non-stationary signals in order to achieve the signal-selectivity and ultimately the processing gains needed, the stationary CRB is only useful as a qualitative comparison. While it will not produce empirical evidence as to the theoretical maximum contribution that cyclostationary techniques make over stationary, this comparison does produce a notion of the power of these new algorithms and the contribution they can make in practice.

In TDOA, the power of the cyclostationary techniques is not as evident in the shorter collect lengths and higher SINR levels as it is in the longer collect lengths and low SINR levels. The RMSE of the three algorithms all exceed that of the CRB for SINR = -3 dB, SINR = -4.8 dB and SINR = -10.4 dB for collect lengths under 4096 samples. I2DMLE begins to perform better than CRB predictions at 8192 samples for these three SINR levels. The same is true at the shorter collect length of 4096 samples for SINR = -10.4 and SINR = -13.2. Neither approximation exceeds the performance of the CRB predictions however, A2DMLE#1 does approach the CRB as the collect length increases to 16384 samples. Both wideband interference and narrowband interference produce similar results.

In FDOA, the reverse pattern appears in the wideband interference environment. I2DMLE performs exceptionally well at SINR = -3 dB exceeding the bound at 4096 samples and continuing out to 16384 samples. However, as the SINR drops, so does the performance of I2DMLE with respect to the CRB. By SINR = -13 dB, only at N = 16384

does I2DMLE exceed the bound. The two approximations again never exceed the bound however, both appear to approach the CRB as N increases to 16384 and beyond.

In the narrowband case, the relative performance of I2DMLE is worse yet. At SINR = -3 dB, only N = 16384 produces a result under the bound. This is true for each of the SINR levels with the difference between I2DMLE and the CRB narrowing as SINR increases. This leads naturally to the conclusion that the cyclostationary algorithms suffer more in narrowband interference than in wideband interference, a trait they share in common with the CAF according to Stein in [7].

The effects of interpolation on the frequency axis definitely affect the performance of the algorithm. Because only a factor of 8 was used to interpolate at each collect length, the minimum error possible for each MLE_{FDOA} range from the maximum of 488 Hz at N = 256 to the minimum of 7.6 Hz at N = 16384. It is likely that the algorithms, the CAF included, would produce RMSE much lower given a greater interpolation factor and thus approach or exceed the CRB in more cases (with the exception of the CAF which of course cannot exceed the CRB). This increased interpolation, which increases the computational burden as the square of the increase in the interpolation factor, was not pursued. It should simply be noted that the RMSE for three cyclostationary algorithms and the CAF are probably conservative estimates in light of this conclusion.

4.   Normalization and Comparison to Heritage Algorithms

In order to compare the RMSE results from above to those for previously derived cyclostationary TDOA algorithms contained in [4] and [22], it is necessary to normalize the RMSE in some way, in order to account for the difference in the bandwidth of the SOI tested here versus that used in each of the two heritage developments. The simplest method for doing involves adjusting the RMSE results for the difference in bandwidth. The bandwidth of the SOI used to test the three new cyclostationary algorithms above is 187.5 kHz. To calculate the performance in the same environments for a SOI with bandwidth of 1.875 kHz, a simple adjustment to the RMSE results is all that is needed.

Equation (7-1) shows that the simple correction factor to accommodate SOI of different bandwidths.

$$20 \log_{10}\left(\frac{187.5 \text{ kHZ}}{B_{\text{desired}}}\right) \qquad (7\text{-}1)$$

The net effect is a decrease in the RMSE for SOI of greater bandwidth and an increase for SOI of lesser bandwidth. For example, for a SOI of 1.875 MHz, the RMSE would decrease by –20 dB. For a SOI with bandwidth 18.75 kHz, the increase is 20 dB.

With this is mind, adjustment can be made for the difference in the bandwidth of the SOI here and that contained in [22]. Although the environments and SINR levels remain different, a qualitative assessment of the comparative performance is possible.

Adjusting the results of Chapter VI for the difference in bandwidth, an adjustment of +3.5 dB, it is clear that while comparable, the performance of I2DMLE and the two approximations, A2DMLE#1 and A2DMLE#2, lag behind the similar heritage algorithms by 2 to 4 dB in similar SINR conditions. At first glance it would appear that the heritage algorithms outperform those newly derived, but at closer examination, the interference environments and specifically the type of interference used here clearly are more difficult an environment in which to operate. Thus, the new algorithms more than likely perform nearly equal to those derived and tested in [22].

Note that these comparisons hold true only for TDOA. While some work into the tolerance of these the TDOA algorithms in [22] to various FDOA has been reported, little development and even less testing has occurred in true cyclostationary TDOA-FDOA, leaving no viable comparison to be made for the FDOA results.

5.   Another Look and Performance vs. Collect Length

Another method for evaluating the performance as collect length increases comes from examining the slope of the lines plotted as RMSE * collect length vs. collect length.

From this, it is easy to tell if the performance of an algorithm is increasing more or less than the collect length is increasing which in turn, gives some sense of the added benefit of collecting and processing more signal data at the cost of computational burden. If an algorithm has a TDOA performance line with shallow slope, more data improves performance at less cost than an algorithm with a relatively steep slope. For FDOA, as explained below, algorithms with slopes equal to or less than the slope of the CRB line are increasing performance better than or proportional to the increase in collect length. Those with greater slopes are not.

An abbreviated examination of this phenomena appears in Figures 7-1 through 7-8, the RMSE * collect length vs. collect length plots for TDOA and FDOA estimation in Environments I and II at SINR = - 3 dB and –13 dB. These eight plots represent the extremes of the performance investigated here and thus, conclusions about the trends in the performance of the algorithms can be noted without the need for plotting the remaining eight middle SINR cases. Again the x-axis containing the collect length is plotted as a $\log_2$-scaled axis.

Note also that because the relationships between collect length, the minimum ε_{FDOA}, and $RMSE_{FDOA}$ are more complex for FDOA than for TDOA, as explained above, the $RMSE_{FDOA}$ plots below are plotted as $\log_{10}$ vs. $\log_2$ plots to obtain a more linear relationship. Again, while a slope of zero does not indicate performance increases equally with collect length for these FDOA plots, it is obvious from the slope of the CRB lines what constitutes a consistent increase in performance with increasing collect length. The CRB lines for FDOA are thus the benchmark here.

The results in Figures 7-1 through 7-8 seem to indicate that the cyclostationary algorithms have minor thresholds at the higher SINR level. This is displayed in the stair-step pattern seen in both Figures 7-1 and 7-5. This pattern is also evident to a lesser extent in the $RMSE_{FDOA}$ plots in Figures 7-2 and 7-6 also confirming that the performance in time and frequency measurement is closely related.

For SINR = -3 dB, with the exception of A2DMLE#2 which must incur a significant increase in computational burden in order to significantly increase its performance, indicated by the sleep slope of its line after $N = 8192$, the cyclostationary

algorithms appear to mimic the CRB. Both I2DMLE and A2DMLE#1 follow the slope of the CRB, concluding at $N = 16384$ with roughly the same slope as the CRB. Two conclusions may be drawn from this: (1) I2DMLE and A2DMLE#1 will gain little in performance relative to the CRB with increasing collect length and (2) these two cyclostationary algorithms require the same increase in computational burden in order to increase performance by a set amount.

This stair-step patterns of thresholds in both TDOA and FDOA are smoothed in the low SINR level plots of Figures 7-3, 7-4, 7-7 and 7-8, dampened by the significant increase in interference at this level. For this SINR level, in TDOA performance, the three cyclostationary algorithms again follow the slope of the CRB with the exception of the two approximations at $N = 16384$ in the narrowband interference case. In FDOA, the three cyclostationary algorithms actually conclude with steeper negative slopes than the CRB. Thus though they rarely exceed the bound up to $N = 16384$, it appears that for longer collect lengths, all three would eventually exceed the CRB. In addition, it would appear that increasing collect length improves the ability of the cyclostationary algorithms to measure FDOA more so than the improvement that could be expected from a stationary-based estimator bounded by the CRB.
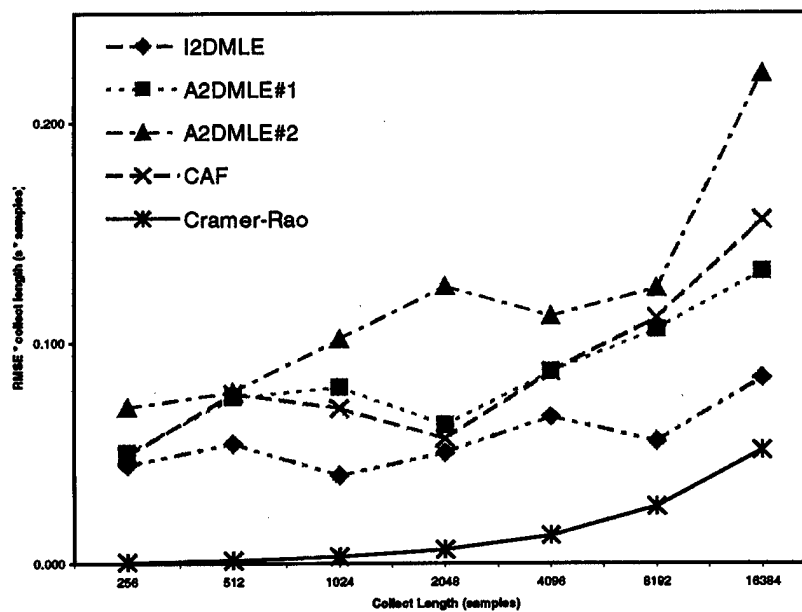
Figure 7-1 – Performance as N increases – TDOA, Environment I, SINR = -3

113
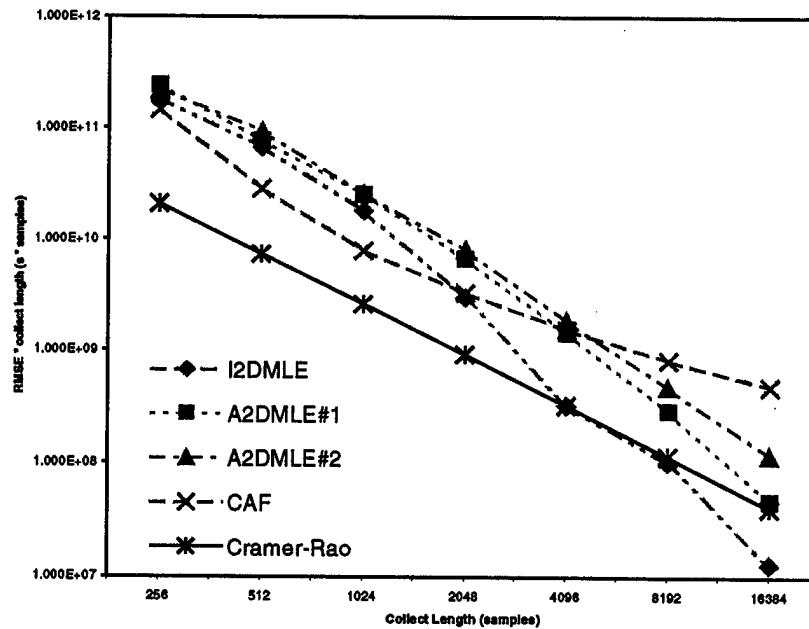
Figure 7-2 – Performance as N increases – FDOA, Environment I, SINR = -3
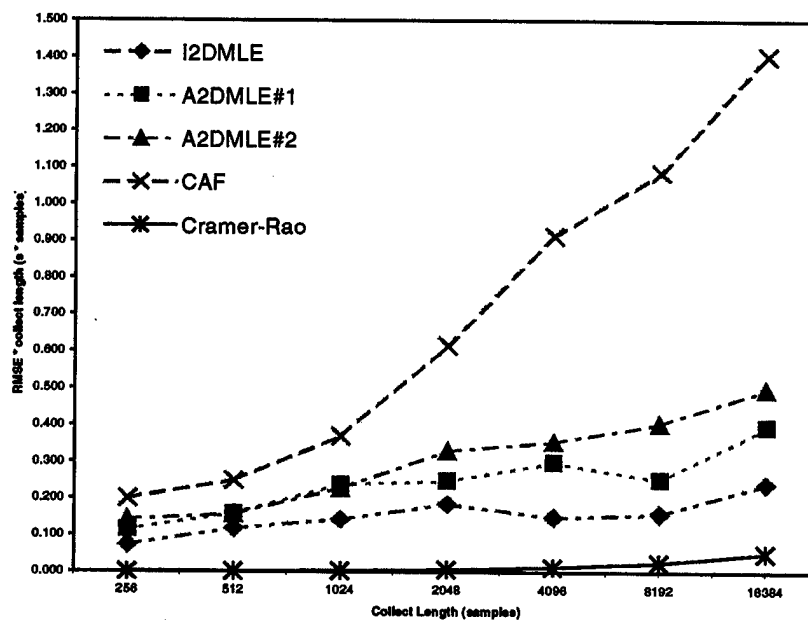
Figure 7-3 – Performance as N increases – TDOA, Environment I, SINR = -13

114
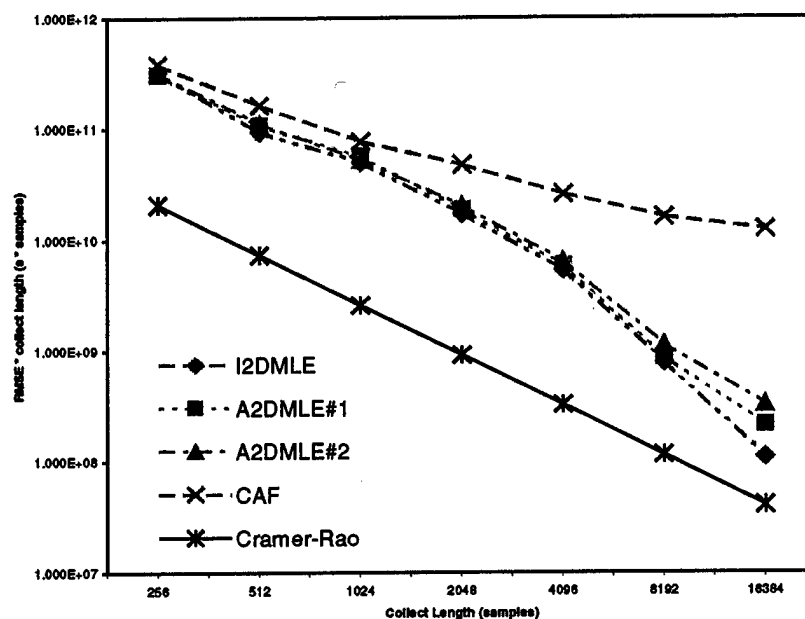
Figure 7-4 – Performance as N increases – FDOA, Environment I, SINR = -13
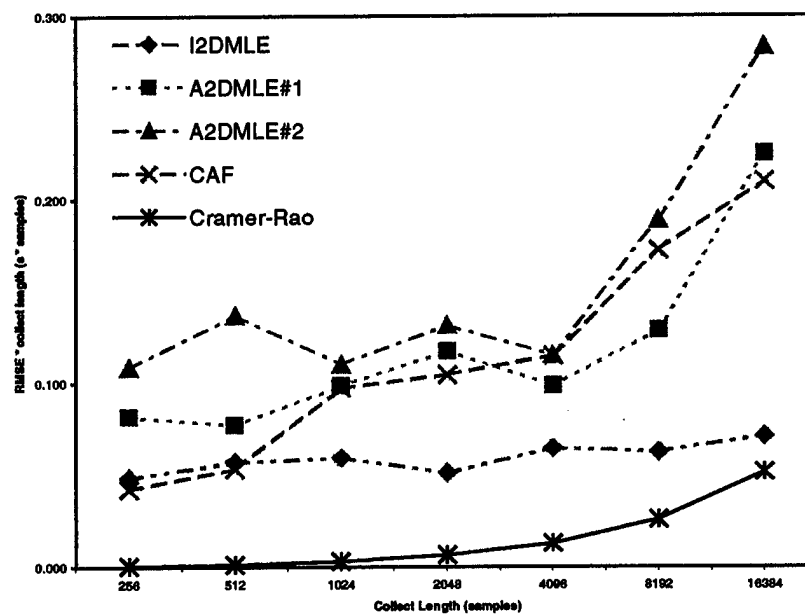
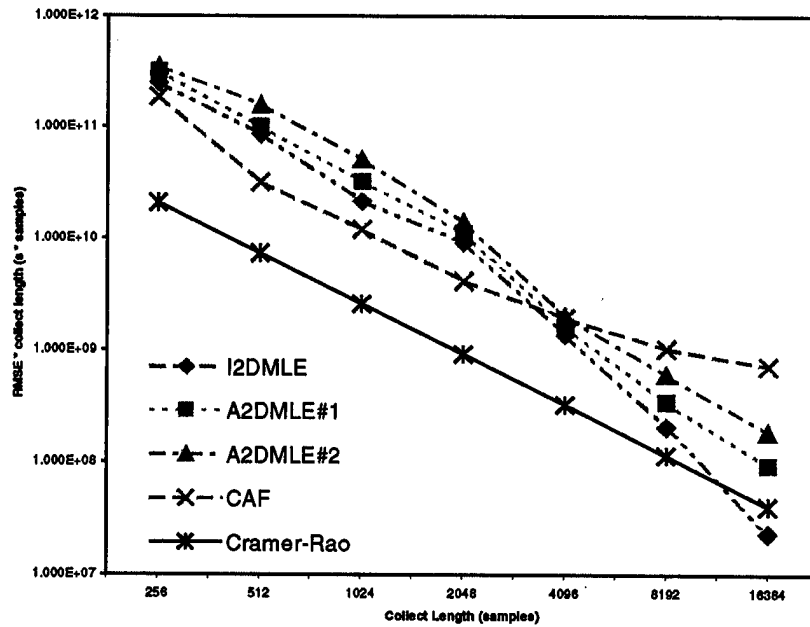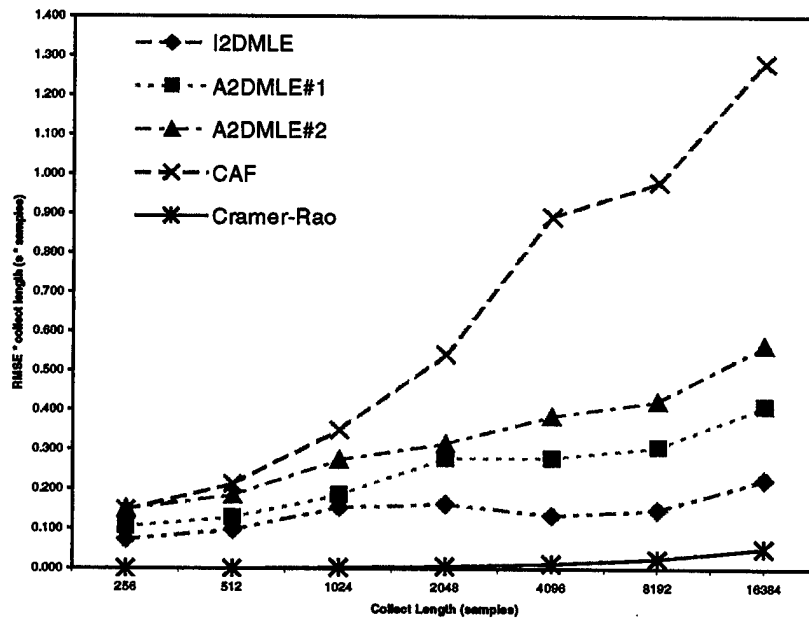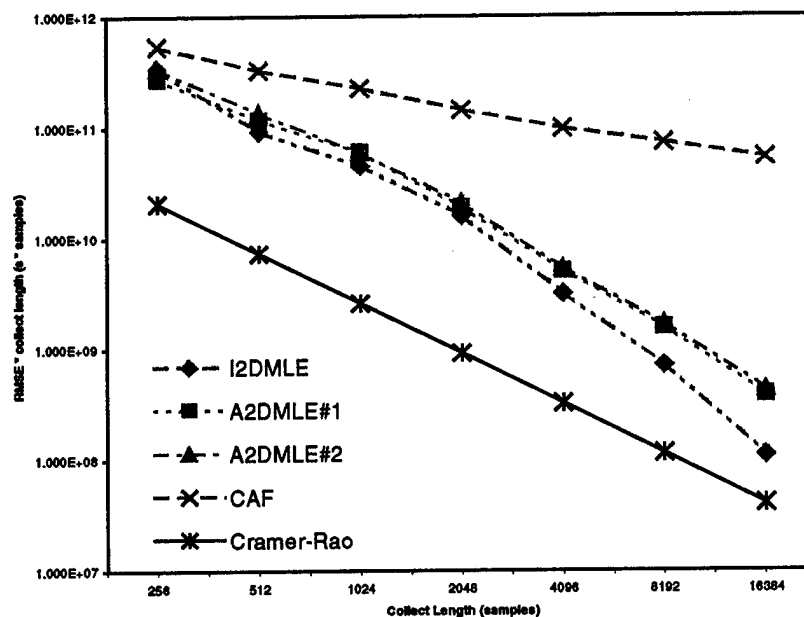Figure 7-5 – Performance as N increases – TDOA, Environment II, SINR = -3

115

Figure 7-6 – Performance as N increases – FDOA, Environment II, SINR = -3

Figure 7-7 – Performance as N increases – TDOA, Environment II, SINR = -13

116

Figure 7-8 – Performance as N increases – FDOA, Environment II, SINR = -13

6. Performance as a Function of Signal to Interference and Noise Ratio

Another comparison that is particularly constructive is that of performance as a function of SINR. One of the theoretical advantages of cyclostationary techniques is the highly signal-selective properties offered by algorithms that take advantage SOI-unique cycle frequencies in order to eliminate energy in the processing bandwidth that is not attributable to the SOI. Thus, cyclostationary algorithms should degrade in performance as SINR decreases much more gracefully than traditional techniques and the stationary CRB.

The fourteen plots in Figures 7-9 through 7-22 illustrate the $RMSE_{TDOA}$ as a function of SINR for each of the seven collect lengths. Figures 7-9 through 7-15 are for Environment I and Figures 7-16 thought 7-22 correspond to Environment II.

117
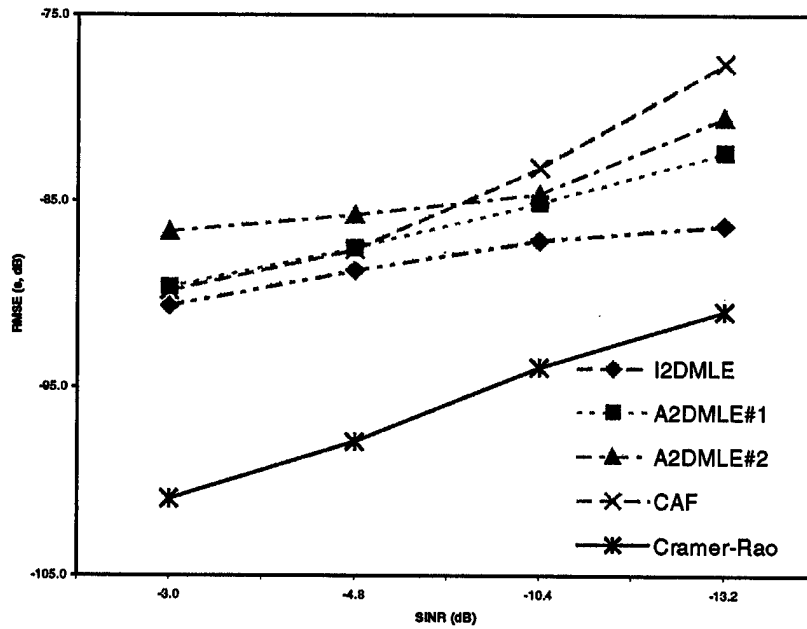
Figure 7-9 – RMSE$_{TDOA}$ vs. SINR, Environment I, $N = 256$
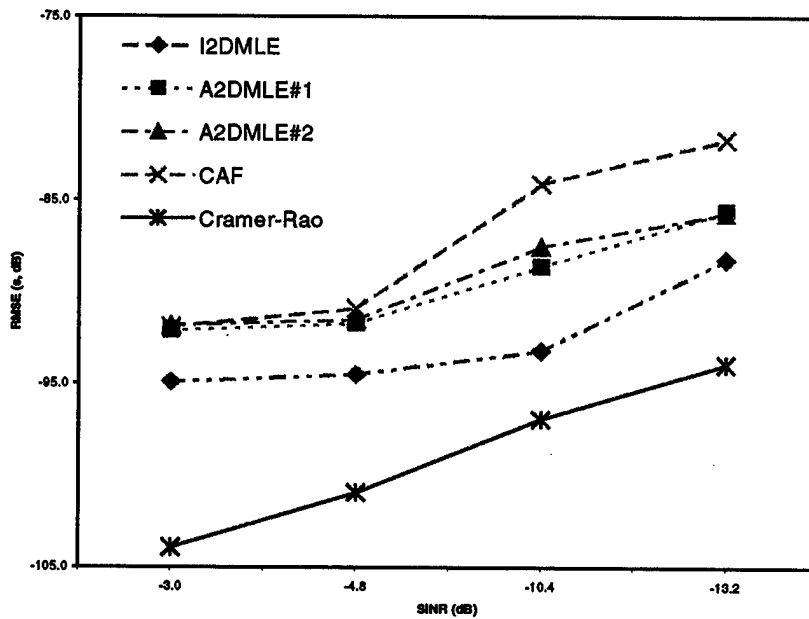
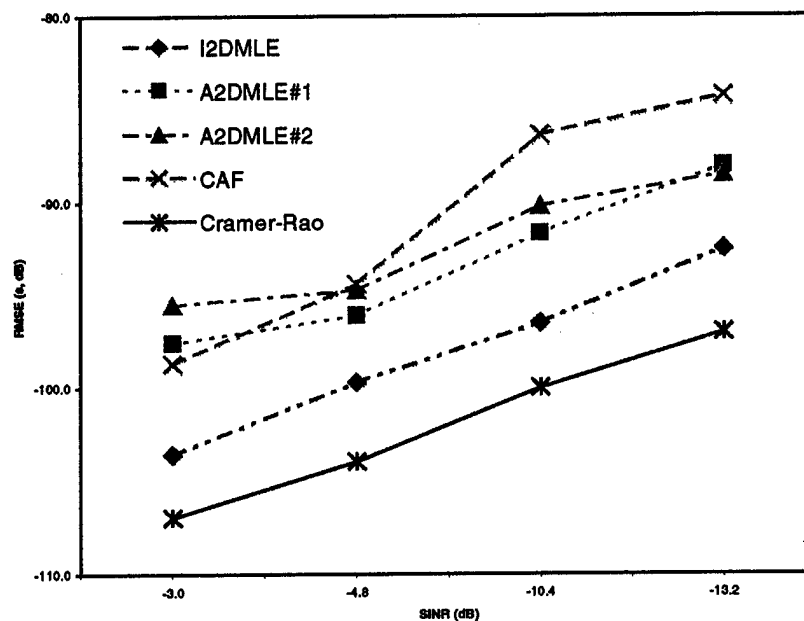Figure 7-10 – RMSE$_{TDOA}$ vs. SINR, Environment I, $N = 512$

118

Figure 7-11 – RMSE$_{\text{TDOA}}$ vs. SINR, Environment I, $N = 1024$
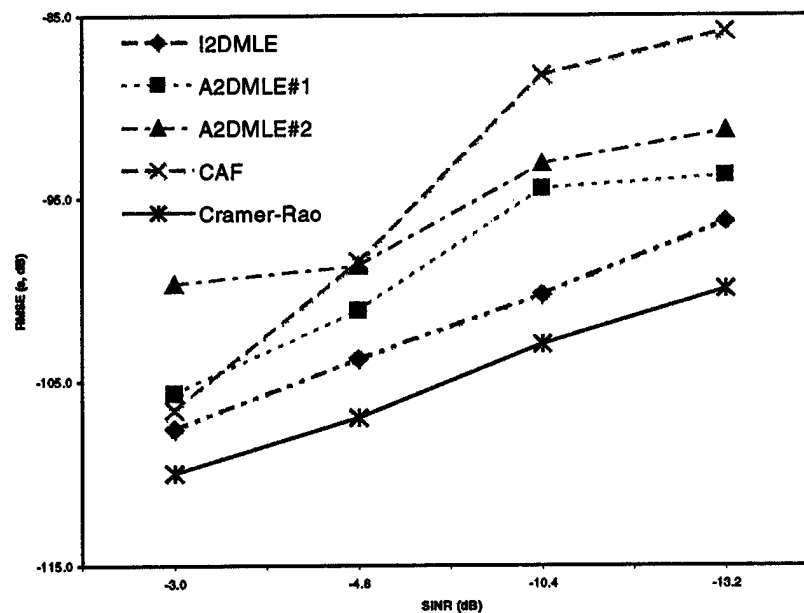

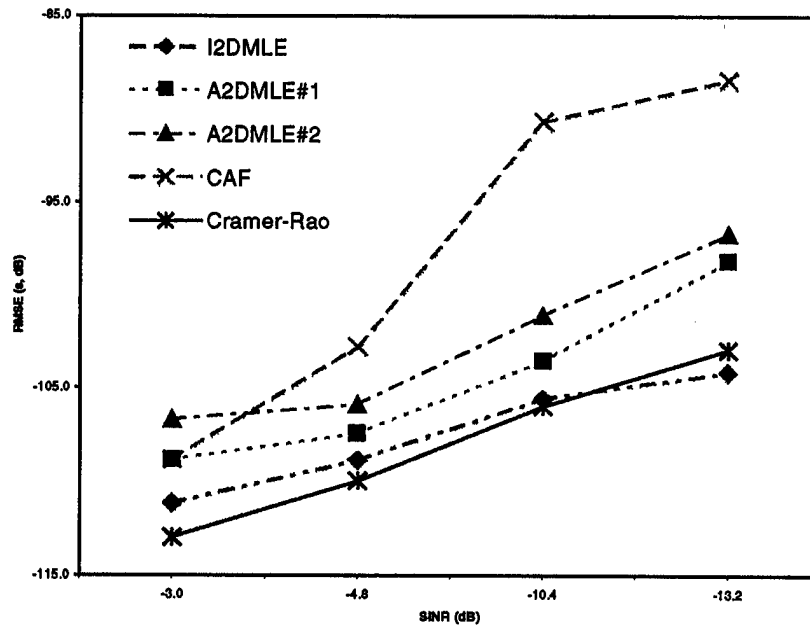Figure 7-12 – RMSE$_{\text{TDOA}}$ vs. SINR, Environment I, $N = 2048$

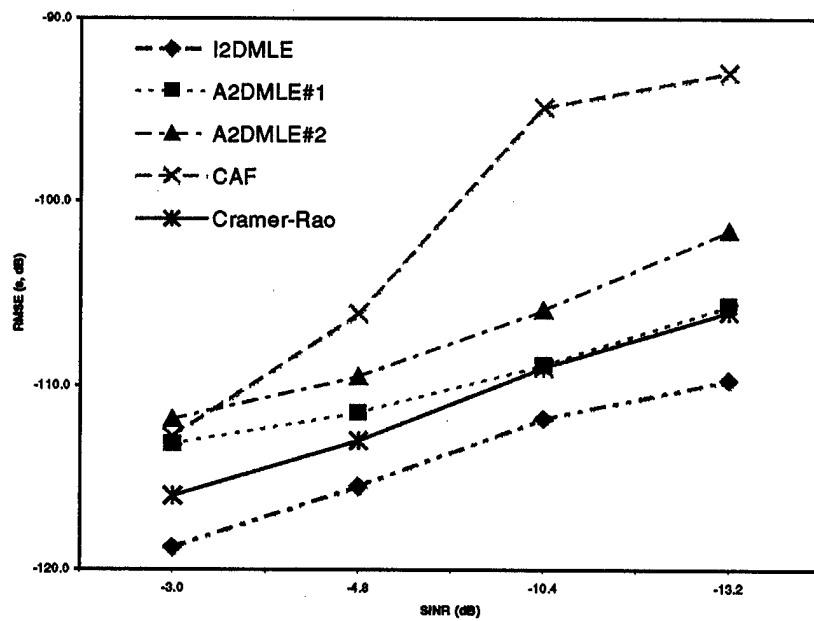Figure 7-13 – RMSE$_{TDOA}$ vs. SINR, Environment I, $N = 4096$

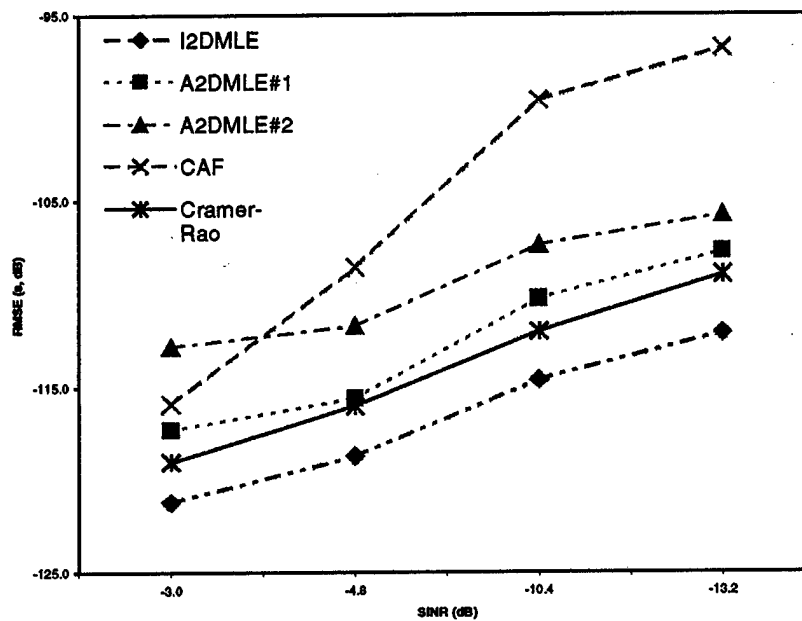Figure 7-14 – RMSE$_{TDOA}$ vs. SINR, Environment I, $N = 8192$

120

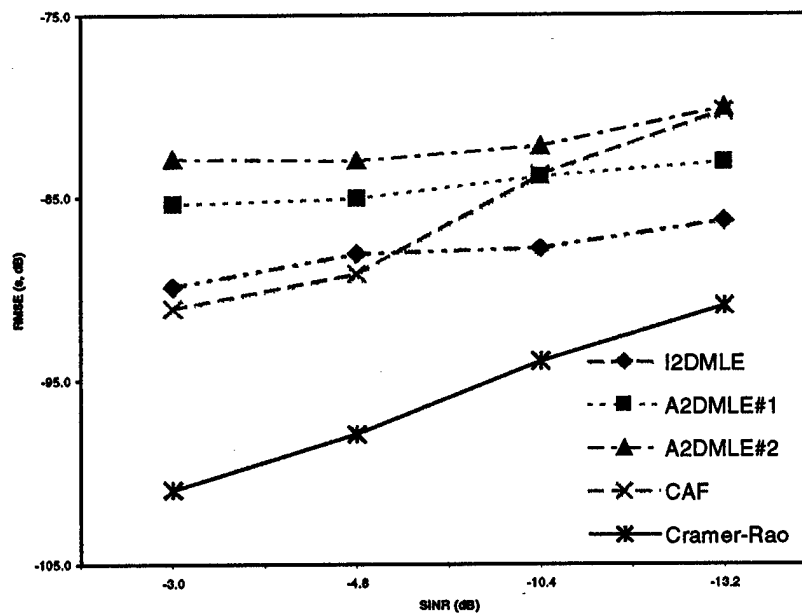Figure 7-15 – RMSE$_{TDOA}$ vs. SINR, Environment I, $N = 16384$

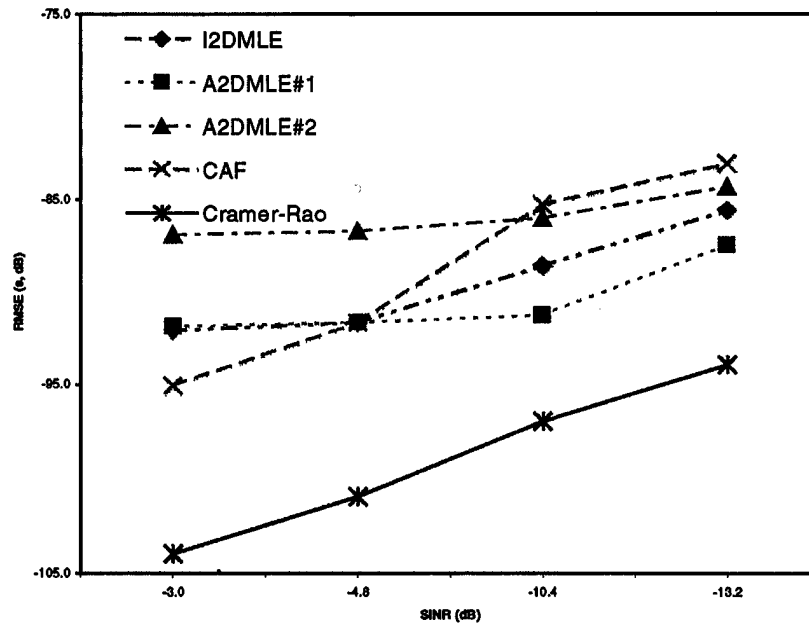Figure 7-16 – RMSE$_{TDOA}$ vs. SINR, Environment II, $N = 256$

121

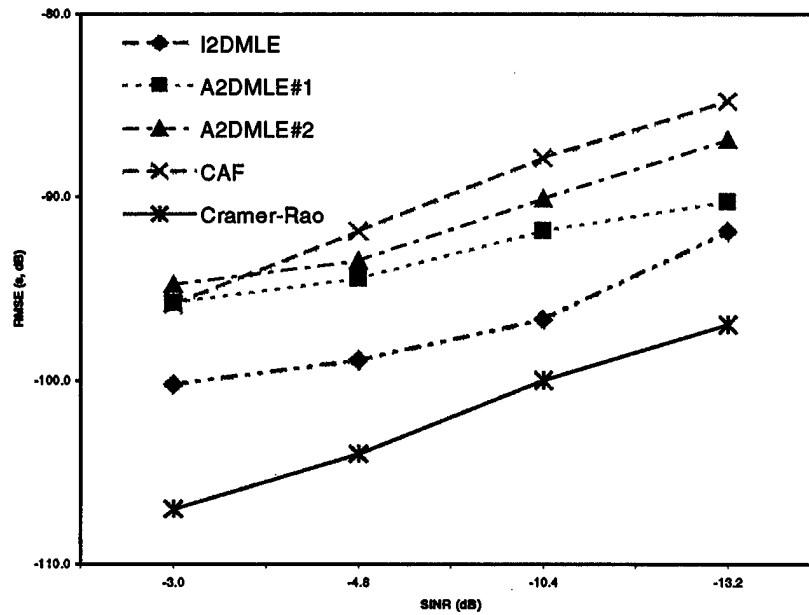Figure 7-17 – RMSE$_{TDOA}$ vs. SINR, Environment II, $N = 512$

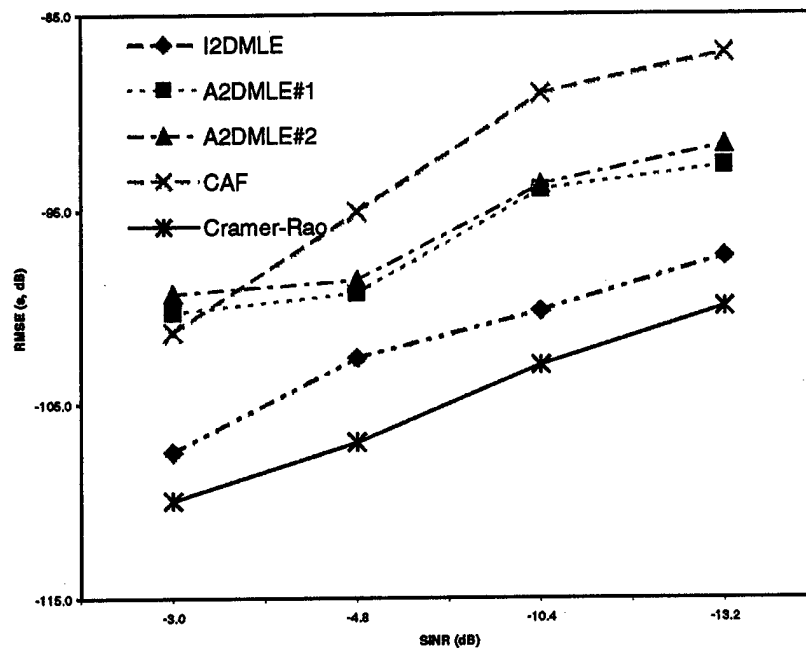Figure 7-18 – RMSE$_{TDOA}$ vs. SINR, Environment II, $N = 1024$

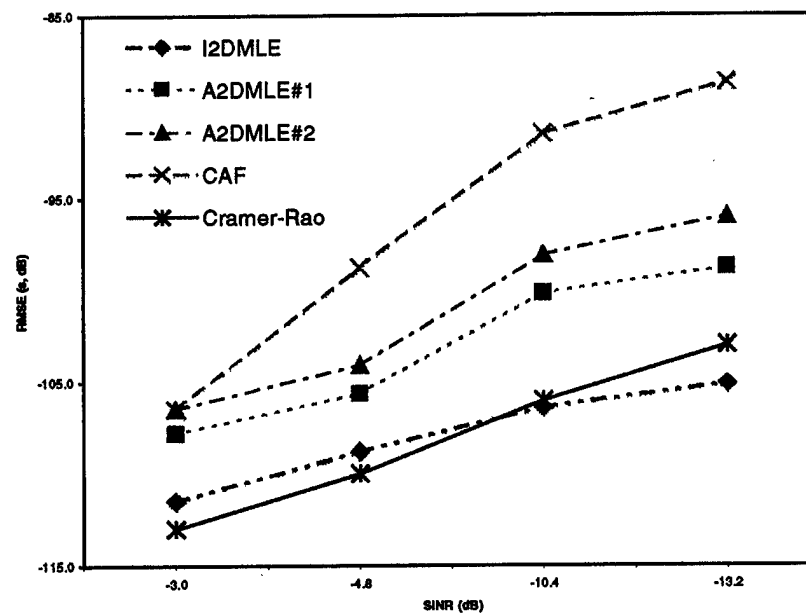Figure 7-19 – RMSE$_{TDOA}$ vs. SINR, Environment II, $N = 2048$

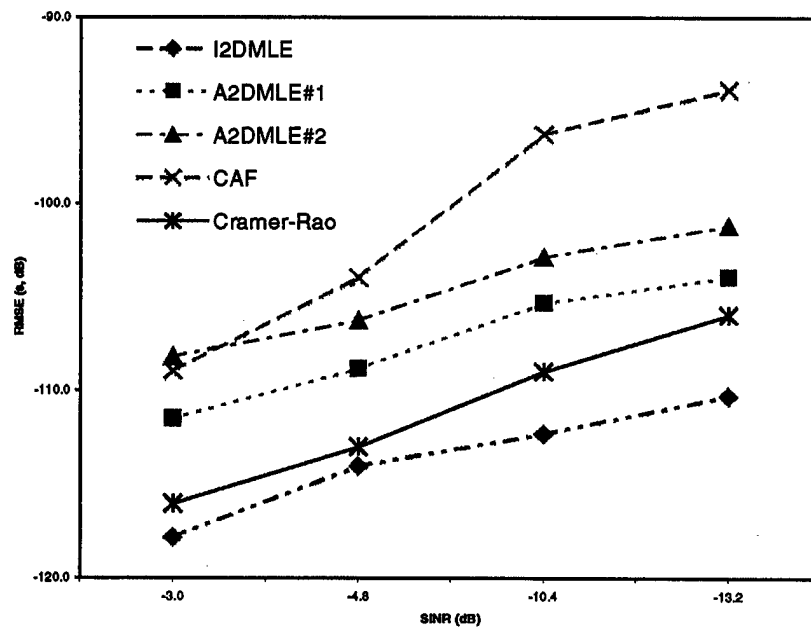Figure 7-20 – RMSE$_{TDOA}$ vs. SINR, Environment II, $N = 4096$

123

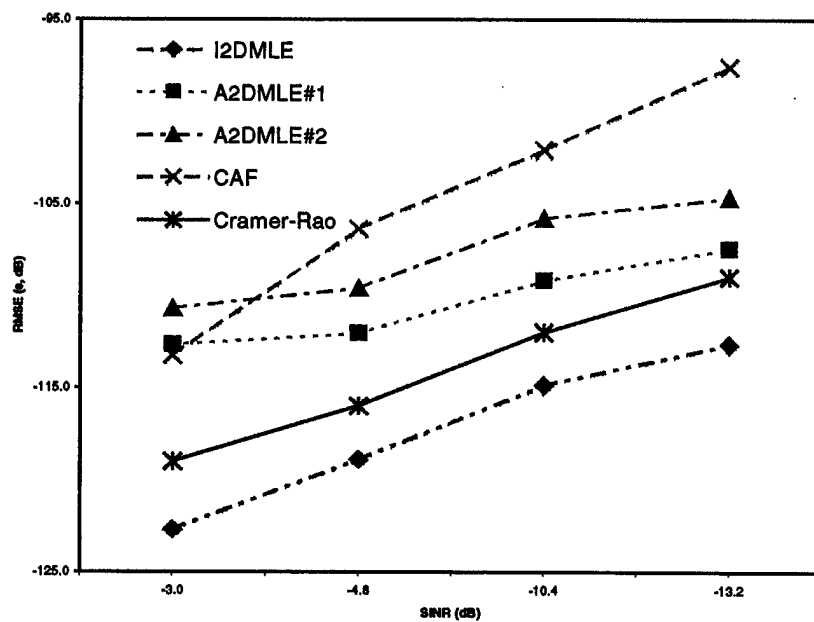Figure 7-21 – RMSE$_{TDOA}$ vs. SINR, Environment II, $N = 8192$

Figure 7-22 – RMSE$_{TDOA}$ vs. SINR, Environment II, $N = 16384$

124

The most obvious result illustrated by these plots is the confirmation of the conclusion from above with respect to the cyclostationary algorithms' performance in shorter collect lengths and lower SINR levels. Beginning with Figures 7-9 and 7-16, for N = 256, the cyclostationary algorithms perform well above the CRB, in the same range as the CAF and do not increase their performance relative to these two stationary benchmarks as SINR decreases. However, as is clear in Figures 7-13 and 7-20, by N = 4096, the true contribution of the cyclostationary algorithms becomes evident. As SINR deteriorates, these three algorithms continue to perform well and significantly increase their performance relative to the stationary techniques. By N = 16384, in Figures 7-15 and 7-22, the cyclostationary algorithms significantly outperform the CAF and appear to suffer less degradation in performance as SINR decreases than even the CRB.

Following the same theme for FDOA, it too is instructive to understand the sensitivity of the algorithms to the SINR level at each of the collect lengths. Figures 7-23 through 7-29 show the $\text{RMSE}_{\text{FDOA}}$ vs. SINR for Environment I and Figures 7-30 through 7-36 illustrate the results for Environment II.

Figure 7-23 – $\text{RMSE}_{\text{FDOA}}$ vs. SINR, Environment I, N = 256

Figure 7-24 – RMSE$_{FDOA}$ vs. SINR, Environment I, $N = 512$

Figure 7-25 – RMSE$_{FDOA}$ vs. SINR, Environment I, $N = 1024$

126

Figure 7-26 – RMSE$_{FDOA}$ vs. SINR, Environment I, $N = 2048$

Figure 7-27 – RMSE$_{FDOA}$ vs. SINR, Environment I, $N = 4096$

Figure 7-28 – RMSE$_{FDOA}$ vs. SINR, Environment I, $N = 8192$

Figure 7-29 – RMSE$_{FDOA}$ vs. SINR, Environment I, $N = 16384$

128

Figure 7-30 – RMSE$_{FDOA}$ vs. SINR, Environment II, $N = 256$
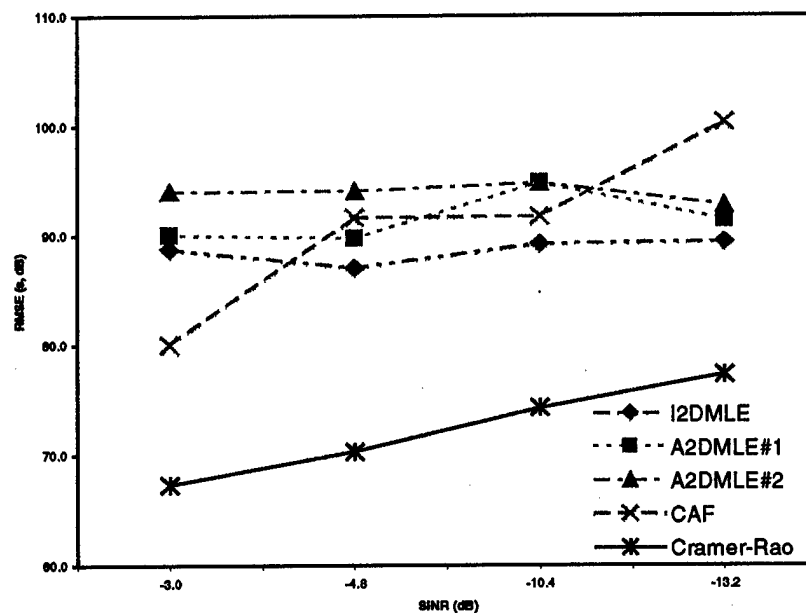
Figure 7-31 – RMSE$_{FDOA}$ vs. SINR, Environment II, $N = 512$

129
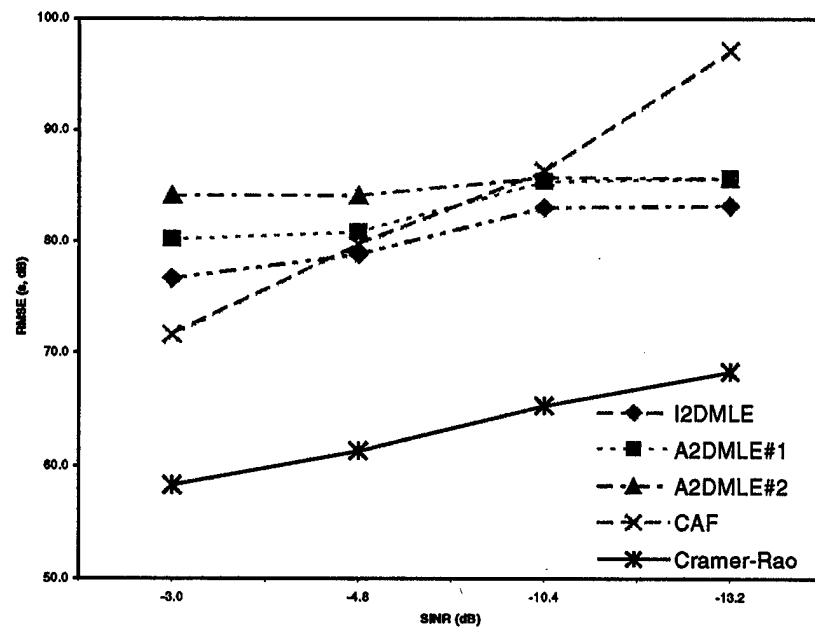
Figure 7-32 – RMSE$_{FDOA}$ vs. SINR, Environment II, $N = 1024$
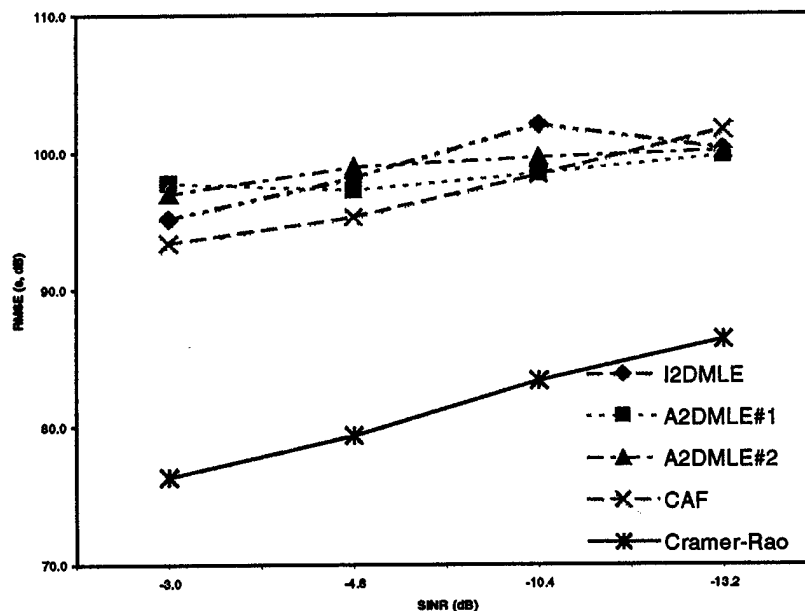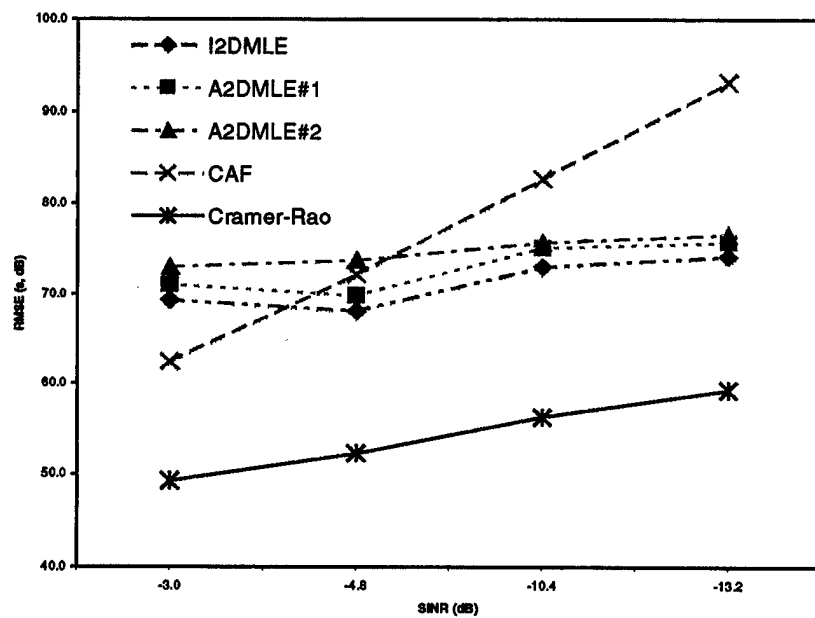

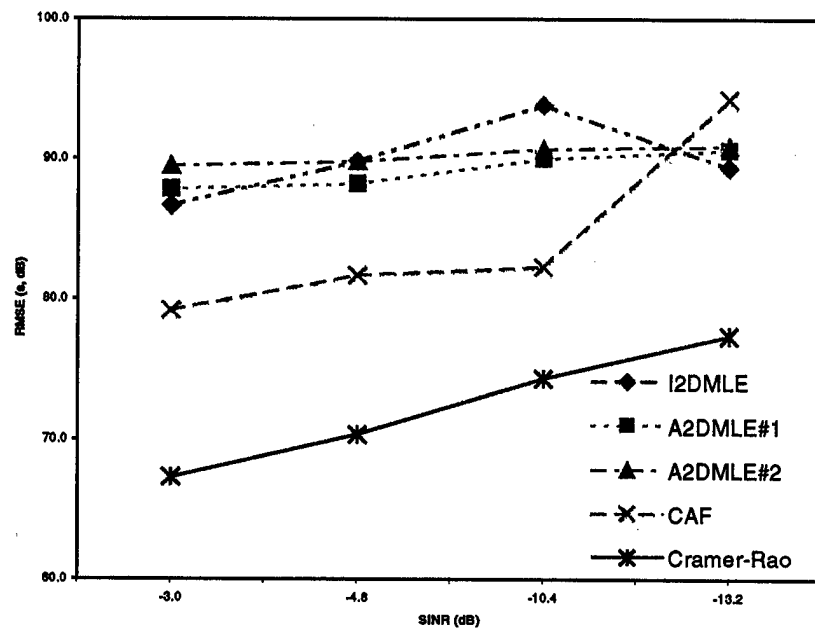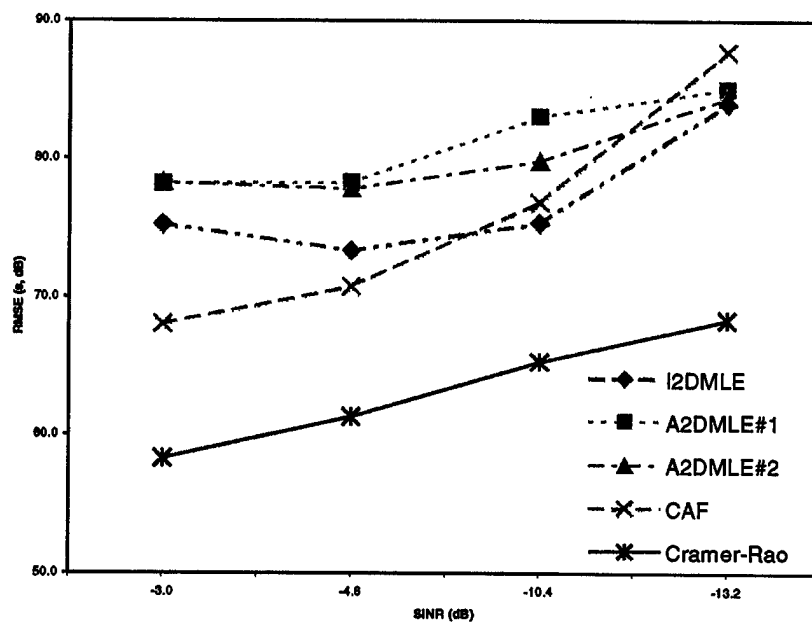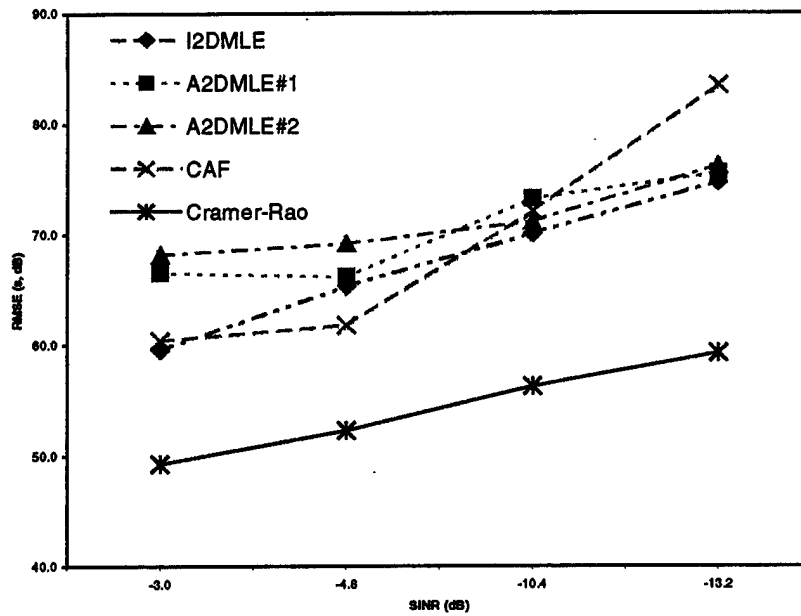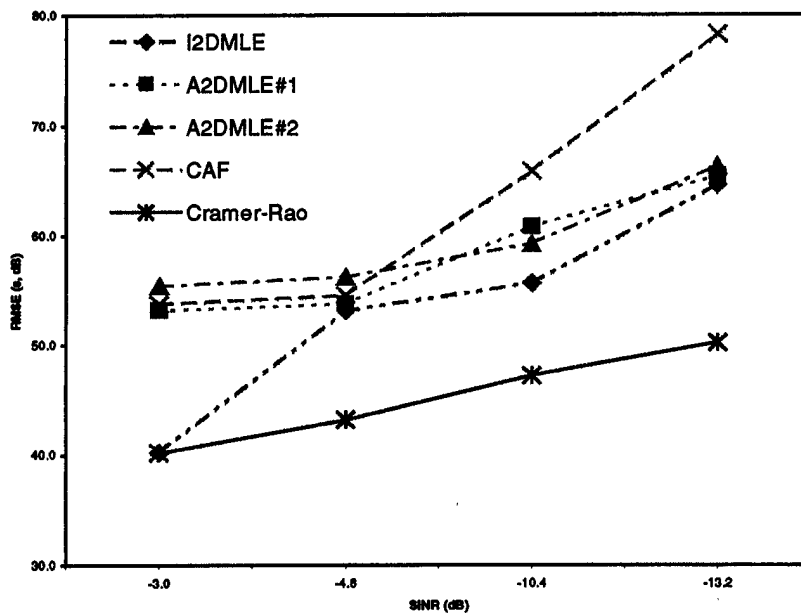Figure 7-33 – RMSE$_{FDOA}$ vs. SINR, Environment II, $N = 2048$

130
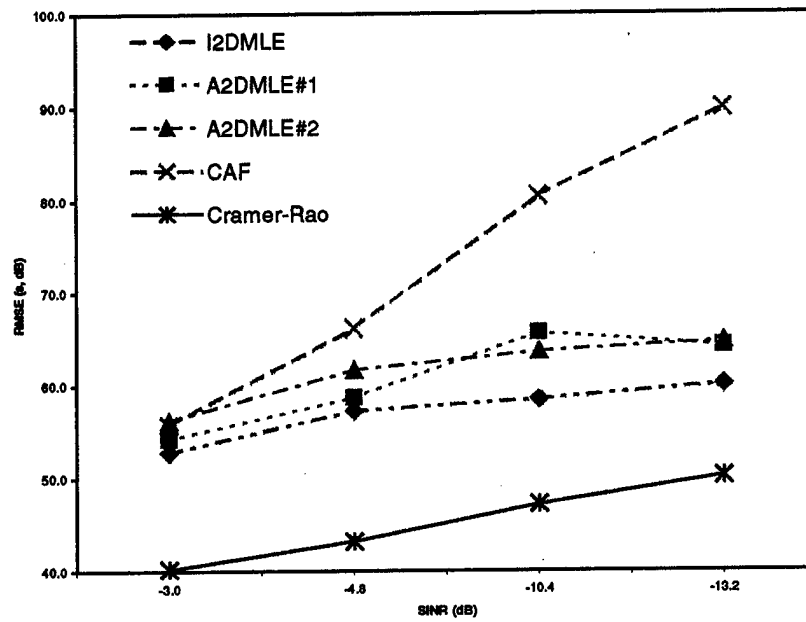
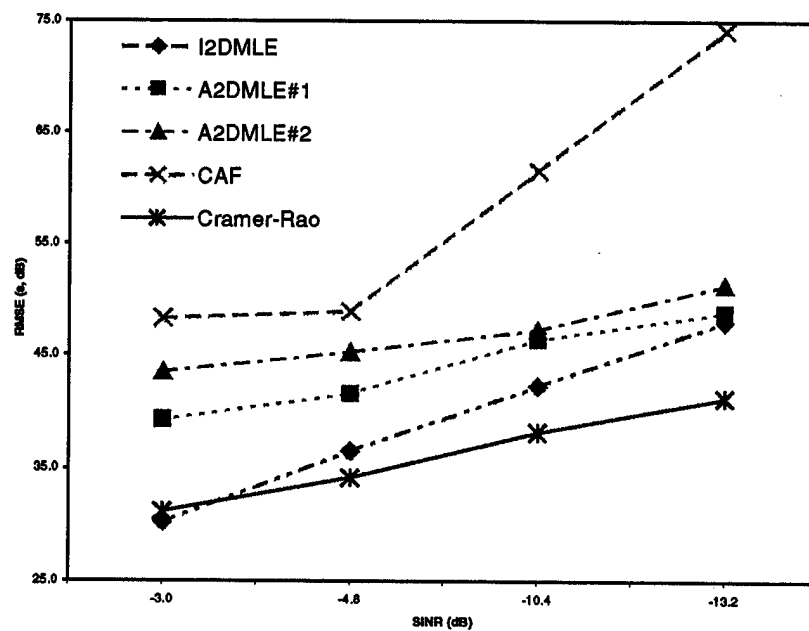Figure 7-34 – RMSE$_{FDOA}$ vs. SINR, Environment II, N = 4096
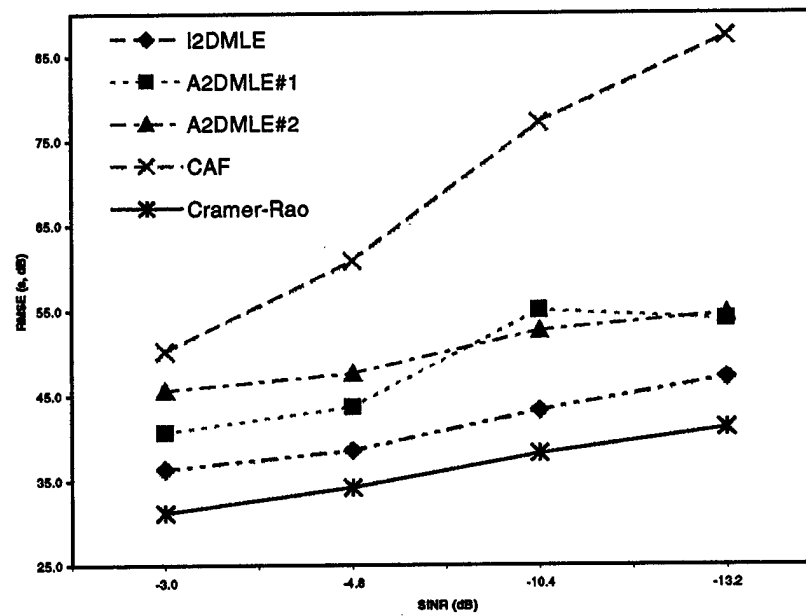
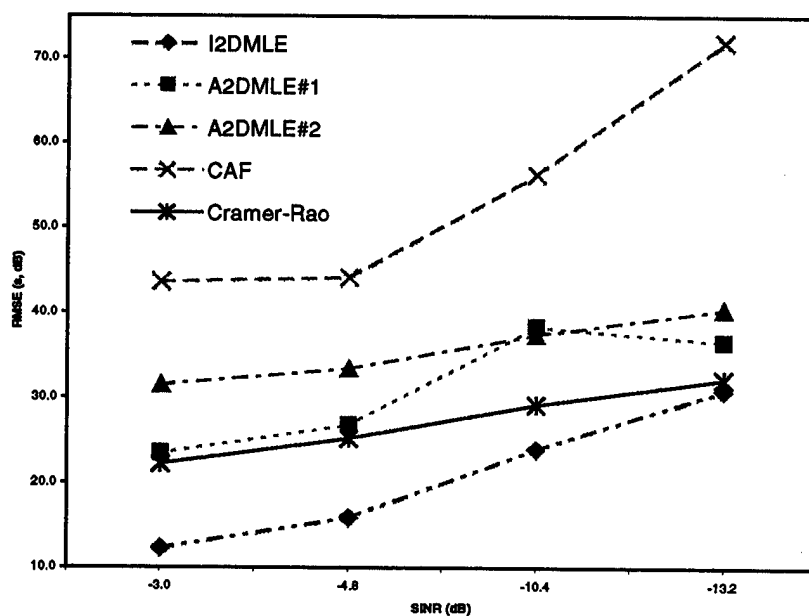Figure 7-35 – RMSE$_{FDOA}$ vs. SINR, Environment II, N = 8192

131

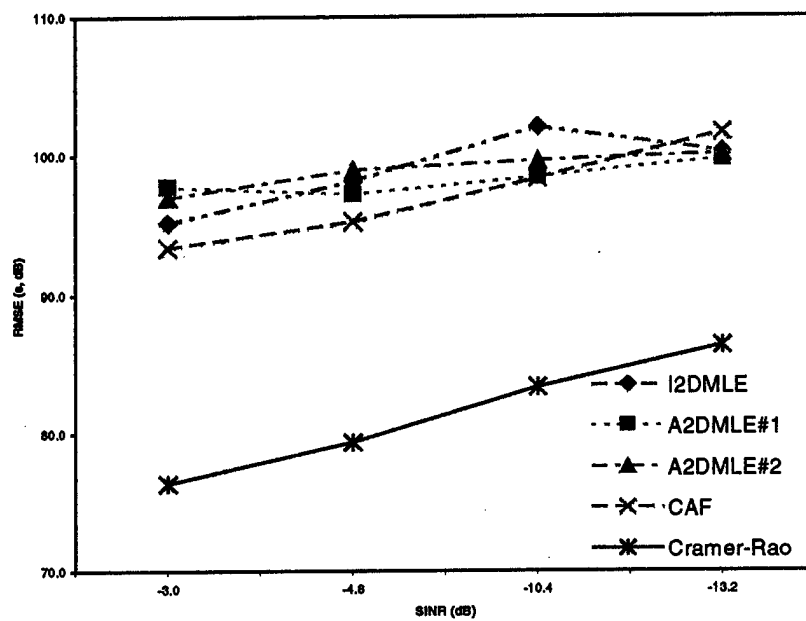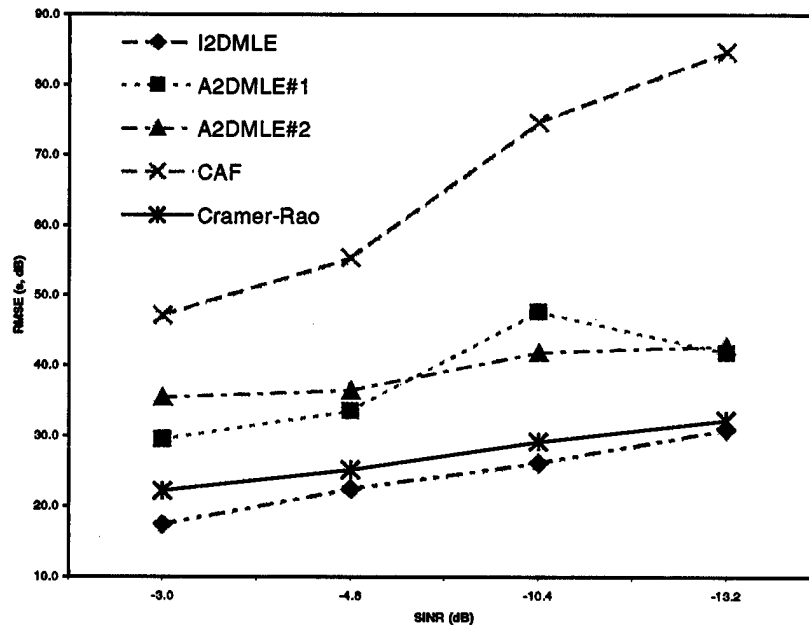Figure 7-36 – RMSE$_{FDOA}$ vs. SINR, Environment II, $N = 16384$

From these RMSE$_{FDOA}$ vs. SINR plots, several conclusions may be drawn. First, the gap between the implemented algorithms and the CRB at short collect lengths is very obvious in Figures 7-23 and 7-30, the gap a bit larger in 7-30 due to the more difficult narrowband interference environment as noted above. In addition, as SINR decreases at this short collect length, the implemented algorithms degrade more rapidly than the CRB. Through the next sets of plots, Figures 7-24 through 7-28 and 7-31 through 7-35, the gradual progression in the performance of the cyclostationary algorithms can be seen. By $N = 8192$ in Figures 7-28 and 7-35, the cyclostationary algorithms have begun to approach the CRB, now degrading at the same rate or even better than the CRB. In this same plot, the fate of the CAF is obvious with its RMSE well above those of the cyclostationary algorithms.

Finally, in Figures 7-29 and 7-36, the cyclostationary algorithms all conclude at SINR = -13 with less degradation than the CRB indicating that as SINR decreases further, all three algorithms will soon exceed the lower bound set by the CRB.

132

7.   Summary

Conclusions in six major areas are available as a result of the MCT presented in Chapter VI. These areas include the effects of approximation on the ideal cyclostationary two-dimensional maximum likelihood algorithm, I2DMLE; a comparison of the new cyclostationary algorithms to their stationary counterpart, the CAF; a comparison of the new cyclostationary algorithms to the stationary theoretical lower bound on the accuracy of TDOA and FDOA estimation, the CRB; a normalization and comparison of the newly derived algorithms to heritage cyclostationary TDOA algorithms; a different illustration of performance as collect length increases; and an investigation of performance as SINR decreases.

The effects of approximation on I2DMLE can be seen in the performance of A2DMLE#1 and A2DMLE#2. The first approximation, A2DMLE#1, followed closely the performance of the ideal algorithm, differing in $RMSE_{TDOA}$ and $RMSE_{FDOA}$ by 2 to 4 dB across nearly all cases. It is deemed a good, practical approximate cyclostationary ML TDOA-FDOA algorithm due to its reasonable performance relative to the ideal and its lack of dependence on a priori information like the spectral correlation function of the SOI. A2DMLE#2 is a compromise between performance and computational complexity. Its performance is 3 to 5 dB above that of A2DMLE#1 and it lacks the steep sloping performance vs. collect length at the longer collect lengths. However, in its implementation, it enjoys computational savings of nearly 2. Thus, it is a good compromise between performance and computational burden.

All three cyclostationary algorithms performed well in comparison to the CAF. In TDOA, the CAF outperforms the cyclostationary implementations at very short collect lengths of 256 or 512 samples, but only at higher SINR. When the signal environment deteriorates, the cyclostationary algorithms continue to improve their performance as collect length increased while the performance curve of the CAF flattens out as a result of the increased interference. Thus, at low SINR and longer collect lengths, the three cyclostationary algorithms outperformed the CAF by as much as 16 dB-(seconds). In FDOA, the cyclostationary algorithms are outperformed at higher SINR by the CAF until

$N = 4096$, quite a bit longer than in TDOA. However again as the signal environment deteriorates, the performance of the cyclostationary algorithms does not deteriorate as rapidly as that of the CAF resulting in a 42 dB (Hertz) gap at SINR = -13 dB and $N = 16384$. Clearly, the advantage of the cyclostationary algorithms over the CAF in heavy interference environments is evident by these results.

Performance of the cyclostationary algorithms in comparison to the stationary theoretical lower bounds on TDOA and FDOA estimation set by the CRB illustrate the contribution that the signal-selectivity and interference tolerance features of the cyclostationary-based algorithms make. In TDOA, I2DMLE exceeds the CRB for larger N and the two approximations approach the CRB as N approaches 16384 samples. This indicates that with increasing N, all three cyclostationary algorithms exceed the CRB. In FDOA, again, I2DMLE exceeds the CRB for $N > 4096$ and SINR = -3 dB. As SINR decreases, however, the number of samples required for the cyclostationary algorithms to exceed the CRB increases. At SINR = -13 dB, only I2DMLE exceeds the CRB and only with $N = 16384$. But, as in TDOA, all three approach the CRB as N approaches 16384 samples. This clearly indicates that in FDOA as in TDOA, as N exceeds 16384, each of the cyclostationary algorithms exceeds the CRB.

Normalization of these results for SOI of different bandwidths is accomplished with a simple adjustment. This adjustment amounts to +3.5 dB for comparison to algorithms outlined in [22]. With this adjustment, the three new cyclostationary algorithms performed within 3 to 5 dB of the heritage algorithms. The more challenging interference environments used in the MCT above can account for at least some of that performance gap. Thus, the results obtained here are consistent with those achieved with previously derived estimators.

Performance as a function of collect length is an important parameter, particularly in making implementation decisions like increasing the number of samples processed. By plotting the RMSE * collect length vs. collect length, it is readily apparent which algorithms benefit most from increasing collect lengths to be processed. With the exception of A2DMLE#2 in TDOA estimation, the cyclostationary algorithms equaled or exceeded any performance gain made by the CRB due to an increase in collect length.

Thus, for improved performance, at the expense of computation time, all three cyclostationary algorithms improve nearly linearly with increased collect length with the exception noted above.

Finally, looking at performance as a function of SINR again illustrates the signal-selectivity and interference tolerant characteristics of the cyclostationary algorithms. While the CAF and it's theoretical lower bound on performance set by the CRB degrade significantly as the SINR decreases to −13 dB, the cyclostationary algorithms do not suffer nearly the same losses in performance. In fact, all three cyclostationary algorithms approach or exceed the CRB as SINR decreases to −13 dB. Again, another indication of the power that these cyclostationary algorithms bring to highly corrupt signal environments.

The results of this work clearly illustrate three joint TDOA-FDOA estimators, optimized in a maximum-likelihood sense, that take full advantage of cyclostationary signal-selectivity and interference tolerance. They perform well in comparison to both the CAF and the stationary CRB, indicating the potential performance gains cyclostationary techniques have to offer over traditional techniques. In addition, their performance in TDOA is comparable to heritage TDOA algorithms when adjusted for SOI bandwidth. Finally, they continue to enjoy performance gains as N increases and also as SINR decreases, not normally seen in traditional techniques.

B.   ORIGINAL CONTRIBUTIONS

The original contribution of this research consists of the new three algorithms developed and the performance testing of these new algorithms. I2DMLE represents the first development of a joint maximum-likelihood TDOA-FDOA estimator for digital cyclostationary communications signals. It is derived from a modified version of Model C, the simple Doppler model, which has yet to be used as the basis for the development of any cyclostationary TDOA or TDOA-FDOA estimators. As noted above, it is an ideal algorithm requiring the a priori knowledge of the spectral correlation function of the SOI in order to be implemented. This situation being difficult to accommodate in practice, a

135

substitution scheme is necessary to form approximations. While an infinite number of substitutions is available to produce an infinite number of approximations, A2DMLE#1 and A2DMLE#2 represent two original approximations to I2DMLE. Thus, they are the first two practical cyclostationary joint ML estimators for TDOA and FDOA requiring only a cycle frequency from the SOI rather than the entire spectral correlation function.

The comparison of the performance of these three original algorithms to that of the CAF and the stationary CRB predictions also marks the first time any cyclostationary TDOA-FDOA estimation algorithm has been evaluated in such detail against traditional techniques. While extensive work has been done in the area of cyclostationary TDOA estimators, the work in cyclostationary TDOA-FDOA determination has been restricted to the investigation of the sensitivity of cyclostationary TDOA estimators to FDOA and to the modification of TDOA algorithms, derived from Model A, to accommodate FDOA. Thus, the performance of I2DMLE, A2DMLE#1 and A2DMLE#2 is the first benchmark to which future cyclostationary TDOA-FDOA algorithms can be compared.

C. AREAS FOR FURTHER INVESTIGATION

1. Time-varying Doppler

The effects of the more-realistic case of time-varying Doppler pose both a challenging and intriguing puzzle. Its first influence in the TDOA/FDOA problem comes in the form of various unknown effects on the calculation of the SCF. How time-varying Doppler changes the SCF surface and affects the determination of cycle-frequencies-of-interest has been investigated little if any. Beyond that, its effect on the two-dimensional optimization problem derived and tested here becomes even less clear. Certainly, allowances have to be made and a proper choice for determining the instantaneous FDOA would have to be determined. In addition, other more subtle changes certainly will be discovered once a detailed analysis is made.

2. Various Spectral Correlation Function Substitution Options

As noted in Chapter V, the derivation concludes with the logical selection of substitutions for the SCF of the SOI based upon the two observation variables. Those substitutions, being driven primarily by arbitrarily chosen rules could be quite different should another set of rules be selected based on one of the other possible motivations outlined in Chapter V as well. These substitutions could change the performance of the algorithm significantly in addition to affecting the digital implementation aspects of the problem. Both accurate determination of the TDOA and FDOA in addition to tractable implementation on general purpose or DSP hardware is relevant and deserves additional attention. Finally, the inclusion of the phase and amplitude mismatch, for highly disparate and non-coherent platforms does add the additional problem of estimating the mismatches first (see below). With this in mind, the substitutions could be made to simplify this process or minimize the reliance on these parameters that themselves may have suboptimal estimates.

3. Amplitude and Phase Mismatch

While arguments outlined in Chapter V supported the disregard of the mismatch in amplitude and phase between the receivers, there may exist an instance where the coherence between platforms is poor enough to play a significant role in the performance of the algorithm. While some work on specific algorithms has been done (SSPI contract), a study that concentrates specifically on the general effects of amplitude and phase mismatch at RF frequencies on TDOA and FDOA determination using cyclostationary techniques has not been published. This work could ideally lay the rigorous mathematical foundation for the inclusion or exclusion of the mismatch in realistic signal models, thus making a fundamental contribution to this field.

4. Modulation Types

As the spectrum crowds evermore, many new and more complex modulation types are in use. The work presented here tested only phase-shift keying schemes, specifically, BPSK with the logical and mathematical extension to QPSK. Higher-order PSK schemes as well as the myriad of other digital and analog modulation types must be investigated before the algorithms can be fully tested.

5. Other Signal Models

Models D and E more accurately reflect the situations most often encountered by systems attempting to measure TDOA and FDOA for SOIs. Algorithms derived directly from these models could prove to perform even better than those derived under simplified conditions. While seemingly mathematically intractable, an investigation into this method seems worthwhile given the possible benefits.

6. Lower Bound Extensions

The extension of the CRLB to the cyclostationary TDOA case has been accomplished and reported by Schell in [6]. According to Gardner [23], this extension would not apply to the TDOA/FDOA case explored here. In addition, the reportedly tighter Barankin and Ziv-Zakai bounds have yet to be investigated for application to the cyclostationary case. Work on these LB extensions could be highly valuable to furthering the understanding of the beneficial effects of modeling signals as cyclostationary.

7. Other Optimization Techniques

Using a different optimization technique, an investigator might discover a more computationally efficient algorithm that performs equally or better than the approximated ML algorithms developed here. A method such as Maximum Entropy might be employed as a different approach with positive results.

LIST OF REFERENCES

[1] C. Larvick, Internal Memorandum, Delphin Systems, Inc., 1998.

[2] R. Steel, *Mobile Radio Communications*, IEEE Press, New York, 1992.

[3] T. S. Rappaport, *Wireless Communications*, Prentice Hall, 1996.

[4] C. M. Spooner and W. A. Gardner, *Algorithm Development for Signals Intelligence Applications, Final Report Part 1 TDOA Estimation for Emitter Location*, Statistical Signal Processing Inc., June 26, 1996.

[5] C. H. Knapp and G. C. Carter, "The Generalized Correlation Method for Estimation of Time Delay", *IEEE Transactions on Acoustics, Speech and Signal Processing*, Vol. ASSP-24, No. 4, August, 1976.

[6] M. Azaria and D. Hertz, "Time Delay Estimation by Generalized Cross Correlation Methods", *IEEE Transactions on Acoustics, Speech and Signal Processing*, Vol. ASSP-32, No. 2, April, 1984.

[7] S. Stein, "Algorithms for Ambiguity Function Processing," *IEEE Transactions on Acoustics, Speech, and Signal Processing*, June 1981.

[8] S. V. Schell, "Corollaries for Cyclostationary Signals for Whittle's Theorem on the Cramer-Rao Bound," submitted to *IEEE Trans. On Signal Processing*, 1997.

[9] W. A. Gardner, *Statistical Spectral Analysis: A Nonprobabilistic Theory*, Englewood Cliffs, NJ: Prentice-Hall, 1987, Chapters 10-15.

[10] W. A. Brown, III, "On the Theory of Cyclostationary Signals", Ph.D. Dissertation, University of California at Davis, 1987.

[11] S. Stein, "Differential Delay/Doppler ML Estimation with Unknown Signals", *IEEE Trans. Signal Processing*, Vol. 41, No. 8, August 1993, pp. 2717-2719.

[12] L. Giulianelli and P. Rusu, "Residual in Time Difference of Arrival Estimates from Cross Correlation Measurements", Internal Memorandum, Applied Research Laboratory, University of Texas at Austin, 1996.

[13] W. A. Gardner, "Exploitation of Spectral Redundancy in Cyclostationary Signals", *IEEE Signal Processing*, Vol. 39, No. 4, April 1991, pp. 14-36.

[14] W. A. Gardner, ed., *Cyclostationarity in Communications and Signal Processing*, IEEE Press, 1994.

[15] W. A. Gardner, "Two Alternative Philosophies for Estimation of the Parameters of Time-series", *IEEE Trans Information Theory*, Vol. 37, No. 1, January 1991, pp. 216-218.

[16] W. A. Gardner and C. K. Chen, "Signal-Selective Time-Difference-of-Arrival Estimation for Passive Location of Man-Made Signal Sources in Highly Corruptive Environments, Part I: Theory and Method, *IEEE Trans on Signal Proc.*, May 1992, pp. 1161-1184.

[17] W. A. Brown, III, *Introduction to Second-Order Cyclostationary Signals*, Mission Research Corp. briefing, April 22, 1996.

[18] R. S. Roberts, W. A. Brown, III and H. H. Loomis, Jr., "Computational Efficient Algorithms for Cyclic Spectral Analysis", *IEEE Trans. Signal Proccessing*, Vol. 39, No. 4, April 1991, pp. 38-49.

[19] W. A. Brown, III and H. H. Loomis, Jr., "Digital Implementations of Spectral Correlation Analyzers", *IEEE Trans. Signal Proccessing*, Vol. 41, No. 2, February 1993, pp. 703-719.

[20] R. S. Roberts, W. A. Brown, III and H. H. Loomis, Jr., "A Review of Digital Spectral Correlation Analysis: Theory and Implementation", Article 6 in *Cyclostationarity in Communications and Signal Processing*, W. A. Gardner, ed., IEEE Press, 1994.

[21] C.W. Therrien, *Discrete Random Signals and Statistical Signal Processing*, Prentice-Hall, 1992.

[22] C.-K. Chen and W. A. Gardner, "Signal-Selective Time-Difference-of-Arrival Estimation for Passive Location of Man-Made Signal Sources in Highly Corruptive Environments, Part II: Algorithms and Performance, *IEEE Trans on Signal Proc.*, May 1992, pp. 1185-1197.

[23] Conversation with W. A. Gardner, August 1998.

BIBLIOGRAPHY

Carter, G. C., "Coherence and Time Delay Estimation", *Proceedings of the IEEE*, Vol. 75, No. 2, February 1987, pp. 236-255.

Franks, L. E., *Signal Theory*, Revised Edition 1981, Dowden & Culver, Inc. Stroudsburg, PA, Chapters 1-3, 5.1-4, & 8.

Gardner, W. A., "Spectral Correlation of Modulated Signals: Part I Analog Modulation," *IEEE Trans on Comm*, June 1987, pp. 585-594.

Gardner, W. A., "Signal Interception: A Unifying Theoretical Framework for Feature Detection", *IEEE Trans. Communications*, Vol. 36, No. 8, August 1988, pp. 897-906.

Gardner, W. A., " The spectral correlation theory of cyclostationary time-series," *Signal Processing*, 11, pp. 13-36, 1986.

Gardner, W. A. and C.-K. Chen, "Interference-Tolerant Time-Difference-of-Arrival Estimation for Modulated Signals", *IEEE Trans. Acoustics, Speech and Signal Processing*, Vol. 36, No. 9, September, 1988, pp. 1385-1395.

Gardner, W. A., W. A. Brown and C. K. Chen, "Spectral Correlation of Modulated Signals: Part II Digital Modulation," *IEEE Trans on Comm*, June 1987, pp. 595-601.

Gardner, W. A. and Chad M. Spooner, "Detection and Source Location of Weak Cyclostationary Signals: Simplification of the Maximum-Likelihood Receiver," *IEEE Trans. on Comm.* June 1993, pp. 905-916.

Gardner, W. A. and R. S. Roberts, "One-bit Spectral-Correlation Algorithms", *IEEE Trans. Signal Processing*, Vol. 41, No. 1, January 1993, pp. 423-427.

Gardner, W. A. and C. M. Spooner, "The Cummulant Theory of Cyclostationary Time-Series, Part I: Foundation", *IEEE Trans Signal Processing*, Vol. 42, No. 12, December 1994, pp. 3387-3408.

Gelli, G., L. Izzo and L. Paura, "Cyclostationarity-Based Signal Detection and Source Location in Non-Gaussian Noise", *IEEE Trans. Communications*, Vol. 44, No. 3, March 1996, pp.368-376.

Ho, K. C., and Y. T. Chan, "Emitter location of a Known Altitude Object From TDOA and FDOA Measurements", *IEEE Trans. Aerospace and Electronic Systems*, Vol. 33, No. 3, July 1997.

Ho, K. C. and Chen, Y. T., "Solution and Performance Analysis of Emitter location by TDOA", *IEEE Transactions on Aerospace and Electronic Systems*, Vol. 29, No. 4, October 1993.

Izzo, L., A. Napolitano and L. Paura, "Modified Cyclic Methods for Signal Selective TDOA Estimation", *IEEE Trans. Signal Processing*, Vol. 42, No. 11, November 1994, pp. 3294-3298.

Izzo, L., L. Paura and G. Poggi, "An Interference Tolerant Algorithm for Localization of Cyclostationary-Signal Sources", *IEEE Trans. Signal Processing*, Vol. 40, No. 7, July 1992, pp. 1682-1686.

Otnes, R., K., "Frequency Difference of Arrival Accuracy", *IEEE Trans. Acoustics, Speech and Signal Processing*, Vol. 37, No. 2, February 1989, pp.306-308.

Piersol, A. G., "Time Delay Estimation Using Phase Data", *IEEE Trans. Acoustics, Speech and Signal Processing*, Vol. ASSP-29, No. 3, June 1981, pp. 471-477.

Spooner, Chad M., "An Overview of Recent Developments in Cyclostationary Signal Processing", Proceedings of the Second Workshop on Cyclostationary Signals, Mission Research Corporation, Monterey, CA, August 1-2, 1994.

Spooner, C. M. and W. A. Gardner, "The Cummulant Theory of Cyclostationary Time-Series, Part II: Development and Applications", *IEEE Trans Signal Processing*, Vol. 42, No. 12, December 1994, pp. 3409-3429.

Spooner, C. M., C.-K Chen and W. A. Gardner, "Maximum Likelihood Two-Sensor Detection and TDOA Estimation for Cyclostationary Signals", *Proceedings of the Sixth Annual Multi-dimensional Signal Processing Workshop*, 1993.

Torrieri, Don J., "Statistical Theory of Passive Location Systems", *IEEE Transaction on Aerospace and Electronic Systems*, Vol., AES-20, Number 2, March 1984, p.183.

Van Trees, H. L., *Detection, Estimation and Modulation Theory, Parts 1, 2 and 3*, New York: John Wiley and Sons, 1968.

APPENDIX

A1. SIGNAL OF INTEREST PARAMETERS

Sampling Frequency: $f_s = 1$ MHz

Carrier Frequency: $f_c = \left(\frac{63}{256}\right) f_s$

Keying Rate: $f_k = \left(\frac{16}{256}\right) f_s$

Bandwidth: $B_{SOI} = \left(\frac{48}{256}\right) f_s$

TDOA: $D_{SOI} = 50 \; \frac{1}{f_s}$

FDOA: $f_d = \left(\frac{5}{256}\right) f_s$

A2. WIDEBAND SIGNAL NOT OF INTEREST PARAMETERS

Sampling Frequency: $f_s = 1$ MHz

Carrier Frequency: $f_c = \left(\frac{54}{256}\right) f_s$

Keying Rate: $f_k = 0.1 f_s$

Bandwidth: $B_{SOI} = 0.3 f_s$

TDOA: $D_{SOI} = 58 \; \frac{1}{f_s}$

FDOA: $f_d = \left(\frac{3}{256}\right) f_s$

A3. NARROWBAND SIGNAL NOT OF INTEREST PARAMETERS

Sampling Frequency: $f_s = 1$ MHz

Carrier Frequency: $f_c = \left(\frac{54}{256}\right) f_s$

Keying Rate: $f_k = 0.025 f_s$

Bandwidth: $B_{SOI} = 0.075 f_s$

TDOA: $D_{SOI} = 58 \; \frac{1}{f_s}$

FDOA: $f_d = \left(\frac{3}{256}\right) f_s$

INITIAL DISTRIBUTION LIST

1. Defense Technical Information Center 2
   8725 John K. Kingman Rd., STE 0944
   Ft. Belvoir, VA 22060-6218

2. Dudley Knox Library 2
   Naval Postgraduate School
   411 Dyer Road
   Monterey, CA 93943-5101

3. Dr. Herschel H. Loomis, Jr. 2
   Naval Postgraduate School
   Code EC/LM
   833 Dyer Road
   Monterey, CA 93943-5121

4. Dr. R. Clark Robertson 1
   Naval Postgraduate School
   Code EC/RC
   833 Dyer Road
   Monterey, CA 93943-5121

5. Dr. Douglas K. Fouts 1
   Naval Postgraduate School
   Code EC/FS
   833 Dyer Road
   Monterey, CA 93943-5121

6. Dr. Gus K. Lott, Jr. 2
   Yarcom, Incorporated
   1475 Terminal Way Suite E
   Reno, NV 89502-3225

7. Dr. William A. Brown, III 1
   Mission Research Corporation
   10 Ragsdale Drive, Suite 201
   Monterey, CA 93940-5776

8. RDML Rand Fisher 1
   14675 Lee Road
   Chantilly, VA 20151-1715